SYSTEM IDENTIFICATION, MODEL UPDATING AND SEISMIC PERFORMANCE ASSESSMENT OF STONE ARCH BRIDGES

by

Emre Aytulun

B.S., Civil Engineering, Boğaziçi University, 2014

Submitted to the Institute for Graduate Studies in
Science and Engineering in partial fulfillment of
the requirements for the degree of
Master of Science

Graduate Program in in Civil Engineering

Boğaziçi University

2017

SYSTEM IDENTIFICATION, MODEL UPDATING AND SEISMIC PERFORMANCE ASSESSMENT OF STONE ARCH BRIDGES

APPROVED BY:

Assoc. Prof. Serdar Soyöz (Thesis Supervisor)	.....
Assoc. Prof. Kutay Orakçal	.....
Prof. Alper İlki	.....

DATE OF APPROVAL: 17.07.2017

ACKNOWLEDGEMENTS

I owe Associate Professor Serdar Soyöz a debt of gratitude for accepting me to his research team and giving the responsibility of this project to me. I am also grateful to Associate Professor Serdar Soyöz for his endless trust and good communication. His valuable guidance and support in every field are absolutely precious. My sincere thanks to him because, my thinking and research skill improved thanks to his knowledge and experience. In addition, he always encouraged me to be unique, which helped me to develop my engineering skill and to stimulate to do my best. Actually, there is actually no words to thanks to him.

Besides, I thank to Prof. Alper İlki and Assoc. Prof. Kutay Orakçal for accepting to be my thesis juries. Their valuable comments and suggestions improved my thesis.

I thank my fellow research assistants in our group: Korkut Kaynardağ, Hüseyin Çolak and Oğuz Şenkardeşler for all the fun and friendship that we have had in the last three years. I specially thank to Korkut for his help through many laboratory and field works. Also, I sincere thank to Oğuz for increasing my awareness to my project with his suggestions and for promoting to continue my project in most proper way with discussions. I would also like to thank ARUP Istanbul office for sharing their project information with us.

Also, I take this opportunity to express the profoundest gratitude from my deep heart to my beloved my parents and my sister for their sacrifices, love, and continuous support – both spiritually and materially. Without their extreme sacrifices, supports and the carefree environment that they provided, it would not be possible for me to follow a graduate degree. Last but not the least, I am very thankful to my wife, Ceren, without her, this thesis would not have been possible. Her unending love, valuable support and incredible tolerance were indescribable. Actually, there is actually no words to thanks to her.

ABSTRACT

SYSTEM IDENTIFICATION, MODEL UPDATING AND SEISMIC PERFORMANCE ASSESSMENT OF STONE ARCH BRIDGES

Modernization of Samsun- Kalin railway line which is 378 km long has been undertaken by Turkish State Railways. Due to their historical significance, 41 stone arch bridges on the line were decided to be preserved. Samsun-Kalin line passes through North Anatolian Fault, resulting in high seismic demand on bridges. In this study, seismic assessment of the bridges was carried out by Finite Element Analysis; however, masonry structures such as stone arch bridges have higher significant uncertainties compared to concrete or steel structures in terms of material properties, boundary conditions and modeling assumptions. Therefore, it becomes almost unavoidable to perform dynamic identification tests to validate Finite Element Models (FEM). In this study, dynamic properties of the bridges were identified by Enhanced Frequency Domain Decomposition method. Vibration measurements were collected under ambient conditions, impact loading and train passage. Based on identified modal parameters, FEM of the bridges were updated to obtain actual values of Young's modulus and soil spring values. FEM updating procedure was performed by minimizing the difference between experimental and analytical modal values. Seismic performance assessment of the bridges was performed by pushover analysis and nonlinear time history analysis. Nonlinear models were created by ANSYS software. As a next step, the results of pushover analysis were compared with 11 nonlinear dynamic analyses in terms of stress distribution of structural components and maximum displacement of determined control node. It was found that capacity of the bridges was affected mostly by the arch length.

ÖZET

TAŞ KEMERLİ KÖPRÜLERİN SİSTEM TANIMLANMASI, MODEL GÜNCELLENMESİ VE SİSMİK PERFORMANSININ DEĞERLENDİRİLMESİ

378 km. uzunlunluğunda olan Samsun-Kalın demiryolu hattının modernizayson çalışmasını Türkiye Devlet Demiryolları üstlenmiştir. Bu köprülerin tarihi öneminden dolayı, bu hat üzerinde olan 41 taş kemerli köprünün korunmasına karar verilmiştir. Samsun-Kalın demiryolu hattı Kuzey Anadolu Fay Hattı'nın yakınında geçmekte ve bu durum köprülerde yüksek deprem talebine neden olmaktadır. Bu çalışmada, köprülerin deprem değerlendirmesi Sonlu Elemenlar Yöntemi kullanılarak tamamlanmıştır, fakat taş kemerli köprüler gibi olan yığma yapılar, çelik ve betonarme gibi diğer türde yapılara kıyasla malzeme özellikleri, zemin özellikleri ve modelleme kabülleri bakımından daha fazla belirsizlik içermektedir. Bu yüzden, Sonlu Elemanlar Yöntemi ile oluşturulan modellerin doğruluğunu onaylamak için dinamik tanımlama methodlarını uygulamak neredeyse kaçınılmazdır. Bu çalışmada, köprülerin dinamik özellikleri Frekans Uzayında Ayrıştırma Metodu (FUAM) kullanılarılak bulunmuştur. Köprülerin titreşim ölçümleri, köprülerin doğal halinde, köprülere etki ile yük yüklenmesi durumunda ve köprülerden tren geçişi sırasında alınmışır. Bu ölçümler sonunucunda tanımlanan yapıların modal özelliklerine bağlı olarak, köprü malzemelerinin gerçek elastisite modulüslerini ve gerçek zemin özelliklerini elde etmek için kurulan modeller güncellenmiştir. Yapıların sismik performans değerlendirilmesi statik itme analizi ve zaman tanım alanında doğrusal olmayan analiz yöntemleri kullanılarak yapılmıştır. Bu çalışma için köprü modelleri ANSYS'de kurulmuştur. Daha sonra, itme analizi ve 11 adet doğrusal olmayan dinamik analiz sonuçları yapısal elemenlardaki stres dağılımları ve kontrol noktasının göstermiş olduğu maksimum deplasman bakımından karşılaştırılmıştır. Sonuçlar, köprünün kapasitesinin daha çok kemer boyundan etkilendiğini göstermiştir.

TABLE OF CONTENTS

ACKNOWLEDGEMENTS iii
ABSTRACT iv
ÖZET v
LIST OF FIGURES viii
LIST OF TABLES xiii
LIST OF SYMBOLS xiv
LIST OF ABBREVIATIONS xvi
1. INTRODUCTION 1
1.1. Overview 1
1.2. Literature Survey 6
1.2.1. Literature Survey on Modal Updating 7
1.2.2. Literature Survey on Tests 9
1.2.3. Literature Survey on Assessment 10
1.2.4. Literature Survey on Retrofitting 12
1.3. Objective 13
1.4. Thesis Outline 14
2. INSTRUMENTATION OF MASONRY BRIDGES 16
2.1. General Description 16
2.2. Instrumentation 18
3. SYSTEM IDENTIFICATION 22
3.1. Enhanced Frequency Domain Decomposition Method (EFFD) 22
3.2. System Identification of Masonry Bridge 23
3.3. System Identification Results of Masonry Bridge 31
4. FINITE ELEMENT MODEL UPDATING 33
4.1. Methodology of FEM Updating 33
4.2. Results of FEM Updating 35
5. SEISMIC ASSESSMENT 40
5.1. Numerical Model 41
5.2. Nonlinear Static Analysis (NSA) 44

5.2.1. Modal Capacity Curve 50
5.2.2. Demand Curve 55
5.2.3. Performance Point Definition 62
5.2.4. Results 65
5.3. Nonlinear Time History Analysis (NLTHA) 67
5.3.1. Ground Motion Record Selection 67
5.3.2. Results 70
5.4. Comparison of NLSA and NLTHA 83
6. CONCLUSION 85
6.1. Summary and Results 85
6.2. Future Works 87
REFERENCES 88

LIST OF FIGURES

Figure 1.1. Structural components of masonry bridges [1] 1

Figure 1.2. Ponte Vecchio Bridge [2] 2

Figure 1.3. Pont du Gar Bridge [3] 3

Figure 1.4. Puente Trajan Bridge [4] 3

Figure 1.5. Examples of bridge from Romans in Turkey [5] 4

Figure 1.6. Examples of masonry bridge in Turkey [5] 5

Figure 1.7. Railway line map of Turkey [6] 6

Figure 2.1. Dynamically identified bridges 17

Figure 2.2. Location of the masonry arch bridge 18

Figure 2.3. Recorder and sensor 19

Figure 2.4. Sensor layout 19

Figure 2.5. Test preparation and data collection 20

Figure 2.6. LDH125 Locomotive [19] 21

Figure 2.7. Hammer impact loading test and train passing 21

Figure 3.1. Ambient vibration response of bridge mid-point transverse direction 24

Figure 3.2. Ambient vibration response of bridge mid-point vertical direction . 25

Figure 3.3. Impact response of bridge mid-point transverse direction 25

Figure 3.4. Impact response of bridge mid-point vertical direction 26

Figure 3.5. Train passage response of bridge mid-point transverse direction . . 27

Figure 3.6. Train passage response of bridge mid-point vertical direction . . . 28

Figure 3.7. Power spectral density of ambient vibration response 29

Figure 3.8. Power spectral density of impact response 29

Figure 3.9. Power spectral density of train passage response 30

Figure 3.10. Impulse response function – damping identification 30

Figure 3.11. Identified transverse mode shapes of bridge 32

Figure 3.12. Identified vertical mode shapes of bridge 32

Figure 4.1. Schema of FEM updating procedure 33

Figure 4.2. Comparison of 1st transverse mode shapes 37

Figure 4.3. Comparison of 2nd transverse mode shapes 37

Figure 4.4. Comparison of 3rd transverse mode shapes 38

Figure 4.5. Comparison of 1st vertical mode shapes 38

Figure 4.6. Comparison of 2nd vertical mode shapes 39

Figure 5.1. Location of the Structure and North Anatolian Fault [21] 40

Figure 5.2. Failure criteria of masonry according to ANSYS [22] 42

Figure 5.3. Stress strain curve for smeared crack model 42

Figure 5.4. FEM of the masonry bridge 43

Figure 5.5. Representation of control point 45

Figure 5.6. Stresses in X Direction 46

Figure 5.7. Stresses in X Direction 47

Figure 5.8. Stresses in Z Direction 48

Figure 5.9. Stresses in Z Direction 49

Figure 5.10. Pushover curve 50

Figure 5.11. Demonstration of participation factor parameters 52

Figure 5.12. Modal capacity curve 54

Figure 5.13. Bi-linearization of modal capacity curve 55

Figure 5.14. Response spectrum 57

Figure 5.15. Design spectrum 60

Figure 5.16. Design curve 61

Figure 5.17. Capacity curve and design spectrum for Case 1 63

Figure 5.18. Capacity curve and design spectrum for Case 2 64

Figure 5.19. Relationship between modal capacity curve and demand curve . . 65

Figure 5.20. Stress distribution in X direction at the performance point 66

Figure 5.21. Stress distribution in Z direction at the performance point 66

Figure 5.22. Response spectra of selected ground motions, their mean and the target spectrum 68

Figure 5.23. Stress distribution for Bingol in X direction 71

Figure 5.24. Stress distribution for Bingol in Z direction 71

Figure 5.25. Stress distribution for Kobe in X direction 72

Figure 5.26. Stress distribution for Kobe in Z direction 72

Figure 5.27. Stress distribution for Manjil in X direction 73

Figure 5.28. Stress distribution for Manjil in Z direction 73

Figure 5.29. Stress distribution for Morgan Hill in X direction 74

Figure 5.30. Stress distribution for Morgan Hill in Z direction 74

Figure 5.31. Stress distribution for Darfield in X direction 75

Figure 5.32. Stress distribution for Darfield in Z direction 75

Figure 5.33. Stress distribution for Hector Mine in X direction 76

Figure 5.34. Stress distribution for Hector Mine in Z direction 76

Figure 5.35. Stress distribution for Malatya in X direction 77

Figure 5.36. Stress distribution for Malatya in Z direction 77

Figure 5.37. Stress distribution for Kocaeli in X direction 78

Figure 5.38. Stress distribution for Kocaeli in Z direction 78

Figure 5.39. Stress distribution for Duzce in X direction 79

Figure 5.40. Stress distribution for Duzce in Z direction 79

Figure 5.41. Stress distribution for Erzurum in X direction 80

Figure 5.42. Stress distribution for Erzurum in Z direction 80

Figure 5.43. Stress distribution for Cankiri in X direction 81

Figure 5.44. Stress distribution for Cankiri in Z direction 81

LIST OF TABLES

Table 2.1. List of bridges 16

Table 3.1. Modal parameter results 31

Table 4.1. Weighting coefficients 35

Table 4.2. Comparison of modal frequencies 36

Table 4.3. Structural parameters of non-updated and updated FEMs 36

Table 5.1. Material properties 41

Table 5.2. Nonlinear behaviors of materials 43

Table 5.3. Participation factor calculation 53

Table 5.4. Values of site factor, F_{a} 58

Table 5.5. Values of site factor, F_{v} 58

Table 5.6. Design spectrum parameters 60

Table 5.7. Performance point parameters 65

Table 5.8. Properties of the selected ground motions 69

Table 5.9. Displacement results of control node for NLTHA 82

LIST OF SYMBOLS

a	Acceleration
C	Damping matrix
C_{R1}	Spectral displacement ratio for the first mode
d_1	Modal displacement demand for first mode of the structure
E	Modulus of elasticity of a material
F_{a}	Short-period site factor
F_{v}	Long-period site factor
f	Frequency
g	Gravitational acceleration
GPa	Gigapascal
G_{xx}	Power spectral density matrix of responses
G_{yy}	Power spectral density matrix of inputs
H	Frequency response function
h	Weightening coefficient for MAC value
Hz	Heartz
K	Stiffness matrix
k	Weightening coefficient for modal frequency
kN	Kilonewton
M	Mass matrix
m_{i}	Lumped mass of i-th point
M_{x1}	Effective mass defined for the first mode of vibration in transverse direction
MPa	Megapascal
R_{y1}	strength reduction factor for the first mode
S_1	horizontal response spectral acceleration coefficient at 1.0 second period on rock
S_{a}	Elastic spectral acceleration
S_{d}	Linear elastic spectral displacement

S_{S}	Horizontal response spectral acceleration coefficient at 0.2 second period on rock
T	Natural period of the structure
T_0	Reference period used to define spectral shape
T_1	Fundamental model period of the structure
T_{L}	Initial period at which constant displacement region starts
T_{S}	Corner period at which spectrum changes from being independent of period to being inversely proportional to period
u_{xN1}	Modal displacement demand for first mode of the structure
V_{x1}	Base shear of the bridge after pushover analysis
α	Rayleigh damping mass coefficient
β	Rayleigh damping stiffness coefficient
ζ	Modal damping ratio
ω	Natural frequnecy
Γ_{x1}	Participation factor defined for the first mode of vibration in the transverse direction
Φ_{xN1}	Amplitude of the first mode shape at the control point of masonry bridge defined for the first mode of vibration in the transverse direction
Φ_{xi1}	Normalized modal displacement for the first fundamental model

LIST OF ABBREVIATIONS

ARMA	Autoregressive Moving Average
DLH	Technical earthquake Regulation Concerning Construction of Coastal and Port Structures, Railroads, Airports by the Ministry of Transport, Maritime and Communication
EFDD	Enhanced Frequency Domain Decomposition
FEM	Finite Element Model
FDD	Frequency Domain Decomposition
MAC	Modal Assurance Criteria
MDOF	Multi Degree of Freedom System
NAF	North Anatolian Fault
NAFZ	North Anatolian Fault Zone
NLTH	Nonlinear Time History
NLTHA	Nonlinear Time History Analysis
NLS	Nonlinear Static
NLSA	Nonlinear Static Analysis
PEER	Pacific Earthquake Engineering Research
PGA	Peak Ground Acceleration
PSD	Power Spectral Density
SDOF	Single Degree of Freedom System
SID	System Identification
SRSS	Square Root of Sum of Squares
SSI	Stochastic Subspace Identification

1. INTRODUCTION

1.1. Overview

Old masonry and stone arch bridges reflect historical heritage of the societies of which cultural history and background are very old. Masonry bridges were constructed all around the world for the transportation, mountain roads, and agriculture and watercourse purposes. The reasons of preference of masonry bridges are ease of natural stones, simple design calculations and construction speed. Masonry bridges mainly consists of series of stone blocks, mortar which connects the stone blocks each other and fill material which provides effective structural integrity and uniform live load distribution due to vehicles. Stone which is the fundamental structural element of masonry bridges is obtained from quarries nearest the construction site, so the properties of stones are changed from one region to another. Mortar is other significant component of these types of structures. It provides structural integrity by connecting stone block and helps the load transfer between them. The types of mortar such as lime and pozzolanic mortar are changed according to purpose and location of structure. However, mortar is the weakest material in structure generally, especially in tension. Fill which is obtained from nature creates dead load on the arches and prevents the tension stresses on the arches of the bridge. The structural components of masonry bridges are showed Figure 1.1.

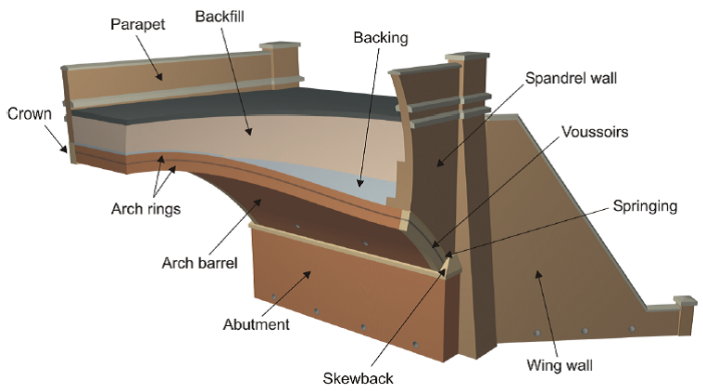

Figure 1.1. Structural components of masonry bridges [1]

First designer and builder of masonry bridges are Romans in the world. Masonry bridges which were constructed by Romans reach form Mesopotamia to Europe. Most of them are in Italy, France, and Spain. The most known masonry bridges from the Romans are Ponte Vecchio Bridge in Italy, Pont du Gard Bridge in France and Puente Trajan Bridge in Spain.

Ponte Vecchio Bridge in Florence which connects two sides of Arno River is stone arch bridge. The bridge consists of three consecutive arches. The main arch has a span of 30 meters the two side arches each span 27 meters. The deck width of bridge is 32 meter. Also, this bridge witnessed important political events and was subject to many mysterious stories. Figure 1.2 represents the Ponte Vecchio Bridge.



Figure 1.2. Ponte Vecchio Bridge [2]

Pont du Gar Bridge which crosses the Gardon River is the highest of all elevated Roman aqueducts and is preserved form UNESCO. This bridge is the most significant part of waterway for the water supply of Roman city, Nimes. The bridge which is showed in Figure 1.3 has a capacity to carry 200 000 m3 water daily. The bridge limestone arch bridge and consist of 47 spans. The total height and width of bridge are 48.8 meter and 6.4 meter.



Figure 1.3. Pont du Gar Bridge [3]

Puente Trajan Bridge which crosses Tagus River is Roman stone arch bridge. Construction years of the bridge is known as 104 AD and 106 AD. The bridge has six arches and the longest span of the bridge is 28.8 meter. The total length and width of the bridge are 181.7 meter and 8.6 meter. The bridge is one of the impressive masonry bridges when thinking its height. Its height is 45 meter. Roman Emperor Trajan who is the builder of the bridges printed on the bridge 'I built a bridge that would last forever. It has been in good shape until this time.'



Figure 1.4. Puente Trajan Bridge [4]

Many masonry bridges from Romans can be seen in Turkey. The best knowns of them are Severan (Cendere) and Taşköprü Bridges (Figure 1.5). Former is known as the oldest bridge in Turkey. Latter was one of the oldest bridges in the world open to motorized vehicles until its closure in 2007.

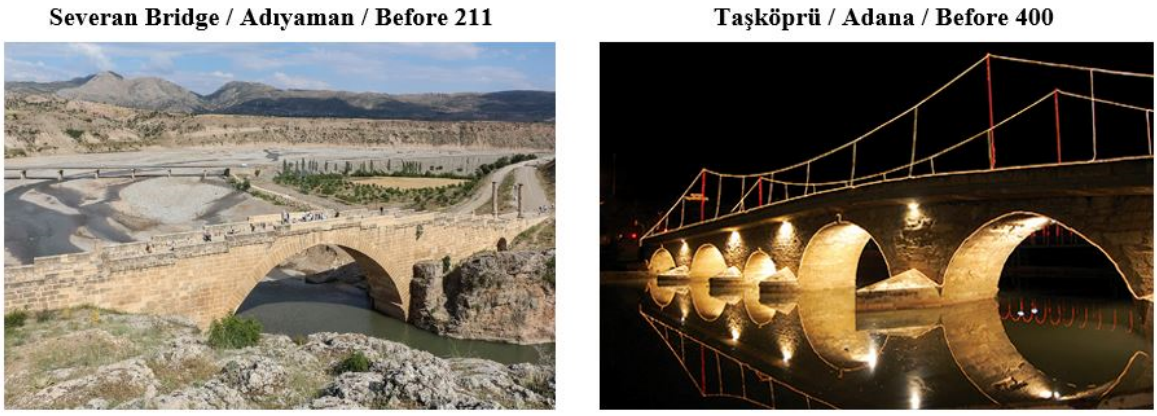

Figure 1.5. Examples of bridge from Romans in Turkey [5]

On the other hand, there are a lot of masonry bridges from Seljuk and Ottoman Empire in Turkey. Especially, Architect Great Sinan designed and constructed many masonry bridges in Ottoman times. Figure 1.6 represents the significant masonry bridges and their construction time in Turkey.

Construction of masonry bridges increased in the recent times of Ottoman Empire and first times of republic. At that times, government of Turkey increased industrial and mining investments in order to pursue industrial revolution. Therefore, the railway installation was necessary in order to carry products to different regions. For this purpose, government agreed French and English companies for railway construction. Railway lines were constructed in seven regions of Turkey. In these railway lines, masonry bridges were preferred in order to cross rivers and valley due to ease of access to materials, simple design calculations and construction speed. Figure 1.7 represents the railway network of Turkey and railway lengths according to intersection cities.

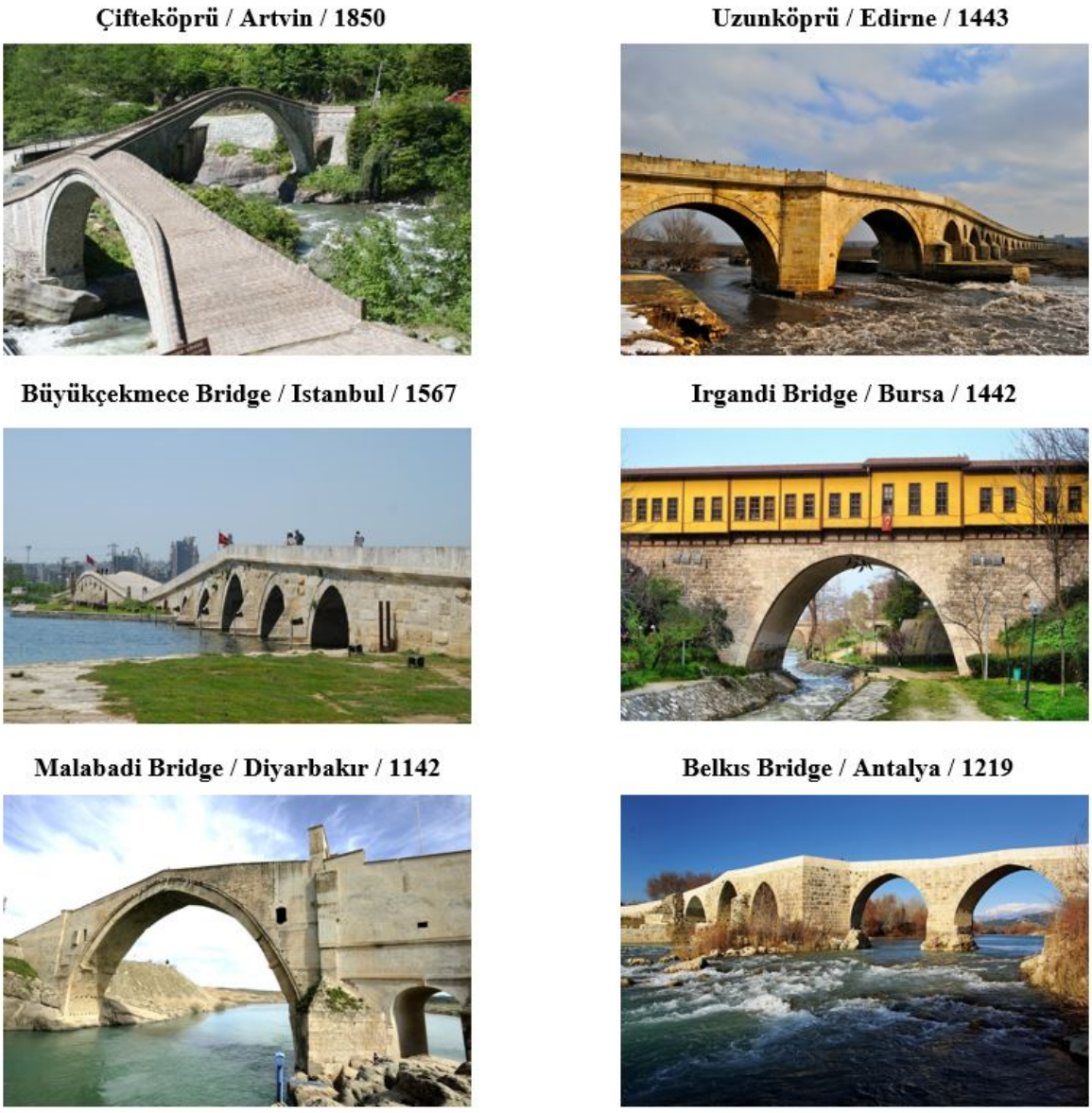

Figure 1.6. Examples of masonry bridge in Turkey [5]

It is a fact that the number of masonry arch railway bridges is estimated around 200 000 in Europe which represents approximately 50% of the total railway bridge stock [13]. It is significant task for engineers to assess and take measurements in the case of requirement in order to protect history when thinking their survival time.

In recent years, Turkish government separated significant amount of money for modernization and restoration of these railway lines. Firstly, modernization of Samsun – Kalin railway line was started with grant of European Union. In the scope of project, the condition of masonry bridges are assessed and railway line was designed again for high speed train passing. It a fact that masonry bridges are strong structures when considering their years of standing. However, durability of these structures may decreased and significant damages and deformation may be created due to seismic action, vehicle loads and humidity. Therefore, assessment and retrofitting of these type of structures are important task in order to protect our architectural heritage when considering the high seismic risk of Turkey.



City	Length (km)
Sivas	570
Afyon	387
İzmir	331
Ankara	310
Konya	298
Elazığ	288
Balıkesir	280
Kütahya	274
Manisa	264
Gaziantep	254

Figure 1.7. Railway line map of Turkey [6]

1.2. Literature Survey

Masonry bridges were preferred in past periods to facilitate daily life due to their construction advantage such as using simple materials, tools and design calculations. Masonry bridges plays important role on the transportation network because they were generally constructed to integrate railways and roads. The durability and maintenance

of the masonry bridges are crucial issues because collapse of masonry bridges would led to abruption of traffic flow, economic loss, in worst case, loss of human lives. However, they were exposed to some damages during their long service time, mainly, due to vehicle loads, earthquake, wind and humidity. The main purposes of the structural and earthquake engineers are to determine behavior of the bridge under the effects of such damages and also take necessary measures in order to prevent collapse of structure. Thanks to the recent technological and technical advances, the current situation of masonry bridges can be evaluated properly. Therefore, the assessment of masonry bridges is very valuable and widespread subject in the recent decades to preserve their magnificent architectural beauty and structural integrity against the external effects. Many notable studies were conducted related to model updating, assessment, and retrofitting of masonry bridges.

1.2.1. Literature Survey on Modal Updating

In order to clearly define the structural characterization of 89.3m long a stone arch bridge, Aoki *et al.* [7] carried out a series of dynamic, non-destructive and destructive tests were carried in visual inspections, material tests on stones and mortar, inspection of inner cavities with radar and fiberscope, and inspections of submerged foundation by camera were the non-destructive and destructive tests. Dynamic properties of the bridge were conducted during micro-tremors and traffic excitations. In the initial FEM, identified young's modulus of the stone and mortar were used whereas the young's modulus of the fill material was assumed as 1/10th of the one of mortar. The boundary conditions were assumed to be fixed at two piers and both abutments. The inverse Eigen - Sensitivity method was utilized for modal updating procedure. This procedure consisted two steps. In the first step, the bridge was divided into 24 subsections and as a result of the updating procedure, the stiffness of the three arch stones was increased whereas the stiffness of the two piers was reduced. At the second step, the bridge was divided into 83 macro elements for a more sensitive updating procedure. The results of the last step demonstrated the following outcomes; the stiffness of the all macro elements at the arch stones was increased to simulate the increased arch thickness that was not considered in the FE model, the stiffness of the macro elements at the

abutments and spandrels near the abutments was reduced probably due to the effect of the boundary condition. The stiffness of the macro elements at other spandrels was increased to simulate the possible behavior of the concrete slab under asphalt because they were not considered in the FEM. The stiffness of the macro elements at the piers, especially pier P1, was reduced probably due to the effect of bridge-soil interaction. The stiffness of the macro elements at the spandrels near pier P2 was reduced probably due to the effect of cracks.

Altunisik *et al.* [8] presented a modal updating study of Mikron historical bridge, located on Firtina River in Rize, Turkey. EFFD and SSI methods were adopted with the aim of identifying the modal properties of the bridge. Excitations from humans and wind were adequate for the identification. The modal shapes obtained from the 3-D FEM and identification were similar whereas some discrepancy was observed between the simulated and identified modal frequencies. Updating of the model resulted in the minimization of the differences between analytical and experimental natural frequencies. The FEM consisted of three different materials for the different structural elements such as the arch, the sideways, and the filler material. Because of the fact that the identification of the properties of historical structures' materials is difficult, material properties were adopted from the previous studies. The intact analytical model assumes all freedoms for the bridge abutments and sidewalls to be fixed at boundaries. During the updating procedure, material properties remained and the boundary conditions were changed. For this purpose, the assumptions were that the stiffness of the sidewalls increased by time because of piling of the earth and stone and the region's ground motions in all directions are fixed.

Banerji and Chikermane [9] carried out modal updating of masonry arch bridge based on the site response data. For FEM updating, the novel algorithm was created in order to optimize multi structural parameters. The algorithm decides most critical structural parameters and converges these variables using sensitivity analysis in order to minimize the difference between numerical model results and experimental recorded data. The comparison of updated FEM result and site data showed good agreement except the results at the abutment springing point due to noise effect. After FEM

updating, the condition of the bridge was assessed according to increased loading standards. The results showed that all the response quantities assessed in this study are within the safe limits.

Costa *et al.* [10] carried out modal updating of three masonry arch bridges based on the modal parameters obtained from operational modal analysis. 2 of those 3 bridges are very old whereas the other one has been constructed recently by considering historical arch bridge characteristics. The material properties of the initial FEM's consisted of the properties obtained from the experimental tests on material samples taken from the bridges, or by assigning properties representative of the experimental tests of previous studies. Detailed micro models were adopted in FEM's, taking mortar and fill-spandrel wall joints into account. Even though large amount of material properties was obtained through laboratory tests, there were still some differences between the analytical and identified modal properties. Therefore, at the final step, the numeric models were tuned by adjusting the material properties in order to simulate defects or including soil conditions in order to represent soil-structure interaction.

1.2.2. Literature Survey on Tests

Fanning *et al.* [11] studied the performance 3-D modelling of three masonry arch bridges by comparing the loading test results with the results determined from the FEM's. The properties of masonry and fill were selected based on the material properties sorted in a previous study by considering the current structural condition of the bridges. The current structural conditions of the bridges were determined by visual inspection. The consistency of the test results with the ones acquired from the simulations indicated that a reasonable set of assumptions that were applied to the construction of an accurate nonlinear 3-D model of a masonry bridge can lead to good results. One important outcome of the study is that the transverse bending may induce cracking in the arch barrel which can alter the response of the bridge.

Orban and Gutermann [12] examined the effectiveness of inspection and testing methods for masonry arch bridges. For this purpose, non-destructive tests (NDTs) such as georadar, conductivity measurements were applied to the masonry arch bridge in order to define clearly geometrical properties of the structure and understand properly the current condition of bridge. Moreover, monitoring systems were installed on the masonry arch bridge to detect damage such as cracks and deformations. In order to identify mechanical properties of the bridge (modulus of elasticity, stress-strain relationship), modified flat-jack which is new minor-destructive test approach was applied on the masonry arch bridge. The test results show that uncertain geometrical properties and unclear physical properties were detected by NDTs. Also, the new minor-destructive test approach can be used to define mechanical properties of the masonry arch bridges.

Domede *et al.* [13] carried out in- situ investigations, laboratory tests and a multi-step calculation based on an orthotropic damage model considering crack reclose possibilities. First of all, the homogenized behavior of masonry was numerically modelled for a representative volume of masonry block based on the experimentally obtained compressive and tensile parameters of stones and mortar. Then, in order to include the current condition of the bridge (several cracks exist on the structure), differential settlement, which resulted in the same actual cracks, were applied to one of the piles in the numerical model. Along this line, the train load was applied. This load was continued to be increased until the collapse of the bridge. The safety margin was fond to be very high, which indicates safety of the studied bridge.

1.2.3. Literature Survey on Assessment

Pela *et al.* [14] investigated the seismic performance of two masonry arch bridges, a stone masonry bridge with brick-made vaults and a stone masonry bridge with concrete made vaults. The analysis was performed by making use of a simplified inelastic procedure. The structural capacity, which was obtained through pushover analysis, was compared with the demand of the earthquake ground motion described by an inelastic response spectrum. The importance of the choice of control node was examined

by selecting the control node from the top of the bridges, their mass centers and energy equivalent displacement. Even though the selection of the energy equivalent displacement gives the most accurate results because of the fact that it produces results on the safe side and representative of the bridge's deformed shape near the collapse, a good choice is the center of mass of the bridge, which is very near to the energy equivalent results but has a clearer geometrical interpretation and requires less computational effort. The analysis results demonstrated that the safety factors of the examined bridges are high for the whole range of the masonry material properties that bounded the actual ones. In the study, core tests allowed the determination of the characteristics of stones and mortar. Dynamic ambient vibration surveys resulted in the tuning of the elastic modulus, unit weight and poison's ratios of the masonry materials in bridges. In particular, the secant young's moduli were set equal to the one half of the determined dynamic ones in the analysis. Because of the fact that it was not possible to obtain large test specimen, several values of compressive and tensile strength of the masonry were selected based on experience of authors and analyses were conducted within those limits.

Pela *et al.* [15] investigated the seismic assessment of triple – arched bridge with brick-made vaults. First of all, the performance of nonlinear static analysis (NSA) was assessed with 84 nonlinear dynamic analysis (NDAs). For this goal, earthquake records which were selected attentively in order to represent seismic properties of the site were scaled according to Eurocode 8 spectra for ground accelerations of 0.15g, 0.30g, and 0.45g. Nonlinear analyses show that performance points of NSA were conservative than the mean of the maximum results obtained from NDAs for all control nodes. After that, the importance of the choice of control node was examined with probabilistic analysis in order to understand clearly its effect on seismic capacity of bridge. The probability analysis show that the possibility that any NDA maximum displacement exceeds the NSA performance point is lower when center of mass displacement is used. The result shows that the selection of center of mass node for NSA gives reliable results.

Zampieri *et al.* [16] examined seismic performance of two different structural configurations of multi – span masonry arch bridges: a three span and a five span

masonry arch bridge. Pushover analysis results showed that the pier base reach its maximum capacity and cracks were created, so the structure was involved in a collapse mechanism. However, shear stresses were lower than the strength of structure at pier base. Moreover, analysis result show that increasing arch length and pier slenderness ratio increased the probability of creation collapse mechanism due to bending failure. On the other hand the probability of shear failure occurrence is small for low piers' slenderness.

1.2.4. Literature Survey on Retrofitting

Tecchio *et al.* [17] investigated the effectiveness of static and seismic strengthening methods on the three masonry arch bridges. In order to increase the load bearing capacity of bridges, many traditional rehabilitation techniques such as adding new layer of brick to old arches was used. Moreover, many innovative repair techniques such as CFRP application were applied to bridges in order to increase seismic capacity. Linear and nonlinear static analysis results show that traditional and innovative strengthening methods increase the seismic resistance of bridges and related seismic demands were satisfied.

Behnamfar and Afshari [18] examined seismic resistance of the three masonry arch bridges which are modelled using the distinct element method with nonlinear dynamic analysis. The seismic resistance of the bridges were assessed considering the transverse displacement of mid-span node of the arch and normal stress distribution of the arch under different earthquake records. The nonlinear dynamic analysis results of the bridges showed that the brittle behavior which is undesirable situation for seismic performance of structures were observed and failure occurred along the arch due to tension instability of sections. Therefore, the arches of the masonry bridges were strengthening in order to prevent collapse. For this purpose, tensile resistance and cohesion between arch stones were increased. The analysis results after retrofitting showed that strengthening method increased seismic resistance of the bridges so that the failure PGA is increased approximately 70%.

1.3. Objective

FEM's of structures involves assumptions due to the uncertainties in structural parameters. Particularly, masonry structures may exhibit even higher uncertainties compared to concrete or steel structures because of the foundation conditions and material properties of masonry. Consequently, establishing realistic FEM's which represent the dynamic properties of these structures accurately is a very difficult task for engineers. Therefore, seismic performance assessment of masonry structures based on computer models has been still a major concern.

In order to minimize the uncertainties and establishing more refined FEM's, carrying out dynamic identification tests becomes almost unavoidable because of the fact that dynamic identification is the only way to validate the "global behavior" of structures.

In this study, dynamic tests of 12 bridges located on Samsun-Kalin railway were carried out. These bridges were selected among 41 historical bridges on the railway route and they form a representative group of all the bridges in terms of masonry type, height, total length, span number and span length. The objective of dynamic tests was to identify the dynamic properties of the bridges and consequently to update the FEM's for more reliable seismic performance assessments. Vibration data from the bridges were collected during ambient conditions, train passage and hammer impact loading. A fine FEMs of the masonry bridges were created based on drawings and site measurements. In many studies, creating FEM's are superficial and the changing of material properties are not accurate because the effect of uncertainness to overall stiffness of bridges are ignored in FEM updating procedure. However in this study, the FEM's of the bridges were updated based on the identified modal parameters such as modal frequencies, mode shapes and damping ratios considering not only material properties but also soil stiffness. That is, the material properties and soil springs were chosen as the updating parameters. The soil and material tests results provided valuable information about the ranges of the updating parameters. To illustrate the importance of modal updating of historical arch bridges, seismic performance assessment of bridges

were carried out with the updated FEM's because the non-updated models consisted of the material and soil properties which were chosen according to the values available in literature and no friction between fill and masonry structure. In addition, a code based spectrums were utilized for seismic assessment of the updated models. As a result, more realistic models associated with code-based spectrum were obtained. It is a fact that dynamic tests as well as material and soil tests of a large number of historical arch bridges, which were built in similar years and on a railway route, uniquely contributes to the understanding the dynamic behaviors of such bridges. Moreover, updating of FEM's by considering identified dynamic behaviors of the bridges and generation of code based spectrums for a representative group of bridges located on a railway route plays an essential role in enhancing the seismic performance evaluation of the railway bridges.

After obtaining FEM's of the bridges and code based spectrums for each bridge separately, pushover analyses were chosen for the assessment due to its simplicity in computation time compared to NLTH analysis. After that, 11 nonlinear dynamic analyses were conducted in order to compare pushover analyses and nonlinear time history analyses. As a conclusion, very similar results were obtained from pushover analyses and nonlinear time history analyses in terms of displacements of control point and stress distribution of masonry structure and the results showed that capacity of the bridges was affected mostly by the arch length. Structural deficiencies were observed on spandrel wall for bridges with wider arches and higher seismic demand.

1.4. Thesis Outline

The layout of the thesis chapters is organized according to order of steps of the project. First chapter is an only introduction part. The short information about masonry bridges and literature survey on FEM of masonry bridges, model updating procedures of FEM, structural identification techniques, assessment and strengthening methods of masonry bridges, the objective of study and scope of work are presented. In second chapter, location and physical properties of evaluated bridges are given. Moreover, the instrumentation configuration and equipment used for structural identification

are presented.

In chapter three, brief information is given about system identification method used in order to obtain modal frequencies, mode shapes and modal damping. Furthermore, modal frequencies, mode shapes and modal damping results obtained from vibration measurements collected under ambient conditions, impact loading and train passage are presented.

In forth chapter, creation and improvement process of FEM are explained. The fundamental purpose of finite element model updating procedure and the importance of structural parameter selection for this procedure are explained in detail. The differences between updated and non-updated model are compared in terms of modal parameters such as modal frequencies and mode shapes and the reasons of these differences are discussed.

In chapter five, creation of nonlinear FEM in ANSYS is described. The information about material properties and nonlinear material model used for FEM are described briefly. Also, target spectrum for the bridge is created according to characteristics of location and local guide line. Moreover, the procedure of nonlinear static analysis (pushover analysis) is explained. The ultimate point and performance point of bridge are obtained. Also, the displacement of control point and stress distribution of masonry structure are given for ultimate point and performance point. Moreover, ground motion selection procedure, based on created target spectrum, for non-linear time history analysis are explained in chapter five. The nonlinear time history analysis results are given in terms of control point displacement and stress distribution in this chapter. Furthermore, the nonlinear static analysis and nonlinear dynamic analysis results are compared by considering maximum displacement of control point and critical stresses on masonry structure.

In the end of study, a brief summary and basic conclusion are presented in chapter six.

2. INSTRUMENTATION OF MASONRY BRIDGES

2.1. General Description

The existing rail transport infrastructure between Samsun and Kalin consists of bridges, culverts and tunnels located within a mountainous region. The region from Black Sea to Central Anatolia is characterized by steep gradients with restrictive horizontal curves. The construction of the line was completed in 1932 and the section between Samsun and Amasya was subject to an essential rehabilitation in 2008. The railway from Samsun to Kalin has a length of approximately 370 kilometers and there are totally 78 bridges throughout the line. Assessing their heritage value, architectural qualities and structural conditions, 41 of the existing bridges are registered as historical and need to be assessed and preserved by effective structural strengthening in the case of requirement.

Table 2.1. List of bridges

ID	Km	Span (m)	Total Length (m)	Height (m)
4	20+533	3x5	15	13.40
5	21+689	6+2x10+2x6	38	17.40
6	21+875	6+2x10+2x6	38	12.30
13	30+153	3x8	24	13.30
14	30+363	6+2x10	26	11.00
18	31+819	3x8	24	10.50
20	33+361	3x8	24	7.60
22	34+962	3x8	24	6.50
23	35+562	3x8+4	28	8.70
28	124+444	6+3x10+6	42	12.50
29	215+540	3+3x5+3	21	3.90
41	360+292	4x10	40	9.75

As the first step, bridges were grouped in terms of their number of spans, longest span, total length, height and structural condition based on the information given to us. Afterwards, one representative bridge was chosen for each group for the validation study of its FEM. Table 2.1 shows the list of selected bridges and Figure 2.1 shows their location on the railway.

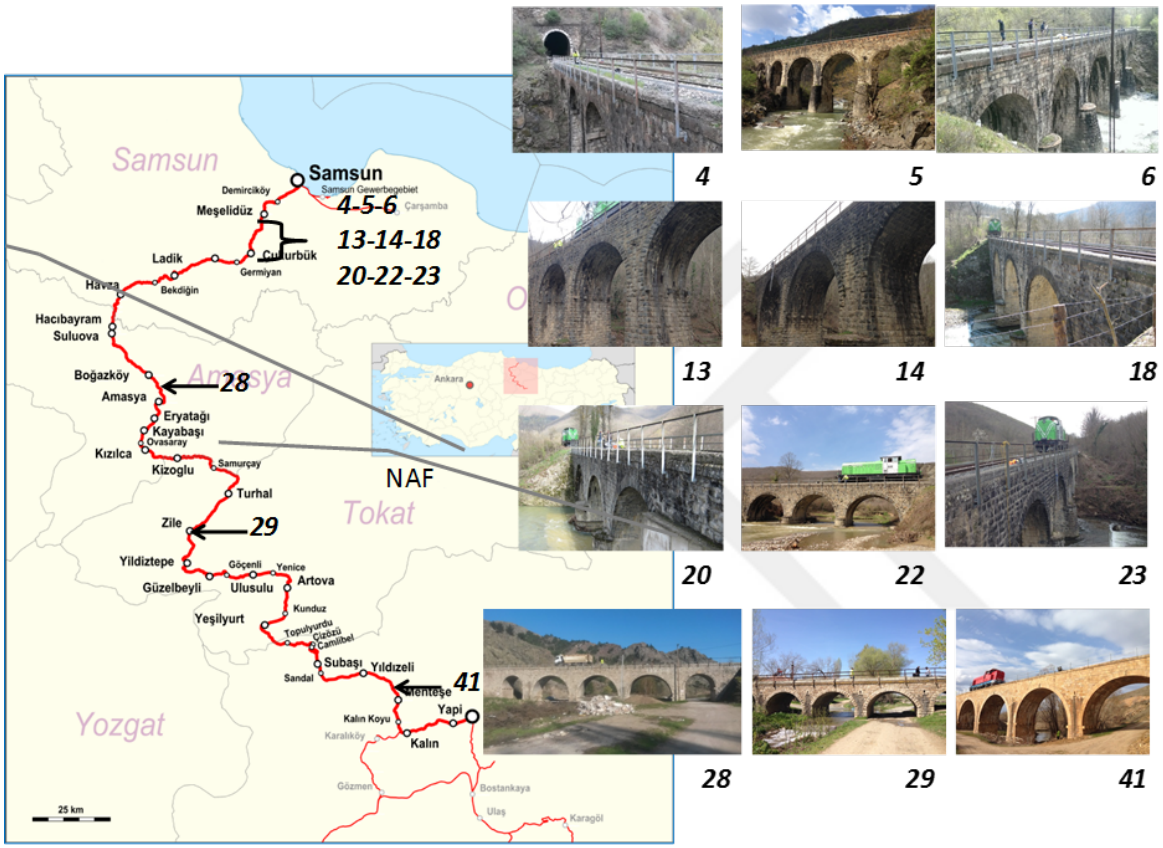

Figure 2.1. Dynamically identified bridges

Material properties of the bridges changes from one location to another. Dark grey non-porous stone is used on the structures nearer to Samsun, gradually towards Sivas buff / beige colored, more porous type of stone is observed. On few structures dark red and pink colored stone is also used. Also, lime and pozzolanic mortar were generally used for bridge constructions.

In the rest of the paper, just one of the bridges (Bridge 6) is focused to represent the dynamic test, FEM updating, pushover analysis results, and nonlinear time history analysis results. This bridge is located at 21.875 km. of Samsun – Kalin railway line.

The construction date of the bridge is believed to be 1926. The coordinates of the bridge which were obtained from GPS on the site are 41.17N, 36.21E. Figure 2.2 represents the location of the stone arch bridge.

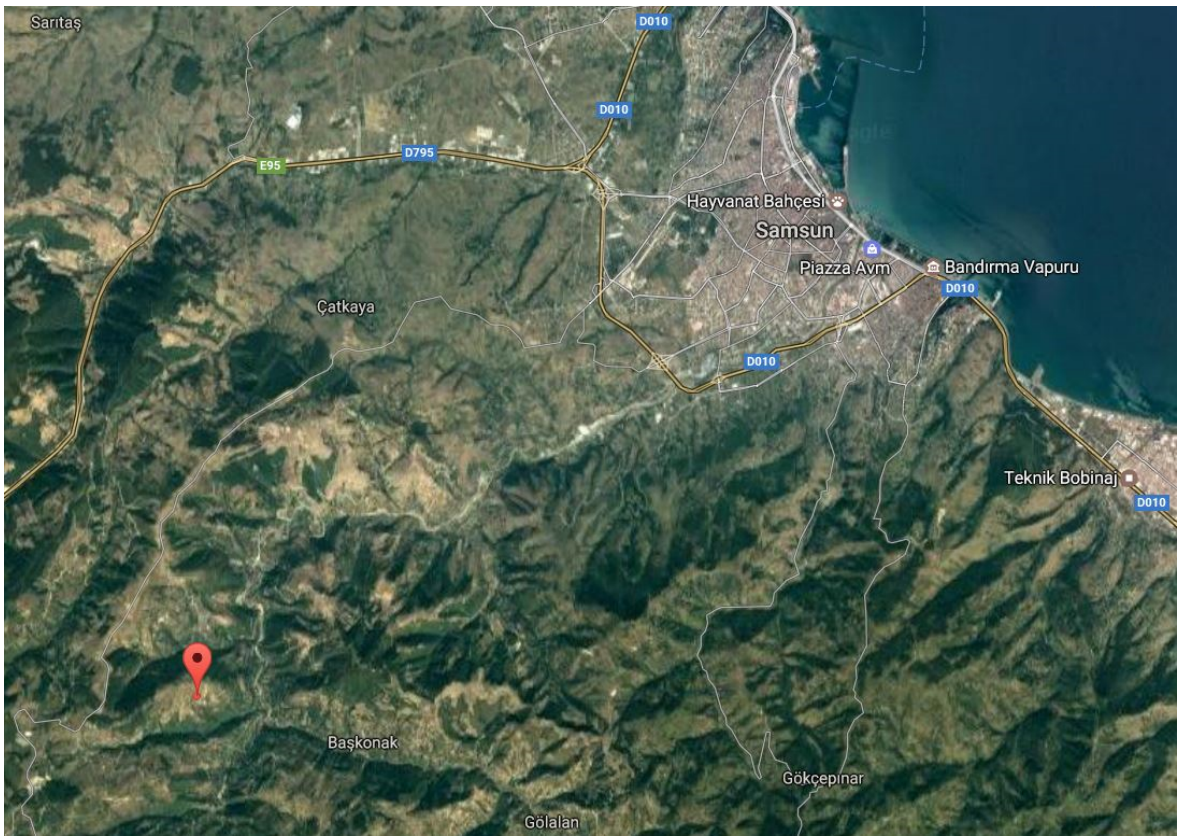

Figure 2.2. Location of the masonry arch bridge

2.2. Instrumentation

Dynamic tests were carried out by Kinemetrics made 24 bit A/D recorder and Forced Balanced Accelerometers (Figure 2.3). These devices are regarded as one of the most precise data recorders and sensors in structural engineering community. It is important to use such devices especially during the collection of ambient vibration data for which signal/noise is very low.

20 acceleration sensors were utilized for the vibration survey of the bridge. 5 acceleration sensors were used in transverse direction at mid-span of arches. 14 acceleration sensors were placed at the mid-span of arches and piers in vertical direction. Furthermore, 1 accelerations sensor is used in longitudinal direction at mid-span of 3rd



Figure 2.3. Recorder and sensor

arch. Figure 2.4 represents the configuration of accelerometers on bridge.

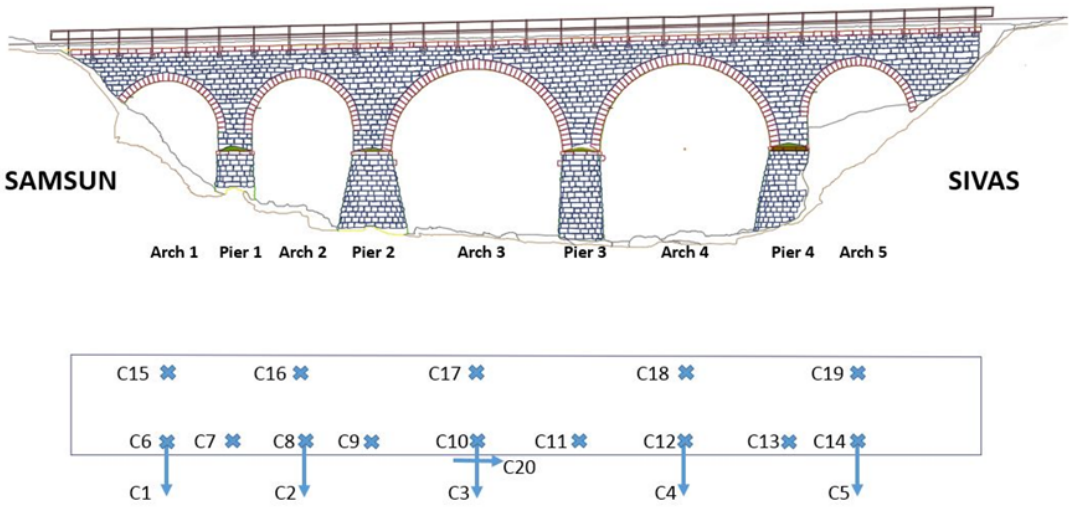

Figure 2.4. Sensor layout

Because of the fact that masonry structures have lower vibration amplitudes compared to the concrete and steel structures, vibration records under train passage and hammer impact loading were also collected. Processing the higher amplitude vibration data allowed to identify the vibration modes which couldn't been identified under ambient vibrations. Therefore, it was seen in this study that conducting load tests and train passing that cause higher amplitude vibrations than the one of ambient vibrations might be crucial in system identification of historical arch bridges. Figure 2.5 represents test preparation, data acquisition setup and data collection.



Figure 2.5. Test preparation and data collection

For hammer tests, simple hammer was used. The model of the locomotive using for train passing was LDH125 (Figure 2.6). The weight of the locomotive was 70 tons during experiments. The locomotive passed on bridge with 2 x 20 km/h, 2 x 40 km/h, and 2 x 60 km/h, respectively. Moreover, mid-point of the locomotive was the center of gravity. Figure 2.7 shows hammer impact loading test and train passing.

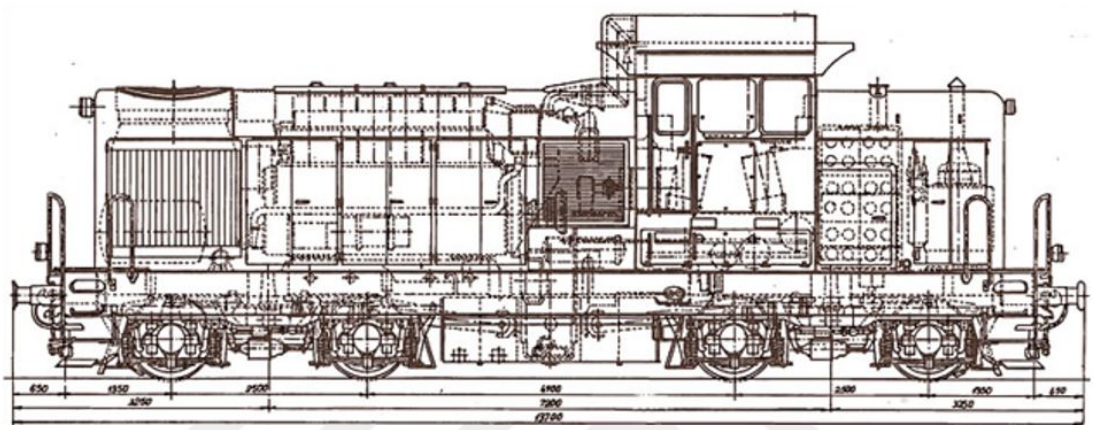

Figure 2.6. LDH125 Locomotive [19]



Figure 2.7. Hammer impact loading test and train passing

3. SYSTEM IDENTIFICATION

Dynamic identification is the only way to validate the "global behavior" of structures. Modal frequencies, mode shapes and damping ratios can be obtained properly from vibration measurements thanks to dynamic identification methods. In this project, the system identification of bridges were carried out with Enhanced Frequency Domain Decomposition (EFFD) method by Brincker *et al.* [20].

3.1. Enhanced Frequency Domain Decomposition Method (EFFD)

In this study, Enhanced Frequency Domain Decomposition (EFDD) method by Brincker *et al.*, (2001) is used to perform system identification. This method is very common and popular output – only modal identification technique nowadays. The main advantages of this technique are to detect the close modes and to estimate modal damping ratios without needed input data. In this method, the relationship between unknown input and measured response is described in the Equation 3.1.

$$G_{yy}(\omega) = \overline{H}(\omega).G_{xx}(\omega).H^{T}(\omega) \tag{3.1}$$

where;

$G_{yy}(\omega)$: (m x m) power spectral density (PSD) matrix of the inputs

$G_{xx}(\omega)$: (n x n) power spectral density (PSD) matrix of the responses

$H(\omega)$: (n x m) frequency response function matrix

In the equation, m represents the number of input, n denotes the number of response. Also, overbar and superscript T indicates the complex conjugate and transpose, respectively.

This method supposes that input is white noise such that power spectral density of input is constant matrix, i.e. $G_{xx}(\omega) = \mathrm{C}$. Also, $G_{yy}(\omega)$ is established by creating cross-correlated relation between the responses of each two sensors for each frequency. Finally, modal decomposition of power spectral density matrix of the responses is obtained by applying some mathematical theorems and manipulations. In order to estimate modal parameters, spectral density matrix of responses is decomposed at each frequency by using singular value decomposition method as described following equation.

$$[G_{yy}(\omega)] = [V].[S].[V^H] \tag{3.2}$$

where;

$[S]$: singular value diagonal matrix

$[V]$: orthogonal matrix of diagonal vectors

First elements of $[S]$ matrix for each frequency establish the acceleration response of the structure which is represented by PSD vs. Frequency graph and the peaks on this graph indicates modal frequencies of the structure. Also, first elements of $[V]$ matrix for each frequency creates mode shapes of the structure at peak points of acceleration response. This method is capable of identifying close modes because of the fact that the singular value decomposition method gives results in frequency domain.

3.2. System Identification of Masonry Bridge

In this project, vibration measurements which are carried out under ambient condition, hammer impact loading and train passage (free vibration of the bridge after train passage were analyzed) were used for dynamic identification. Modal parameters such as modal frequencies, shapes and damping ratios were identified from these vibration measurement records. Modal parameters are obtained by converting the recorded

vibration data from time domain to frequency domain thanks to EFDD.

It is the fact that, the amplitude of the excitations levels are different for these three cases. Excitations levels of hammer impact loading and train passing are higher than excitation level of ambient condition. Identification under the train passage and hammer impact loading were very beneficial because of the fact that the vibration modes, which could not been identified under ambient conditions, were successfully identified under these loadings. Damping ratios were obtained based on train passage as it gives the highest level of excitation. Hammer impact loading test records were used for dynamic identification when no clear results were obtained from ambient vibration response data for certain modes.

Figure 3.1 and Figure 3.2 show the ambient vibration responses of the bridge mid-point transverse and vertical directions. Figure 3.3 and Figure 3.4 demonstrate the impact response of the bridge mid-point transverse direction and vertical direction while Figure 3.5 and Figure 3.6 show the train passage response of the bridge mid-point transverse direction and vertical direction.

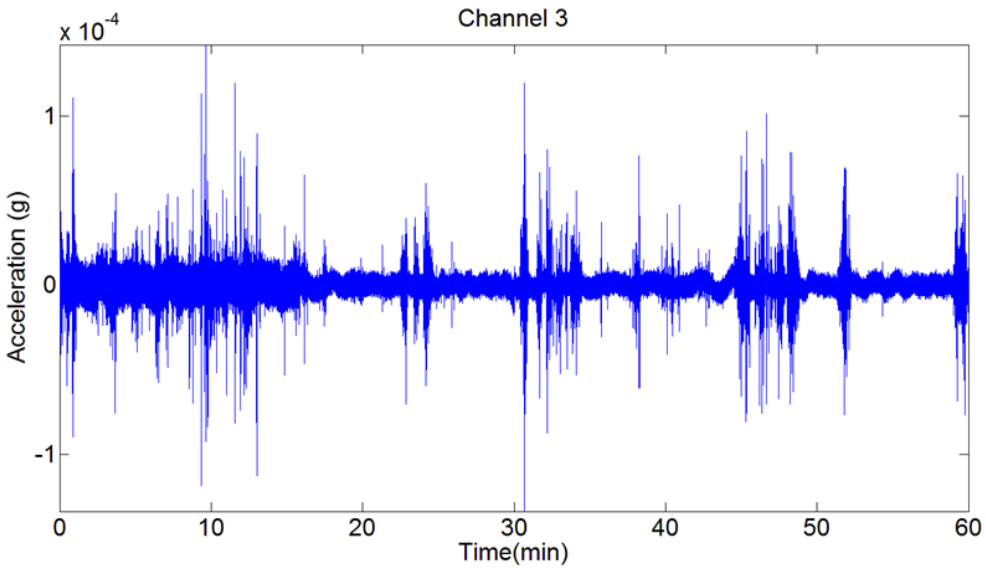

Figure 3.1. Ambient vibration response of bridge mid-point transverse direction

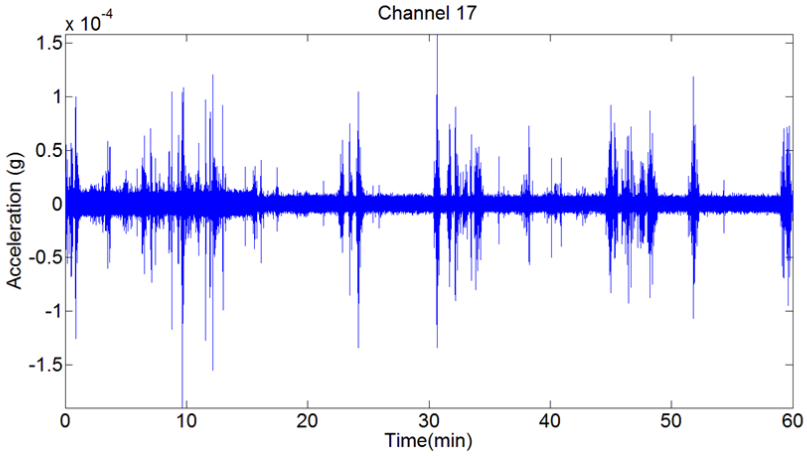

Figure 3.2. Ambient vibration response of bridge mid-point vertical direction

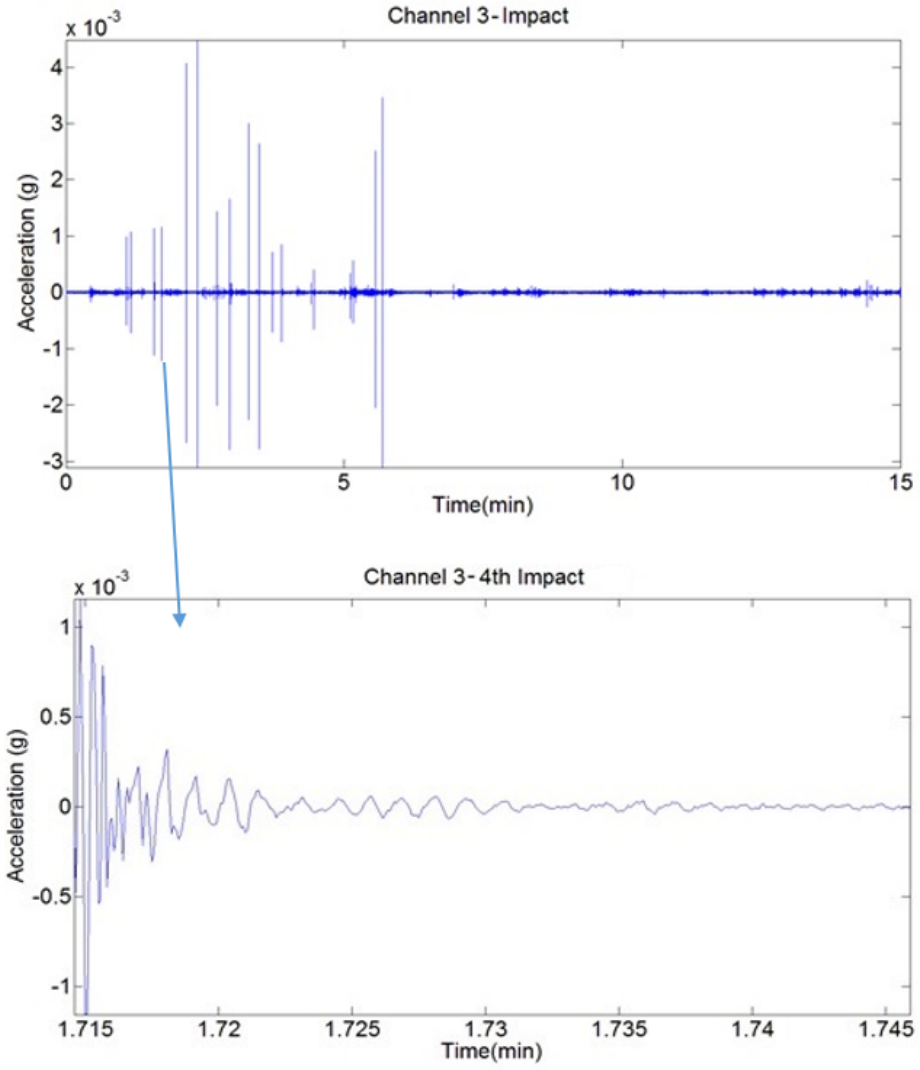

Figure 3.3. Impact response of bridge mid-point transverse direction

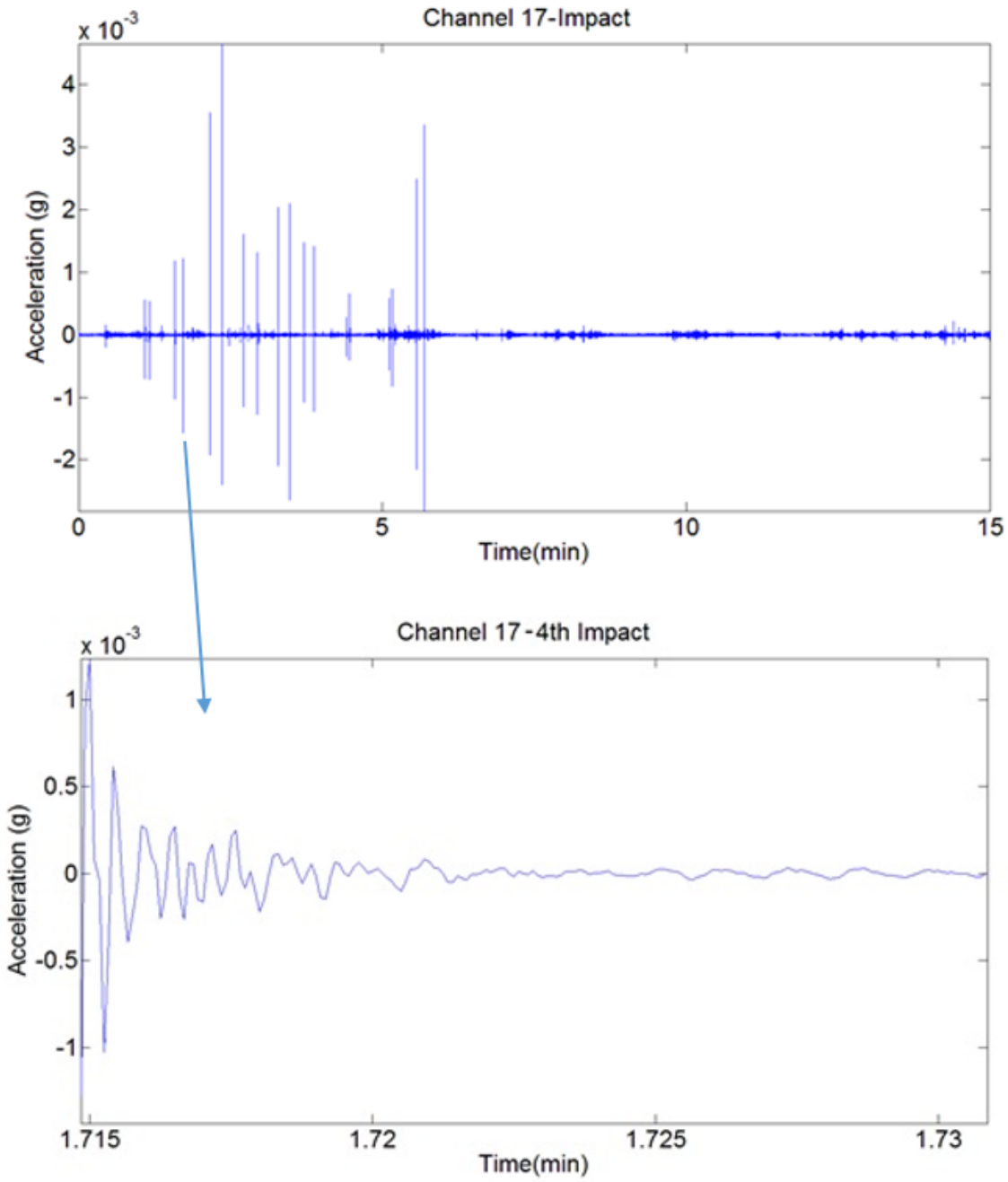

Figure 3.4. Impact response of bridge mid-point vertical direction

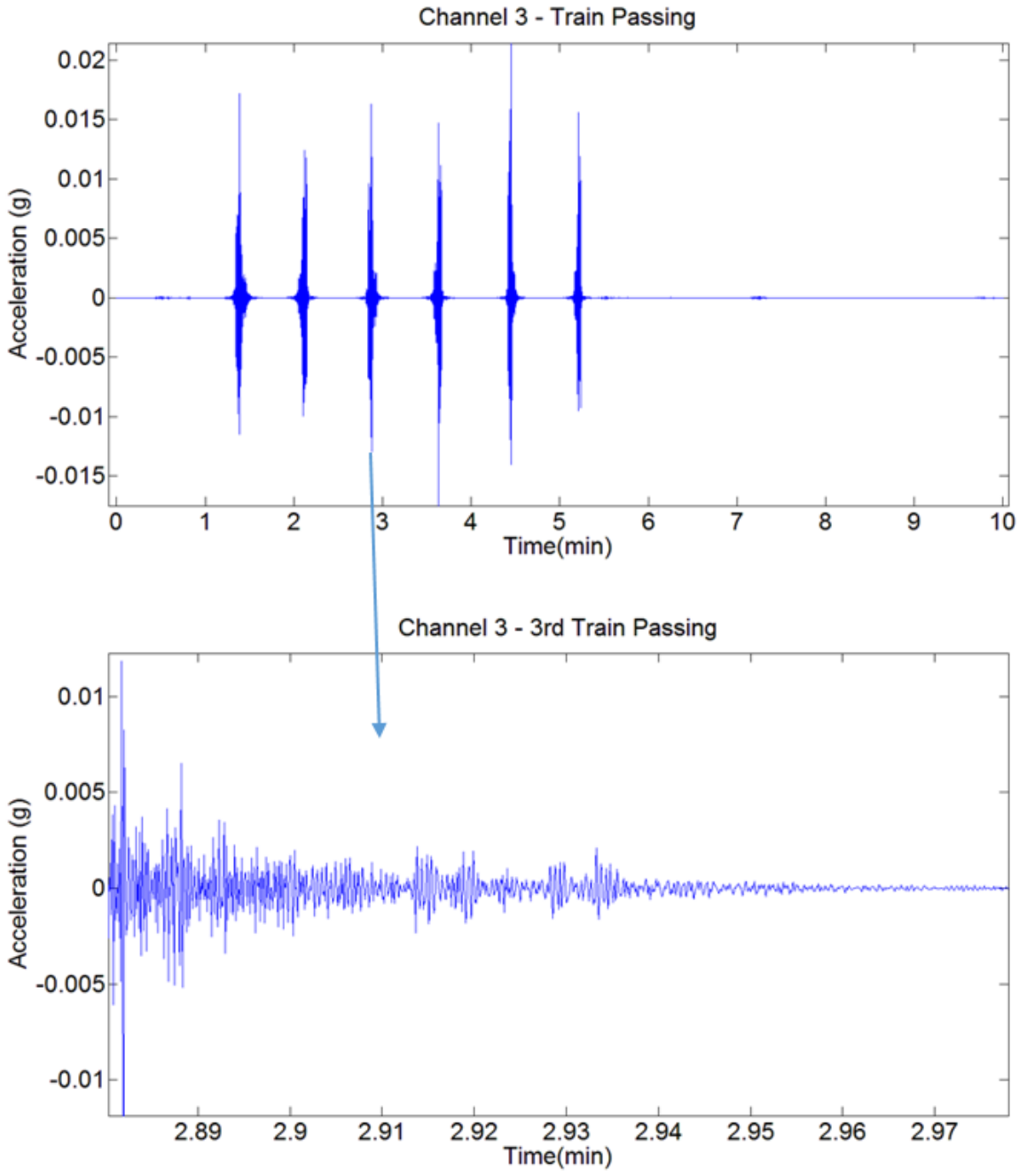

Figure 3.5. Train passage response of bridge mid-point transverse direction

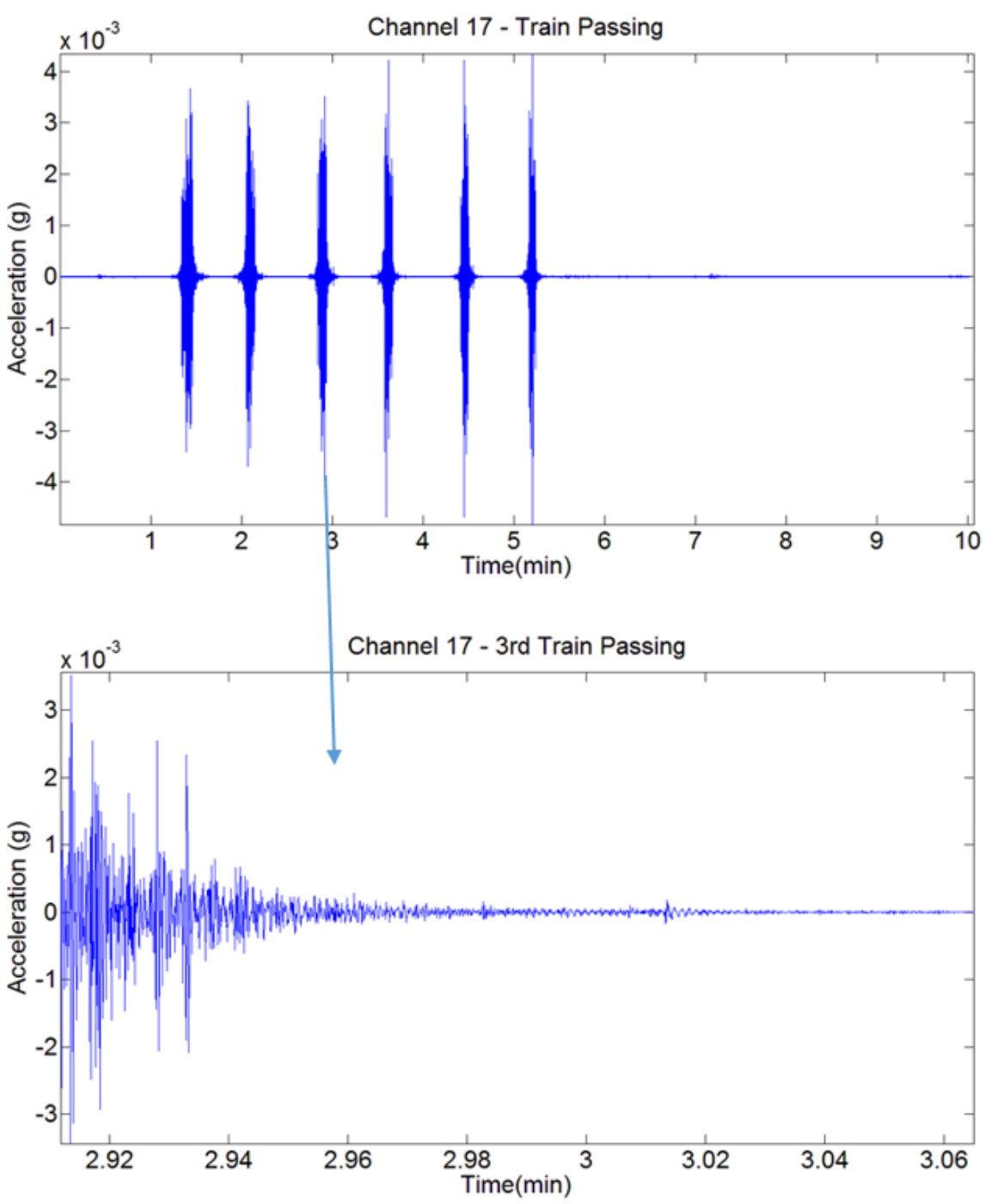

Figure 3.6. Train passage response of bridge mid-point vertical direction

Figure 3.7, 3.8 and 3.9 depict the cross-power spectra density under ambient vibrations, train passage and impact loadings. The peaks of PSD vs. frequency graphs show the natural frequencies of the bridge.

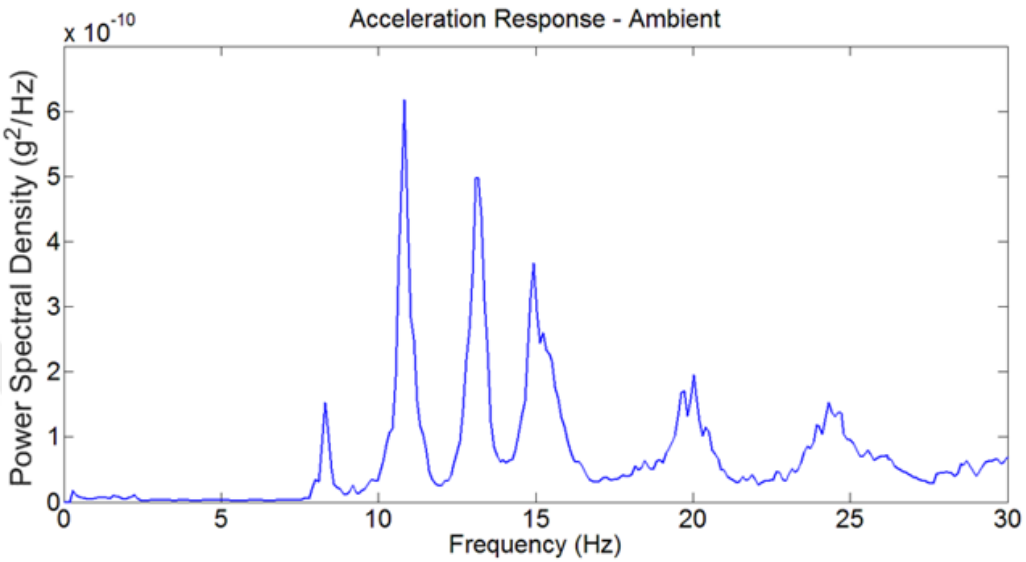

Figure 3.7. Power spectral density of ambient vibration response

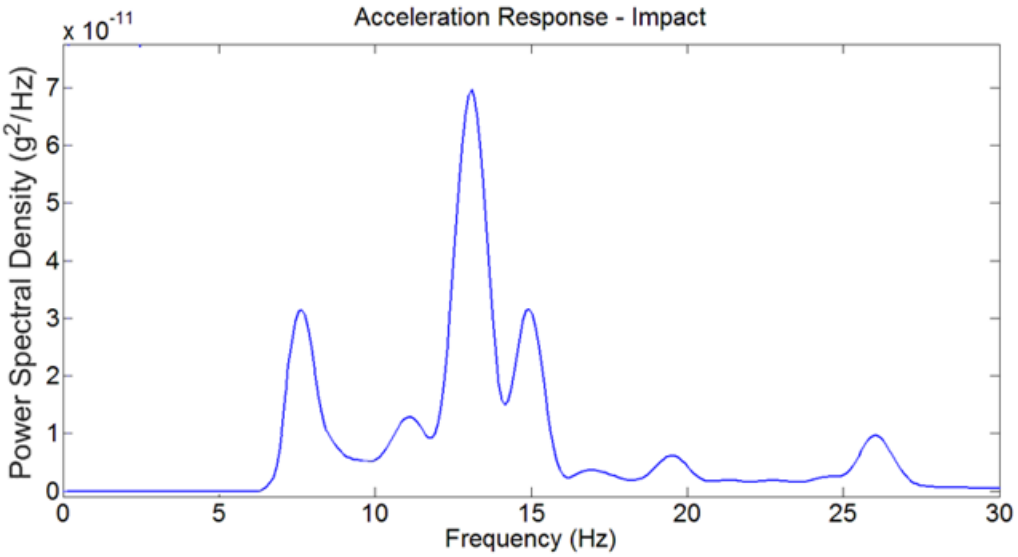

Figure 3.8. Power spectral density of impact response

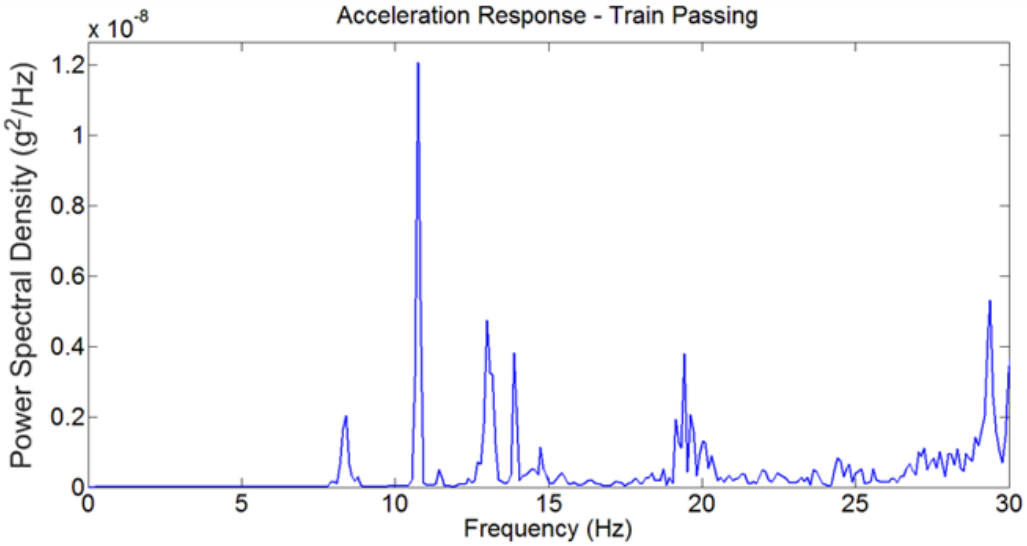

Figure 3.9. Power spectral density of train passage response

It is a well-known fact that the damping ratios of structure tend to increase as the vibration amplitude increase. Therefore, as the higher vibration amplitudes were adopted in the identification, the identified damping ratio gets closer to the damping ratio under a seismic event. In this study, damping ratios of vibration modes were determined from vibrations under train passage loadings because highest vibrations amplitudes were generated under this type of loading. Figure 3.10 illustrates the impulse response function of the 1st mode of the bridge. This function was generated by transforming the response of 1st mode in frequency domain to time domain. The exponential decay of this function gives the damping ratio.

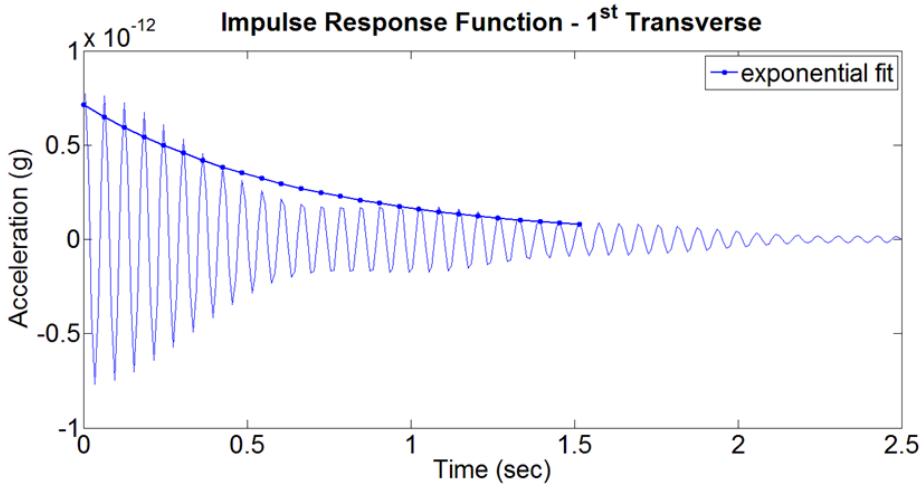

Figure 3.10. Impulse response function – damping identification

3.3. System Identification Results of Masonry Bridge

Modal frequencies and mode shapes were identified from vibration measurement records under ambient conditions. On the other hand, damping ratios were obtained from vibration data under train passing due to its high excitation level. For this bridge, recorded data under hammer impact loading is just used for to check identification results due to fact that vibration data under ambient condition is clear and gives rational results.

The identified frequencies and damping ratios of the first 3 transverse, first 2 vertical and first longitudinal modes of the bridge are presented in Table 3.1. The sum of mass participation ratios of these modes are 69%. Therefore, considering these modes was considered adequate in the identification procedure.

Table 3.1. Modal parameter results

Mode	**Shapes**	**Frequency (Hz)**	**Damping (%)**
1	1st Transverse	8.31	1.40
2	2nd Transverse	10.84	1.97
3	3rd Transverse	13.18	2.04
4	1st Longitudinal	14.94	2.83
5	1st Vertical	20.02	2.89
6	2nd Vertical	24.32	4.82

The identified mode shapes of the first 3 transverse and first 2 vertical modes of the bridge are presented in Figure 3.11 and Figure 3.12, respectively.

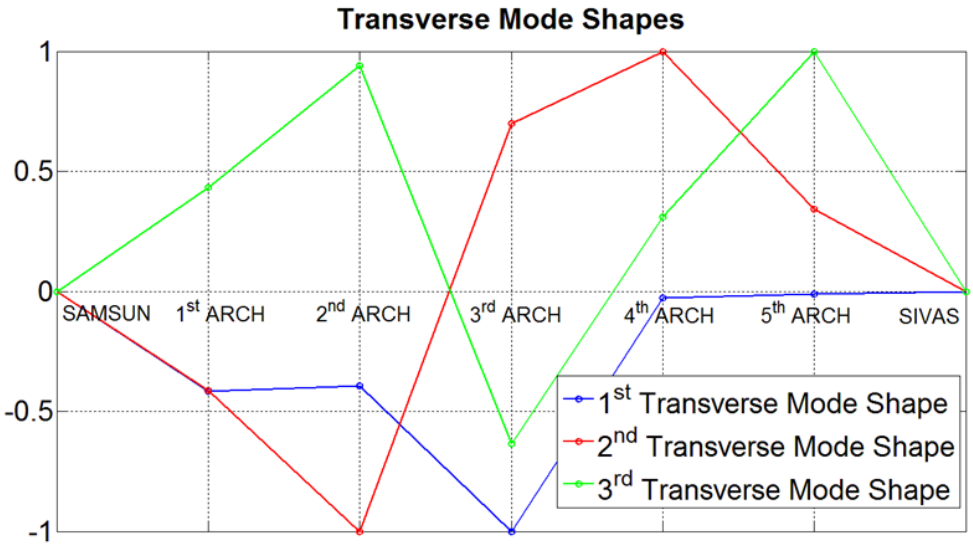

Figure 3.11. Identified transverse mode shapes of bridge

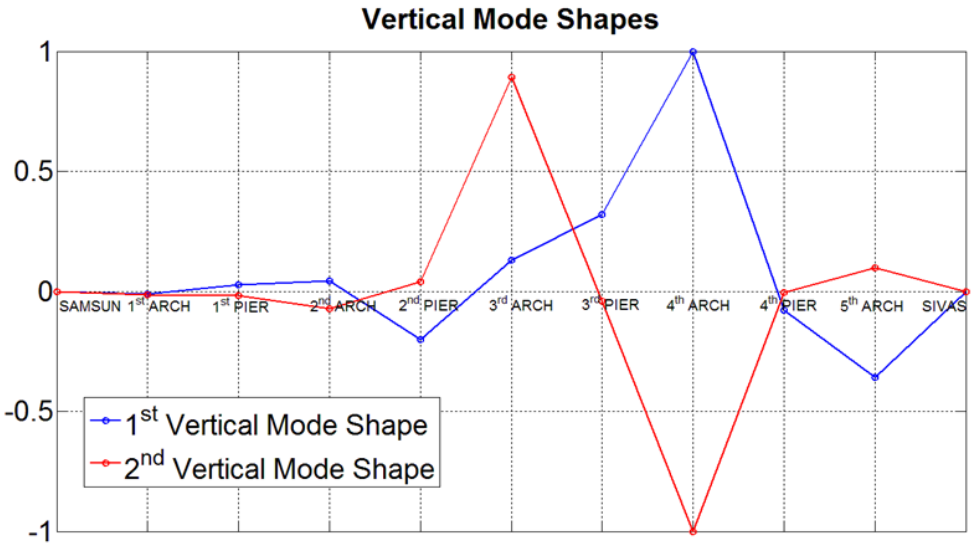

Figure 3.12. Identified vertical mode shapes of bridge

4. FINITE ELEMENT MODEL UPDATING

4.1. Methodology of FEM Updating

In order to minimize the differences between experimental and analytical modal values, FEM updating is performed. For the purpose of updating the FEM's, a Matlab code, which automatically creates FEM's by changing the values of the chosen structural parameters within pre-determined limits, was utilized. As a next step, an error function compared the MAC values and frequencies of the structural modes of each created FEM with the ones of identified one. At the last step, the FEM, which gave the minimum error between the modal parameters of generated FEM's and identified modal parameters were chosen as the final updated model. Figure 4.1 represents the procedure of FEM updating briefly.

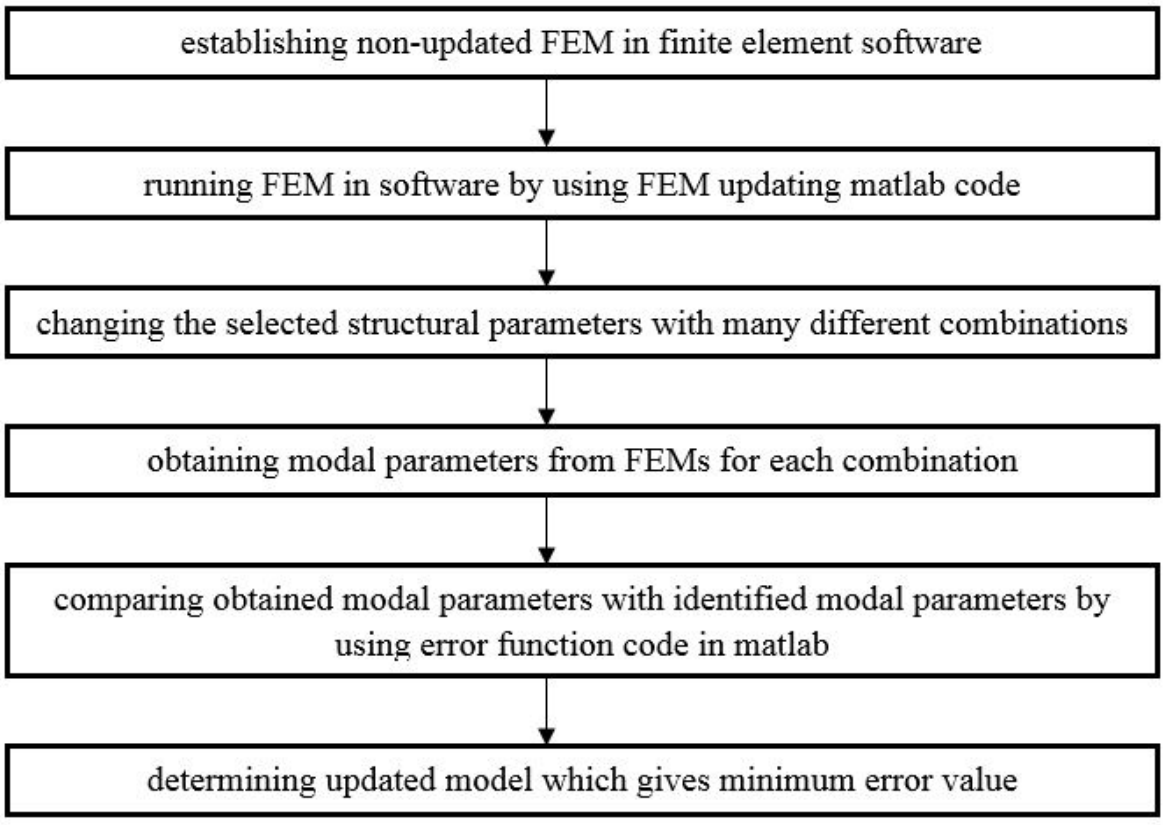

Figure 4.1. Schema of FEM updating procedure

The objective function which is utilized in order to quantify the error between the analytical and the experimental results is indicated in Equation 4.1.

$$E(\alpha) = \sum (k_i.[(f_i^* - f_i)/f_i^*]^2 + h_i.[1 - MAC_i]^2) \tag{4.1}$$

where;

α : stiffness correction coefficient

i : mode number;

k_i : the weighting coefficient for i^{th} modal frequency

h_i : the weighting coefficient for i^{th} modal assurance criteria

f_i^* : the measured modal frequency of ith mode

f_i : the simulated modal frequency of ith mode

MAC_i : the modal assurance criteria for i^{th} mode shape

The formulation of Modal Assurance Criteria (MAC) is used to indicate the level of similarity between the simulated and measured mode shapes by comparing them with the following equation.

$$MAC = \frac{|\psi_*^T.\psi|^2}{(\psi_*^T.\psi_*).(\psi^T.\psi)}. \tag{4.2}$$

where;

ψ: the measured mode shape of the corresponding mode

ψ^* : the simulated mode shape of the corresponding mode

The value of MAC changes between 0 and 1 based on Equation 4.2. Approaching of MAC value to 1 shows that measured and simulated mode shapes are quite similar.

Weighting coefficients were determined by considering contribution of different modes for error function because analysis results show that more than one mode have higher effect on the dynamic behavior of the masonry bridge. Decoupling of modes in linear analysis point outs that the first three transverse modes and first two vertical modes produce large portion of seismic force. Therefore, the first three transverse modes and first two vertical modes are adequate to be considered in updating procedure. The weighting coefficients are chosen according to the modal participation factors of corresponding modes.

Table 4.1. Weighting coefficients

Mode Shapes	**Weighting Coefficients**
1st Transverse	0.45
2nd Transverse	0.15
3rd Transverse	0.05
1st Vertical	0.20
2nd Vertical	0.15

4.2. Results of FEM Updating

For FEM updating procedure, initial FEM of the bridge was established SAP2000 structural engineering software considering drawing and site investigation reports. For the initial FEM, Young's modulus of the bridge materials and soil spring constants are used 7.80 GPa and 75000 kN/m respectively for non-updated model. These values are chosen according to literature. Optimal modal parameters which are Young's modulus of the bridge materials and soil spring constants were obtained from FEM updating to minimize the difference between identified and analytical modal values. Table 4.2 represents the comparison of modal frequencies obtained from non-updated FEM and

updated FEM with identified modal ones. On the other hand, the differences of updated structural parameters for non-updated FEM and updated FEM is depicted in Table4.3.

Table 4.2. Comparison of modal frequencies

Mode Shapes	**Non-updated Frequency (Hz)**	**Updated Frequency (Hz)**	**Identified Frequency (Hz)**
1st Transverse	3.28	7.40	8.31
2nd Transverse	5.79	10.84	10.84
3rd Transverse	9.29	15.33	13.18
1st Vertical	12.95	23.38	20.02
2nd Vertical	13.80	25.64	24.32

Table 4.3. Structural parameters of non-updated and updated FEMs

Parameter	**Non-updated Model**	**Updated Model**
Material Modulus of Elasticity (GPa)	7.80	14.05
Vertical Spring Coefficient (kN/m)	75 000	Fixed
Horizontal Spring Coefficient (kN/m)	37 500	Fixed

Comparison of the transverse and vertical mode shapes obtained from system identification, the non-updated FEM and the updated FEM are demonstrated in below figures.

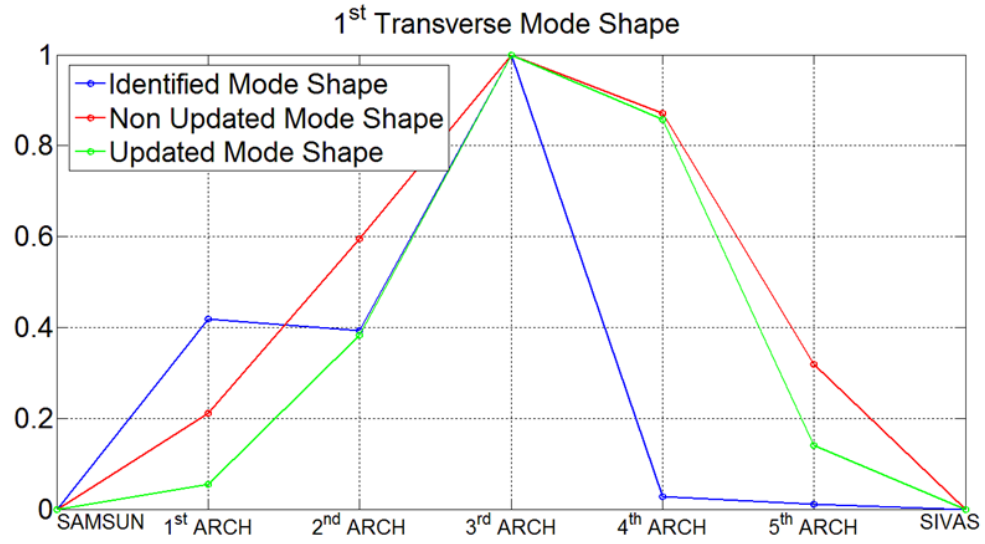

Figure 4.2. Comparison of 1st transverse mode shapes

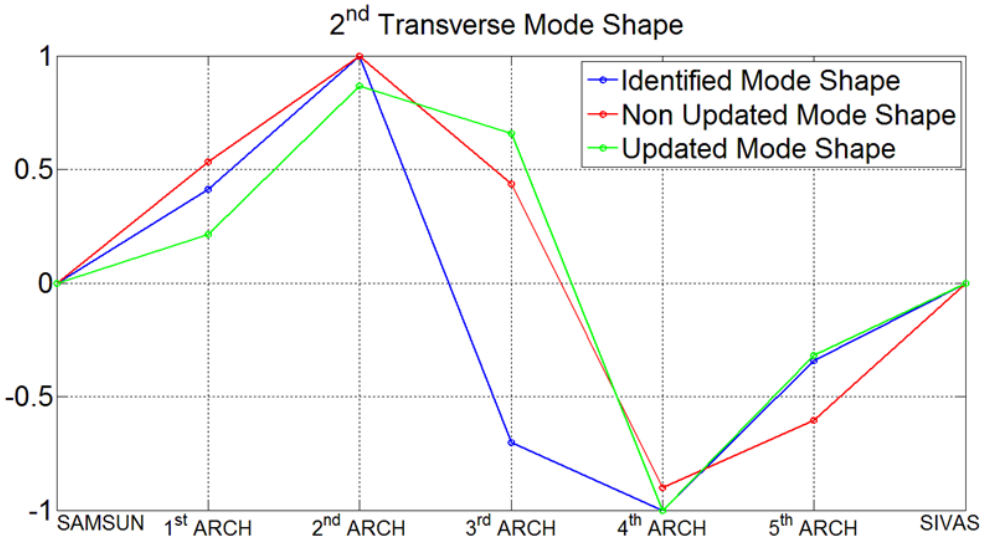

Figure 4.3. Comparison of 2nd transverse mode shapes

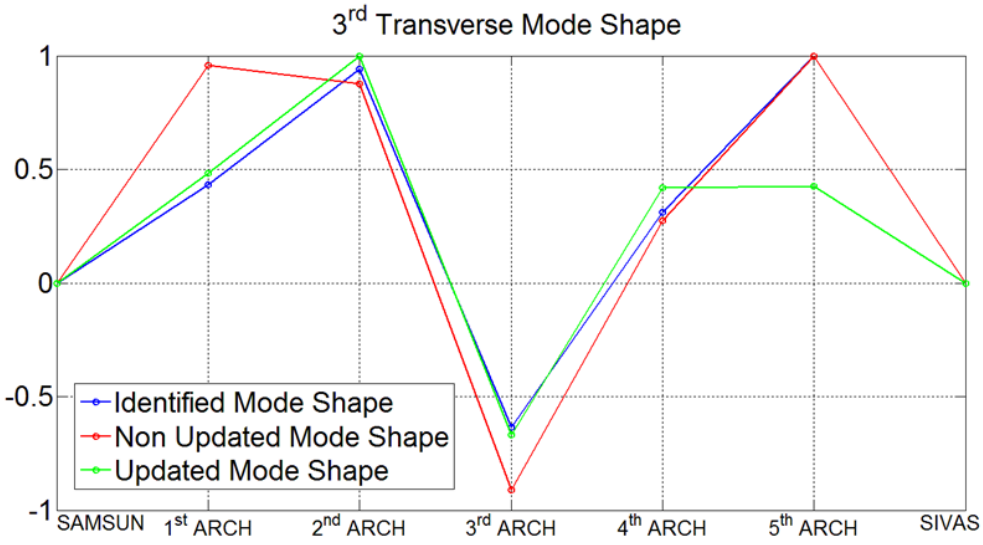

Figure 4.4. Comparison of 3rd transverse mode shapes

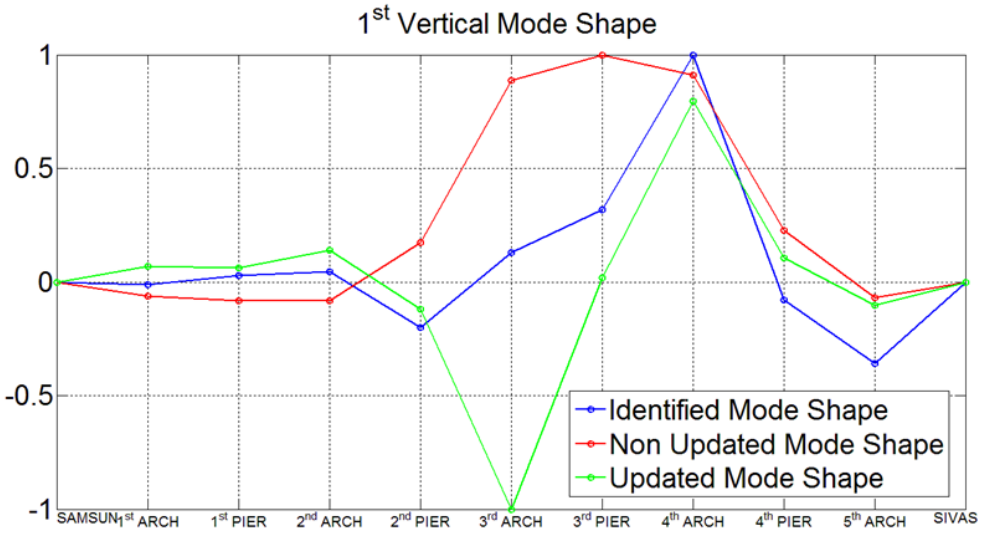

Figure 4.5. Comparison of 1st vertical mode shapes

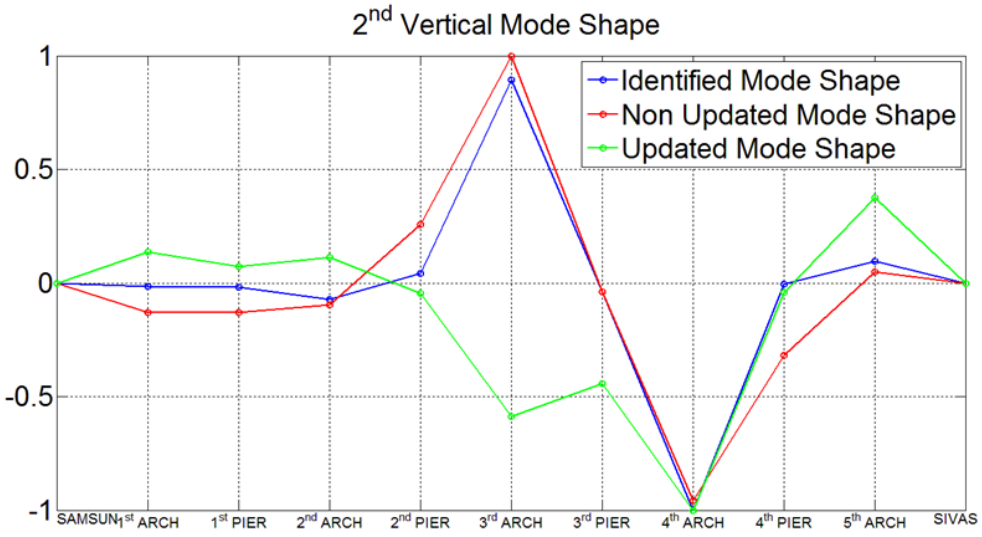

Figure 4.6. Comparison of 2nd vertical mode shapes

5. SEISMIC ASSESSMENT

Seismic performance of the bridge is essential issue by considering the location of the bridge such that North Anatolian Fault passes very close to the structure. For this reason, the probability of taking damage of the bridge is high during seismic actions. Therefore, performing seismic analyses is inevitable in order to define current situation of the bridge and to take measurements if they are necessary. Figure 5.1 represents the location of bridge and Black Sea region segment of North Anatolian Fault.



Figure 5.1. Location of the Structure and North Anatolian Fault [21]

The ability of linear analysis is limited, when comparing to nonlinear dynamic analysis, to obtain structural response to external effects such as earthquake loads where expected level of nonlinearity is high. For this project, the nonlinearity level of the masonry bridge is high due to material properties of structural component and soil properties, so the nonlinear analyses are inevitable and common way to assess this type of structures.

5.1. Numerical Model

For nonlinear analyses, the FEM of the bridge is established ANSYS engineering software according to drawing and site investigations. For FEM of the masonry bridge, homogenized model was considered because this modelling method is very effective way to define the mechanical behavior of composite material without considering any damage and deformation in macro modelling approach. Homogenized model is used in order to represent mechanical parameters of a masonry representative volume mainly consists of mortar and stone in this study. Physical properties of masonry structures, fill and soil are represented according to material test reports and FEM updating results in Table 5.1.

Table 5.1. Material properties

	Density (kN/m^3)	**Elastic Modulus (GPa)**	**Poisson's Ratio**	**Compressive Strength (MPa)**	**Tensile Strength (MPa)**
Masonry	25.40	14.05	0.25	56.50	0.80
Backing	20.00	14.05	0.25	56.50	0.80
Fill	20.00	14.05	0.25	56.50	0.80
Soil	20.00	30.00	0.25	10.00	0.10

For nonlinear analyses, nonlinear element type option of masonry structure for FEM of the bridge in ANSYS is limited. The most suitable and effective nonlinear element type for masonry components such as arches, spandrel walls and piers is smeared crack model. This model is eight–noded isoparametric solid element and called as Solid 65 in ANSYS. This solid element model has an ability to capture cracking in tension and crushing in compression of structural components. This solid element model predicts and changes stress – strain relationships of components in the case of cracking and crushing. That is, this solid element model assumes that a plane of weakness exists in the normal direction of crack surface under tension condition and material strength of structural component decreases for crushing under compression condition. Moreover, the degradation of shear strength can be considered thanks to this solid element model.

Shear strength of component can be decreased for open crack and closed crack conditions with reduction factors. Figure 5.2 represents failure criteria of smeared crack material model according to ANSYS. Also, stress strain curve for smeared crack model is represented in Figure 5.3 for tension and compression conditions.

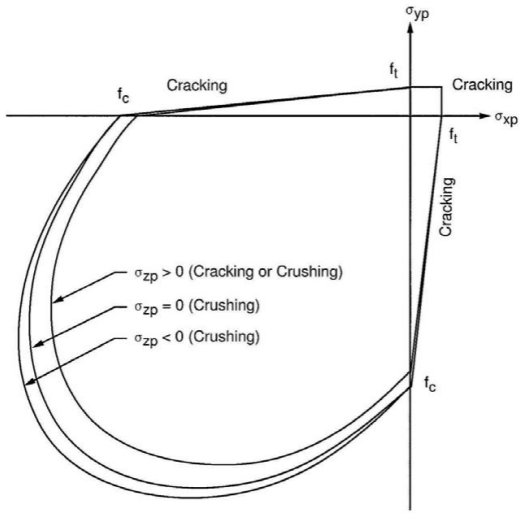

Figure 5.2. Failure criteria of masonry according to ANSYS [22]

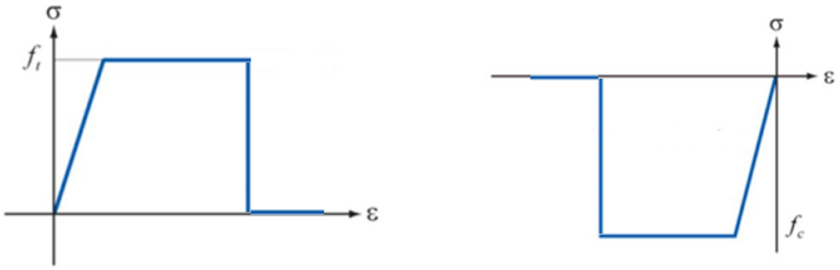

Figure 5.3. Stress strain curve for smeared crack model

Fill material in FEM is also modelled with Solid 65 in order to account nonlinear behavior of the element. The significant issue of FEM is the definition of interface between fill material and masonry. This subject is important especially for nonlinear dead load analysis. For coarse FEM in ANSYS, the interface between two different materials is defined as bonded contact. This type of contact is not allow the relative motions of different materials. In these case, fill and masonry want to move together although the settlement of fill will be greater due to its low stiffness, so extra tension stresses will be created on spandrel walls under gravity load. However, it is possible to define frictional contact interface between two different materials in ANSYS. This type

of contact allows to relative motion so that stress distribution can be obtained accurately for masonry and fill materials. The friction coefficient between fill and masonry is assumed as 0.5 for nonlinear analyses. Solid 65 is also used for soil in order to properly account plastic soil behavior. The different yielding strength of soil in tension and compression can be defined thanks to Solid 65. Therefore, this model gives advantages to obtain local damages at piers of bridge and proper stress distribution for structural components in overturning condition during nonlinear analyses. Defined nonlinear material properties of Solid 65 element type are depicted for masonry structure, fill and soil in Table 5.2.

Table 5.2. Nonlinear behaviors of materials

	Masonry	**Fill**	**Soil**
Shear transfer coefficient for open crack	0.1	0.1	0.1
Shear transfer coefficient for closed crack	0.9	0.9	0.9
Uniaxial tensile cracking stress (MPa)	0.8	0.8	0.1
Uniaxial compressive cracking stress (MPa)	56.5	56.5	10

Figure 5.4 shows the FEM of the masonry bridge in ANSYS software.

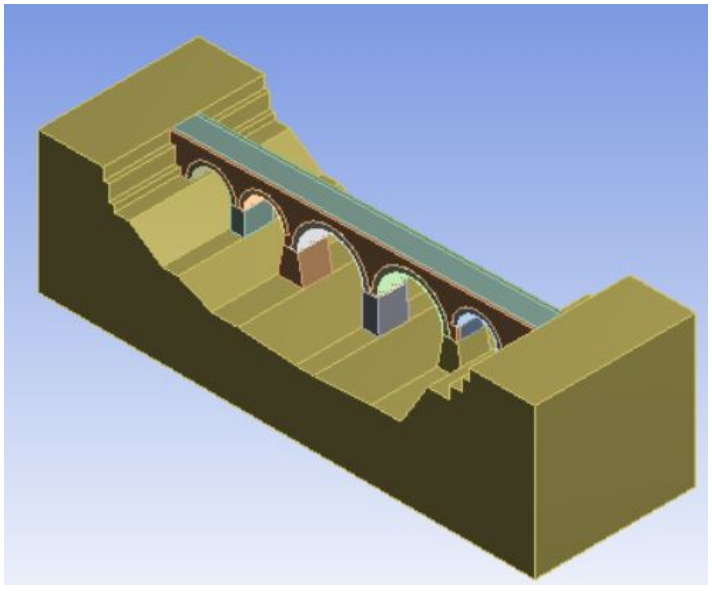

Figure 5.4. FEM of the masonry bridge

5.2. Nonlinear Static Analysis (NSA)

In this study, nonlinear static analysis is performed according to Technical Earthquake Regulation Concerning Construction of Coastal and Port Structures, Railroads, Airports by the Ministry of Transport, Maritime and Communication, DLH-2008. Many seismic codes recommend pushover analysis, so it is very common analysis method for performance based design and performance assessment. Pushover analysis is more suitable method and gives more reliable results for short and regular bridges because the higher mode effects are limited for these types of structures. The mass participation in the first mode should be 70% according to DLH-2008 but the contribution of the mode shapes other than the first fundamental mode shape may decrease the percentage.

Pushover analysis of the masonry bridge was carried out applying monotonically increasing lateral loads along the height of the structure under conditions of constant gravity loading. The load representing inertia forces in an earthquake will be increased incrementally until the target displacement (e.g. the displacement expected in an earthquake) is exceeded or until collapse of the structure. The lateral loads were applied to the structure in transverse direction and longitudinal direction. The amount of lateral force in longitudinal direction is 0.3 times of that of transverse. A uniform pattern based on lateral forces that are distributed proportional to the mass regardless of elevation will be used in the analysis.

After pushover analysis, capacity curve of the masonry bridge was obtained. Capacity curve showing global behavior of structure is the relationship between applied lateral load and lateral displacement of control point. The selection of control node is complicated issue for pushover analysis. Although there are many recommendations in codes and articles in order to select proper control point for concrete, steel and masonry buildings, selection of control node for stone arch bridges is complex task. The straightforward way of defining control node is to select top of the structure. However, many studies show that using top of the structure gives more conservative results although choosing this point is a conventional procedure. Other suggestion for selecting

control node is to use Energy Approach which uses principles of virtual work, but this method is quite time consuming. Recent studies show that using center of mass of the stone arch bridge is very effective to represent the global behavior of the structure for pushover analysis. Therefore, center of mass at the upper level of the arch barrel which is in the same direction with keystone of middle arch was selected as a control point due to its closeness to center of mass of the bridge. Figure 5.5 shows control point on the bridge.

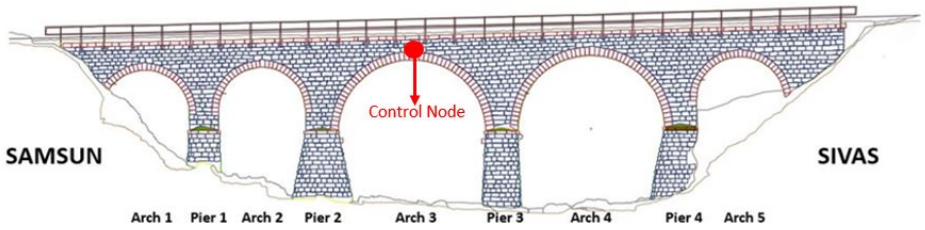

Figure 5.5. Representation of control point

The failure point of the structure is determined by controlling the distribution of element stresses along the global X and Z directions. The stresses of the structural elements were redistributed gradually and cracks, especially along the arch barrel and spandrel wall, were created during progressive loading. The load step at which tension or compression stresses are at the specified limit values within a region that is probably causes failure was defined as the ultimate point. At the ultimate point, the cracks along the arch barrel and spandrel wall due to high stress concentration cause mass movement which was called failure mechanism.

In this study, crack (or crush) shows that a section of structural component reaches its tensile (or compressive) strength. After that point, this section could not carry any extra load, and stress of this section drops to zero for successive loading. In pushover analysis, width of the area reaching the capacity which was represented by black dashed line in the below figures increased during progressive loading. Consequently, the collapse of spandrel wall above the middle arch was observed at the failure point. Figure 5.6-5.7 and Figure 5.8-5.9 represent the stresses in X direction and Z direction, respectively, step by step from first critical point to the ultimate point.

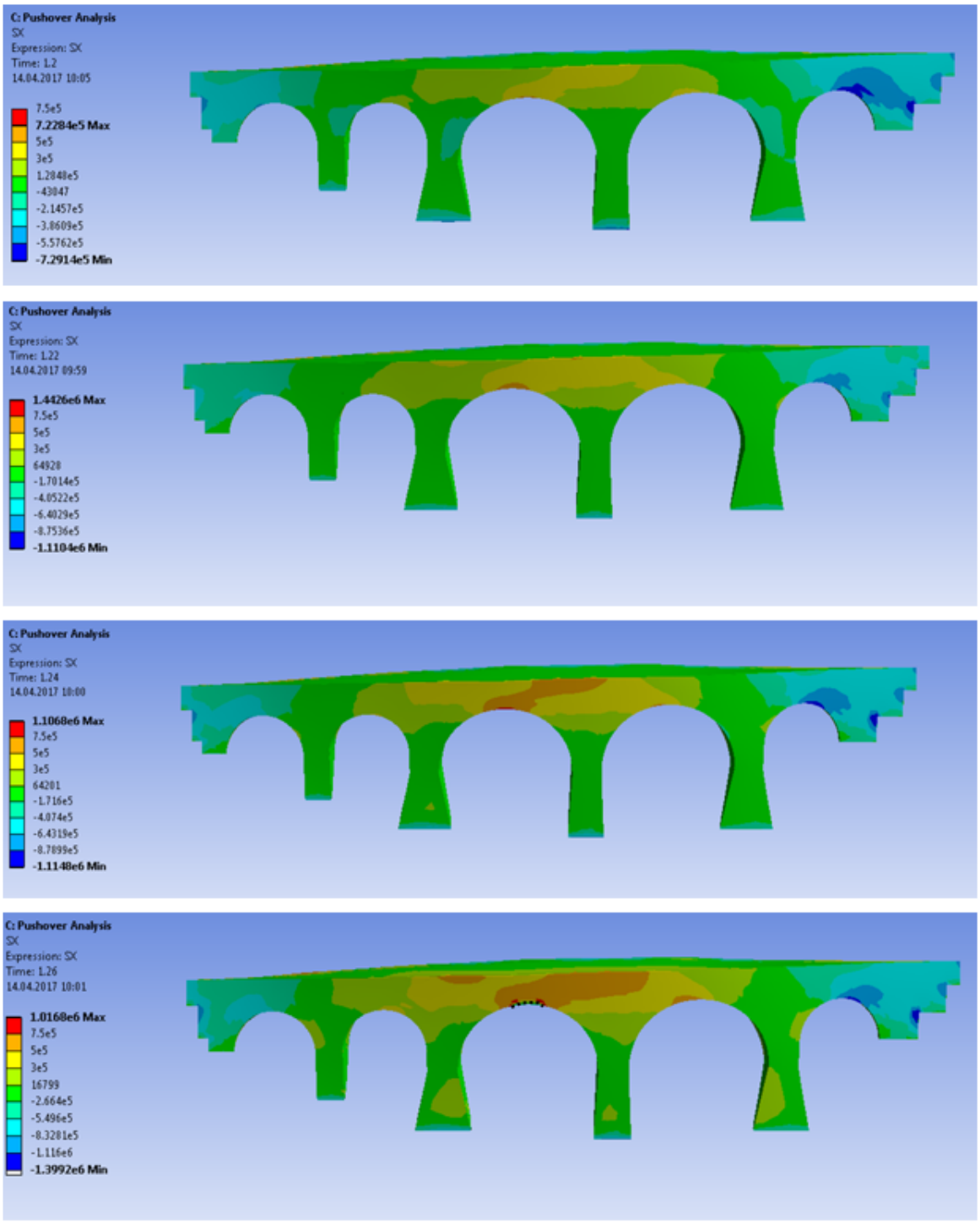

Figure 5.6. Stresses in X Direction

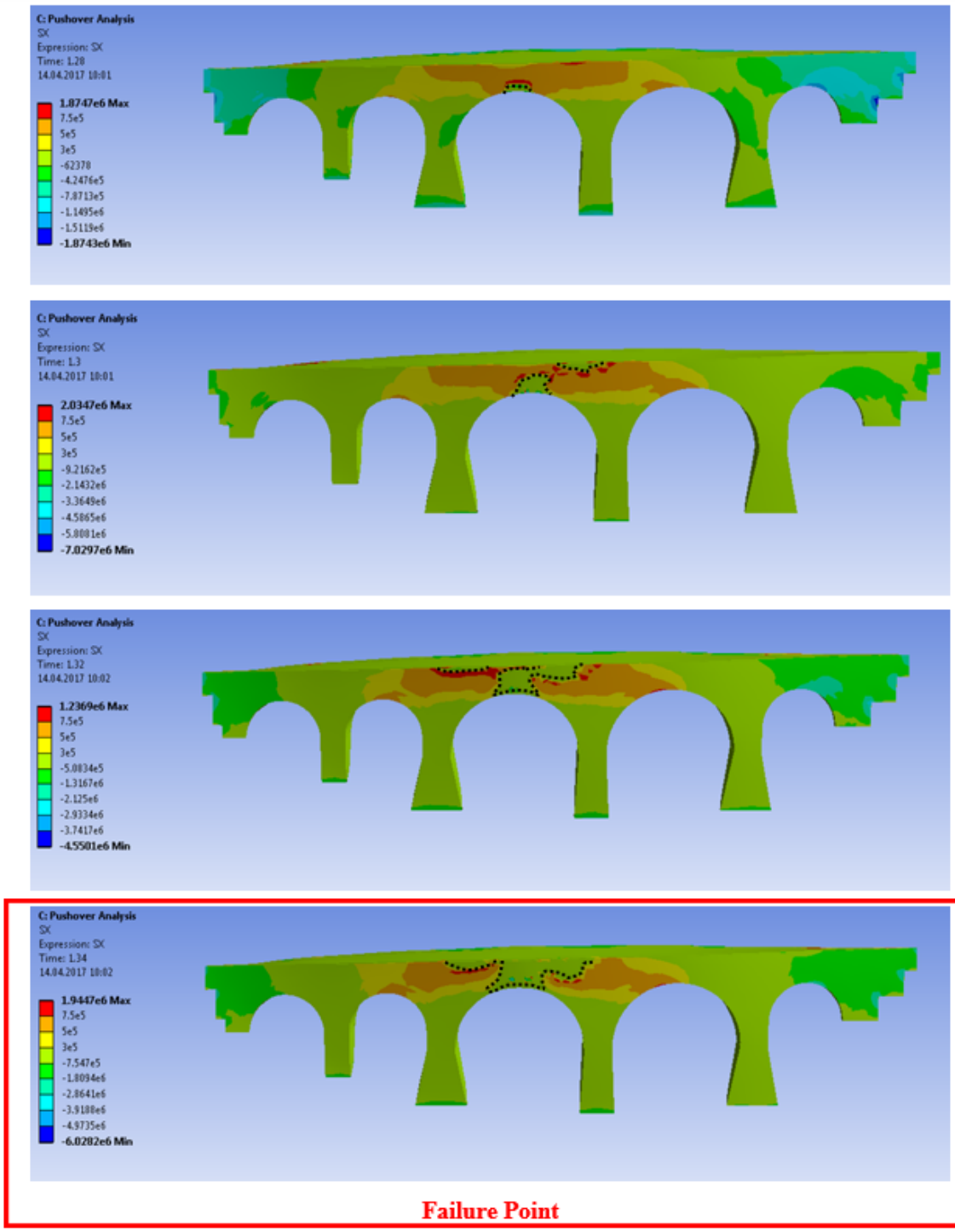

Figure 5.7. Stresses in X Direction

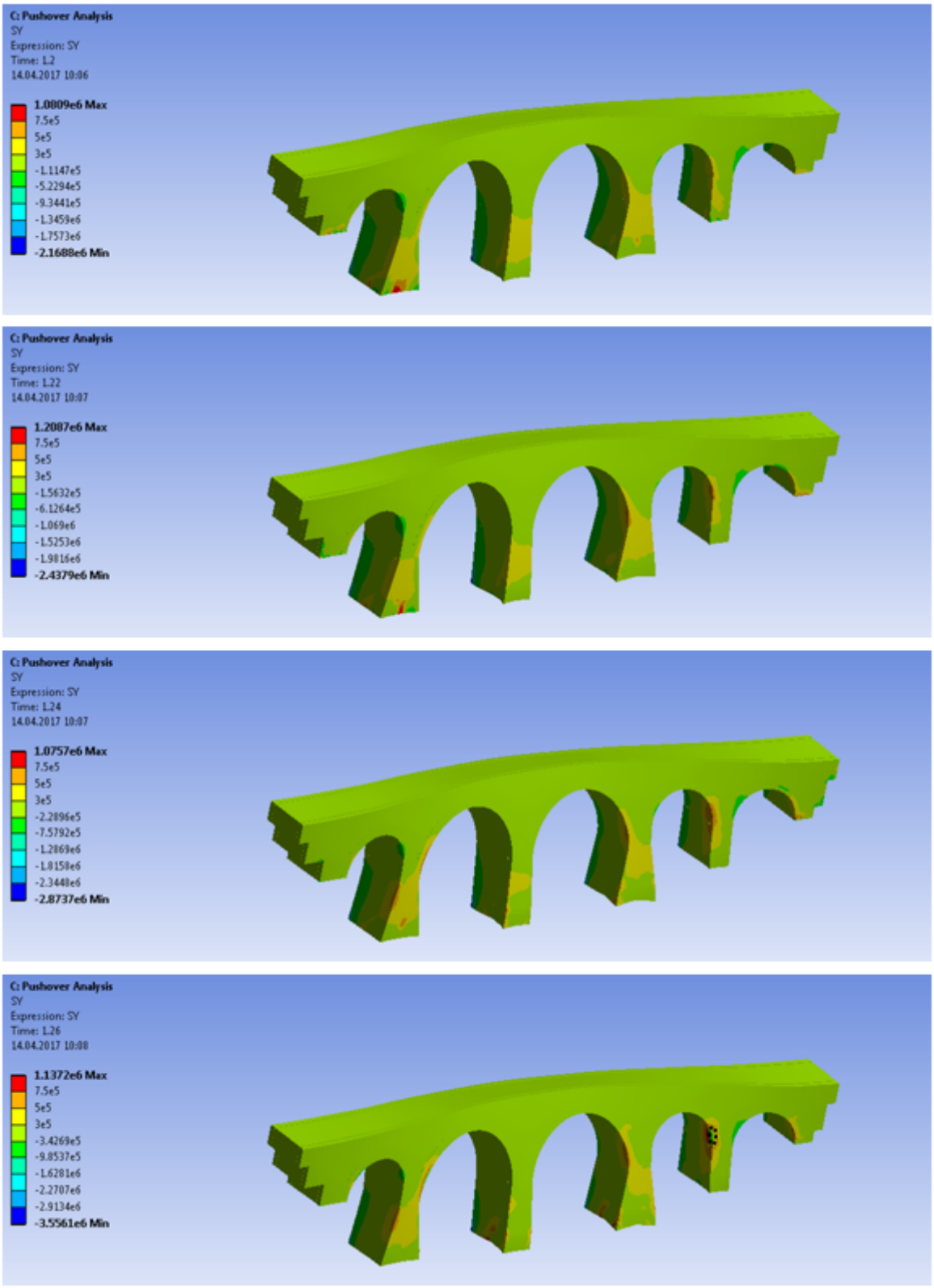

Figure 5.8. Stresses in Z Direction

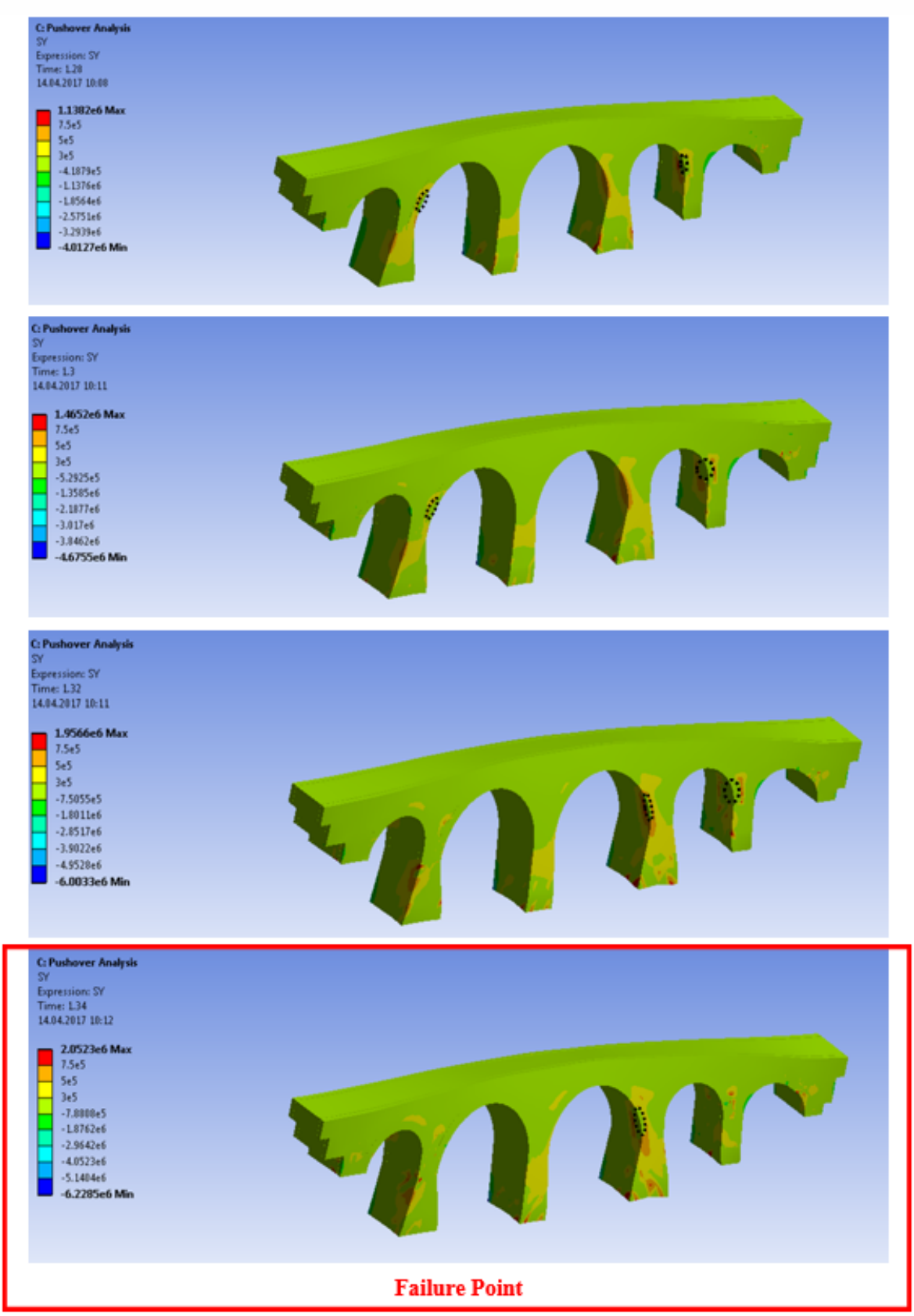

Figure 5.9. Stresses in Z Direction

Figure 5.10 represents the capacity curve of the structure obtained from nonlinear static analysis.

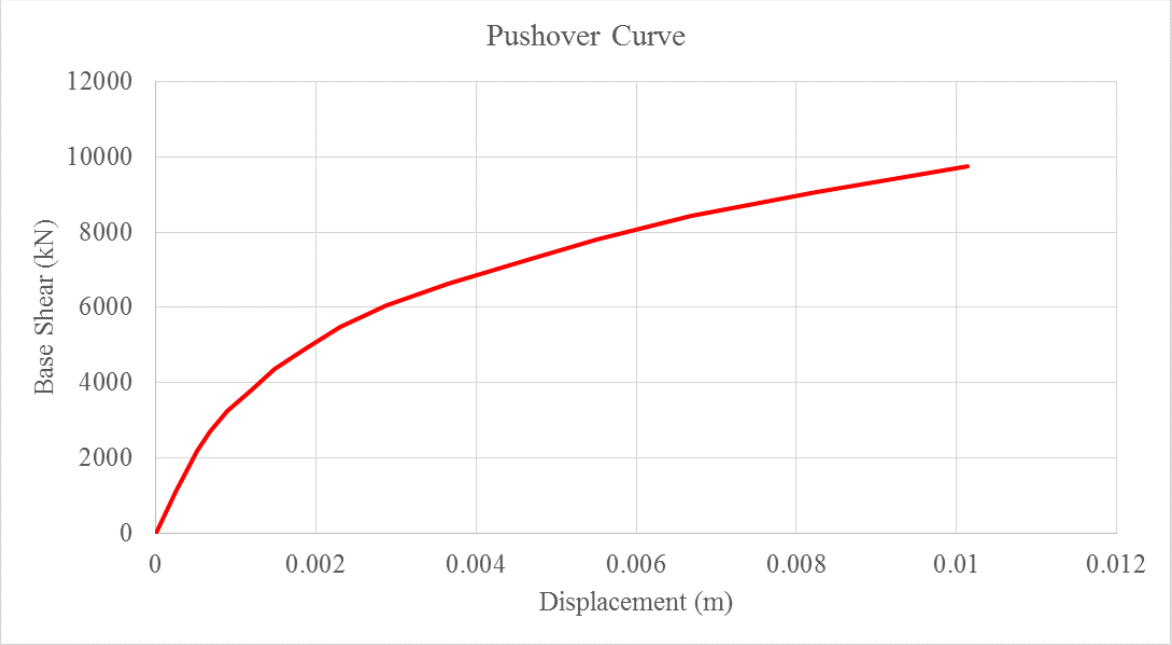

Figure 5.10. Pushover curve

5.2.1. Modal Capacity Curve

Modal capacity cure obtaining from pushover analysis was transformed to spectral acceleration versus spectral displacement graph in order to develop performance point of the bridge. For this purpose, DLH 2008, Chapter 3 was used. The modal displacement demand for the first mode is computed as:

$$d_1{}^{(i)} = \frac{u_{xN1}{}^{(i)}}{\Phi_{xN1}.\Gamma_{xN1}} \tag{5.1}$$

Also, the modal acceleration demand for the first mode is calculated as:

$$a_1{}^{(i)} = \frac{V_{x1}{}^{(i)}}{M_{x1}} \tag{5.2}$$

where;

M_{x1} : effective mass defined for the first mode of vibration in transverse direction

Φ_{xN1} : amplitude of the first mode shape at the control point of masonry bridge defined for the first mode of vibration in the transverse direction

Γ_{x1} : participation factor defined for the first mode of vibration in the transverse direction

V_{x1} : base shear of the bridge after pushover analysis

u_{xN1} : displacement demand (target displacement) at the control point of the masonry bridge in the transverse direction

Calculation formulas of M_{x1} and Φ_{xN1} are represented in below equations.

$$M_{x1} = \frac{{L_{x1}}^2}{M_1} \tag{5.3}$$

$$\Gamma_{x1} = \frac{L_{x1}}{M_1} \tag{5.4}$$

$$M_1 = \sum_{i=1}^{N} (m_i . {\Phi_{xi1}}^2) \tag{5.5}$$

$$L_{x1} = \sum_{i=1}^{N} (m_i . \Phi_{xi1}) \tag{5.6}$$

where;

m_i : lumped mass of i-th point

Φ_{xi1} : normalized modal displacement for the first fundamental model

In calculations, normalized modal displacements are used in such a way that $\Phi_n = 1$, where n is the control node. Also, N represents the number of nodes.

Effective mass defined for the first mode of vibration in transverse direction (M_{x1}) and participation factor defined for the first mode of vibration in the transverse direction (Γ_{x1}) are defined as below equations.

$$M_{x1} = \frac{\sum_{i=1}^{N} (m_i . \Phi_{xi1})^2}{\sum_{i=1}^{N} (m_i . {\Phi_{xi1}}^2)} \tag{5.7}$$

$$\Gamma_{x1} = \frac{\sum_{i=1}^{N} (m_i . \Phi_{xi1})}{\sum_{i=1}^{N} (m_i . {\Phi_{xi1}}^2)} \tag{5.8}$$

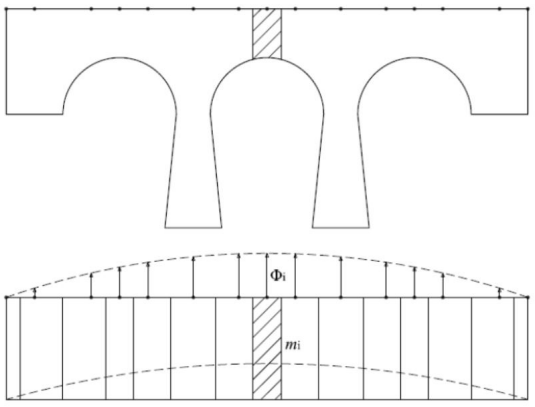

Figure 5.11. Demonstration of participation factor parameters

Table 5.3. Participation factor calculation

Partial Masses of Bridge	**Mass (ton),** m_i	**Modal Displacement,** $u_{T,1}$	**Normalized Modal Displacement,** Φ_i	$m_i.\Phi_i$	$m_i.\Phi_i^2$
M1	102.41	0.00	0.002	0.20	0.00
M2	230.88	0.07	0.045	10.31	0.46
M3	170.93	0.25	0.169	28.94	4.90
M4	189.51	0.55	0.365	69.23	25.29
M5	307.65	0.88	0.585	180.08	105.41
M6	334.49	1.38	0.919	307.28	282.29
M7	280.98	1.50	1.000	280.98	280.98
M8	336.91	1.29	0.860	289.74	249.18
M9	306.56	0.70	0.467	143.06	66.76
M10	183.77	0.25	0.167	30.63	5.10
M11	137.33	0.03	0.020	2.75	0.05
M12	87.06	0.00	0.002	0.17	0.00
				1343.39	**1020.43**

From calculations, $M_{x1}(= (1343.92)^2/1020.43 = 1768.565$ ton) and $\Gamma_{x1}(= 1343.39$ $/1020.43 = 1.317)$ were obtained.

The modal capacity curve obtained from pushover curve by using defined equations was depicted in Figure5.12. Defining bilinear curve is a common way to idealize

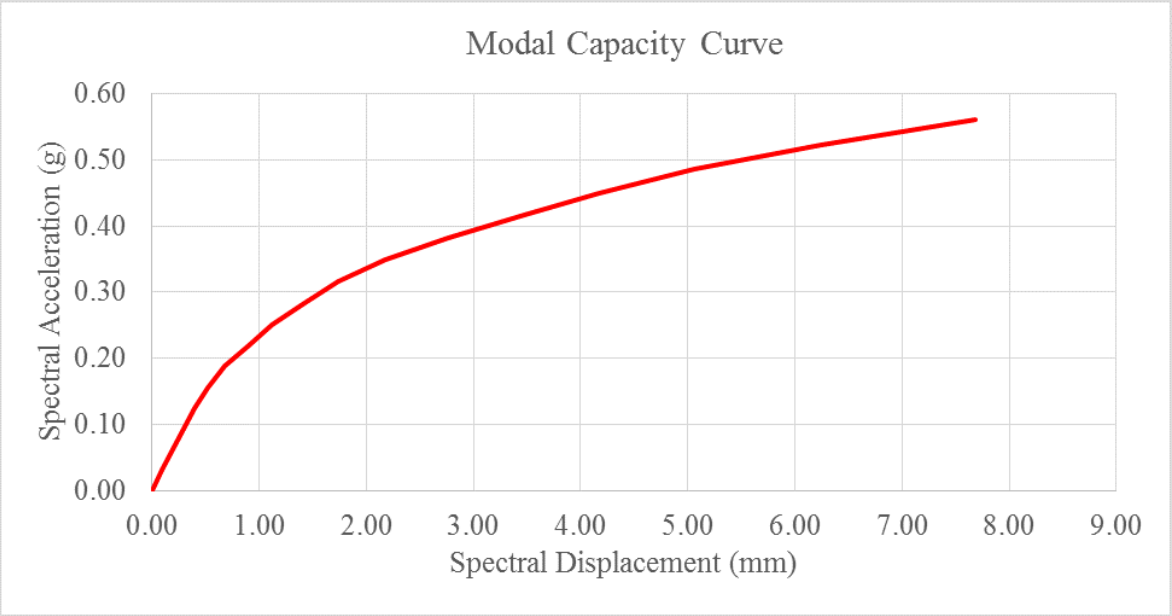

Figure 5.12. Modal capacity curve

the nonlinear spectral acceleration – spectral displacement relationship in the modal capacity curve of the structure for performance assessment. For this purpose, the initial slope will be determined by a line segment that passes through 40% of the ultimate acceleration, a_{u1}.

The ultimate acceleration, a_{u1} is the failure point of the structure which is determined by controlling the distribution of element stresses along the global X and Z directions. Line segments on the idealized acceleration-displacement curve will be located using a graphical procedure that approximately balances the area above and below the modal capacity curve. The horizontal line segment located as to balance the areas defines the yield acceleration, a_{y1}. Bi-linearization of the modal capacity curve is demonstrated in Figure 5.13.

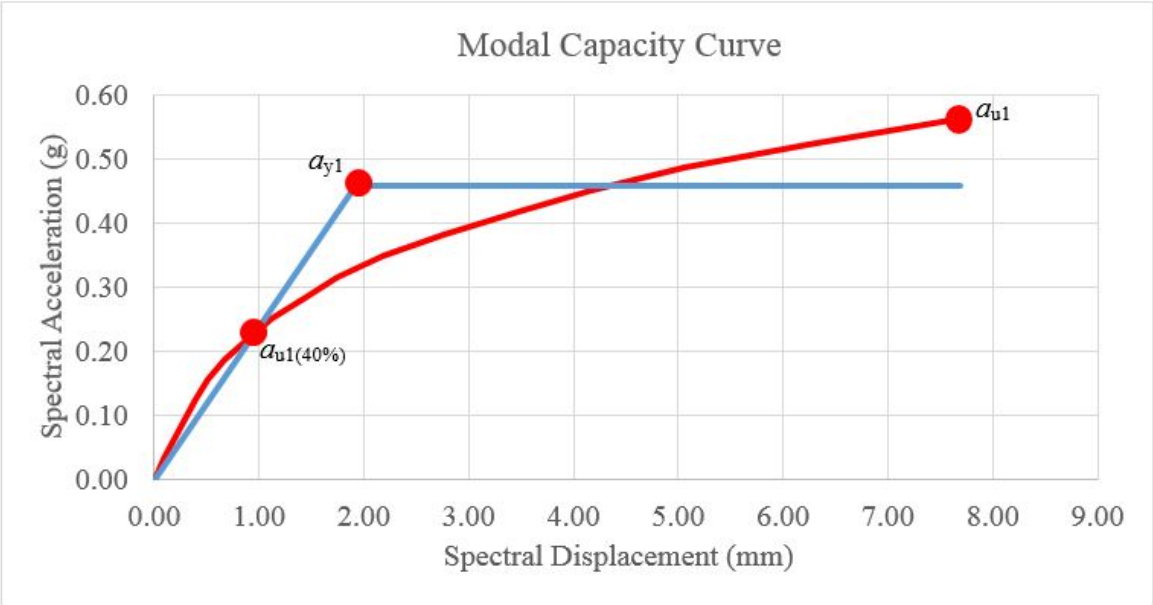

Figure 5.13. Bi-linearization of modal capacity curve

In Figure 5.13; a_{u1} is ultimate acceleration, $a_{u1(40\%)}$ is acceleration corresponding to 40% of ultimate acceleration, a_{y1} is equivalent yield acceleration.

5.2.2. Demand Curve

Earthquake creates critical lateral displacements changing with time in structures. Displacement demand is expected maximum response of the structure, which is the maximum lateral displacement in this project, against the ground motion. Therefore, a spectral representation of ground motion is needed in order to attain expected maximum displacement against the earthquake. In this study, the five-percent-damped-design response spectrum was created according to DLH 2008, Section 1.1.2, to obtain spectral representation of ground motion.

Earthquake design spectrum is defined in the following expressions according to DLH 2008;

$$S_{\mathrm{ae}}(T) = 0.4S_{\mathrm{MS}} + 0.6\frac{S_{\mathrm{MS}}}{T_0}T \qquad (0 \leq T \leq T_0) \tag{5.9}$$

$$S_{\mathrm{ae}}(T) = S_{\mathrm{MS}} \qquad (T_0 \leq T \leq T_{\mathrm{S}}) \tag{5.10}$$

$$S_{\mathrm{ae}}(T) = \frac{S_{\mathrm{M1}}}{T} \qquad (T_{\mathrm{S}} \leq T \leq T_{\mathrm{L}}) \tag{5.11}$$

$$S_{\mathrm{ae}}(T) = \frac{S_{\mathrm{M1}}\,T_{\mathrm{L}}}{T^2} \qquad (T_{\mathrm{L}} \leq T) \tag{5.12}$$

where;

T_{L} : 12 s.

T_{S} : S_{M1} / S_{MS}

T_0 : $0.2T_{\mathrm{S}}$

T: period of vibration of mth mode (sec.)

T_0 : reference period used to define spectral shape (sec.)

T_{S}: corner period at which spectrum changes from being independent of period to being inversely proportional to period (sec.)

T_{L} : initial period at which constant displacement region starts

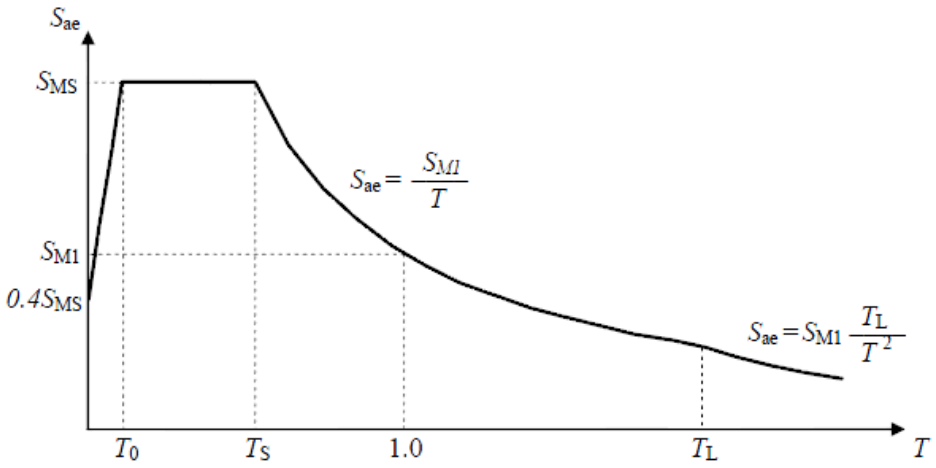

Figure 5.14. Response spectrum

The five-percent-damped-design response spectrum was used as defined in Figure 5.14. This spectrum was calculated in accordance with DLH-2008, using the mapped spectral acceleration coefficients, S_S and S_1, scaled by short-period and long-period site factors, F_a and F_v, respectively.

$$S_{MS} = F_a.S_S \tag{5.13}$$

$$S_{M1} = F_v.S_1 \tag{5.14}$$

where;

S_S : horizontal response spectral acceleration coefficient at 0.2 second period on rock

S_1 : horizontal response spectral acceleration coefficient at 1.0 second period on rock

F_a : short-period site factor

F_v : long-period site factor

Table 5.4. Values of site factor, F_a

Site Class	**Values of Site Factor, F_a for Short Period Range of Acceleration Response**				
	$S_S < 0.25$	$S_S = 0.50$	$S_S = 0.75$	$S_S = 1.00$	$S_S > 1.25$
A	0.8	0.8	0.8	0.8	0.8
B	1.0	1.0	1.0	1.0	1.0
C	1.2	1.2	1.1	1.0	1.0
D	1.6	1.4	1.2	1.1	1.0
E	2.5	1.7	1.2	0.9	0.9
F	-	-	-	-	-

Table 5.5. Values of site factor, F_v

Site Class	**Values of Site Factor, F_v for 1.0 sec. Period Range of Acceleration Response**				
	$S_1 < 0.10$	$S_1 = 0.20$	$S_1 = 0.30$	$S_1 = 0.40$	$S_1 > 0.50$
A	0.8	0.8	0.8	0.8	0.8
B	1.0	1.0	1.0	1.0	1.0
C	1.7	1.6	1.5	1.4	1.3
D	2.4	2.0	1.8	1.6	1.5
E	3.5	3.2	2.8	2.4	2.4
F	-	-	-	-	-

The site factors F_{a} and F_{v} which are determined depending on the site class, S_{S} and S_1 are given in Table 5.4 and Table 5.5.

First of all, the earthquake level was determined according to DLH 2008 to define parameters needed for design spectrum. Earthquake hazard levels in DLH 2008 are described as following definitions by considering probabilistic approach .

(i) D1 Earthquake Level is the earthquake level which has a 50% probability of exceedance in 50 years and a return period of 72 years.
(ii) D2 Earthquake Level is the earthquake level which has a 10% probability of exceedance in 50 years and a return period of 475 years.
(iii) D3 Earthquake Level is the earthquake level which has a 2% probability of exceedance in 50 years and a return period of 2475 years.

On the other hand, in the new Turkish Seismic Code, expected to enter into force in 2017, new earthquake level is described. This earthquake level is D4 Earthquake Level which has a 68% probability of exceedance in 50 years and a return period of 43 years.

The (D2) Earthquake Level was selected for the performance assessment of the masonry bridge in this study. The bridge is classified as 'ordinary bridge' where the seismic performance target is 'controlled damage performance level' for D2 earthquake level. This earthquake level permits limited and repairable structural damages after an earthquake and there can be operation interruption for a few days or a few weeks. Also, soil investigation reports show that site class for the masonry bridge is A according to DLH 2008. Table 5.6 represents essential parameters needed to establish design spectrum for the earthquake level D2.

Table 5.6. Design spectrum parameters

Site Class	Coordinates		Parameters for D2 Earthquake Level					
	Latitude	Longitude	S_S	S_1	F_a	F_v	T_0(sec.)	F_S(sec.)
A	41.2	36.2	0.60	0.28	0.8	0.8	0.093	0.467

Design spectrum which was established using defined parameters was showed in Figure 5.15.

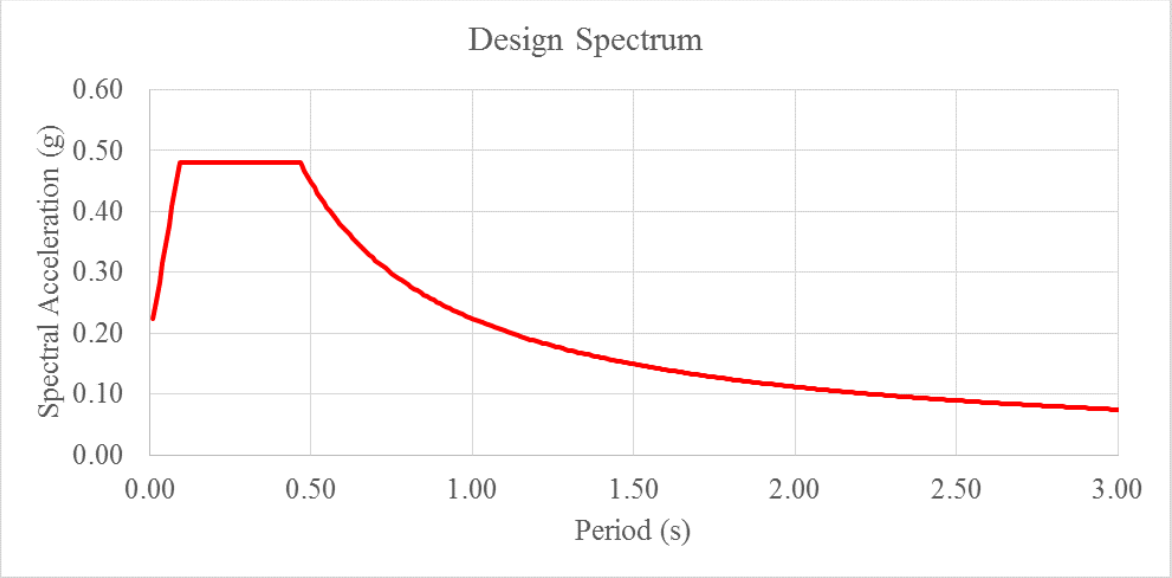

Figure 5.15. Design spectrum

After, spectral acceleration – spectral displacement spectrum was obtained by transforming design response spectrum according to DLH 2008, Appendix C. Spectral acceleration – spectral displacement spectrum is needed to attain spectral demand of the masonry bridge. Linear elastic spectral displacement is calculated from elastic spectral acceleration by the following equations.

$$S_d = \frac{S_a}{\omega^2} \tag{5.15}$$

$$\omega = 2\pi f = 2\pi \frac{1}{T} \tag{5.16}$$

where,

S_{d} : linear elastic spectral displacement

S_{a} : elastic spectral acceleration

ω : natural angular frequency

T : period

Figure 5.16 depicts the demand curve which was established by using design response spectrum where spectral displacement is defined a function of spectral acceleration.

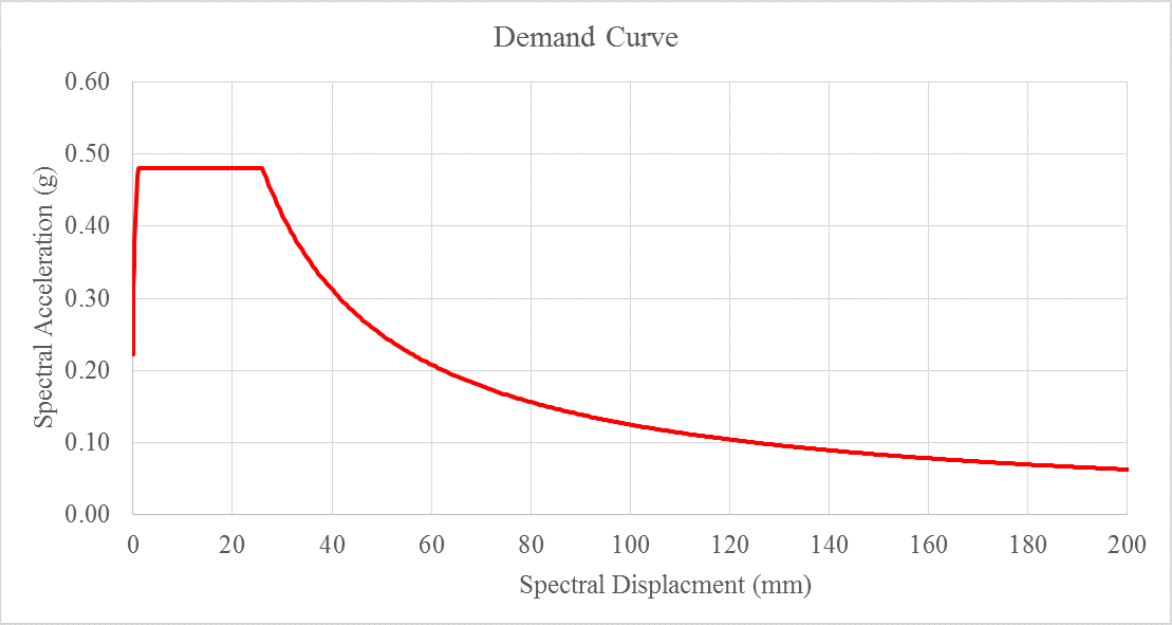

Figure 5.16. Design curve

5.2.3. Performance Point Definition

Performance of the structure was evaluated using modal capacity curve and demand curve relationship. The nonlinear response of the structure can be estimated thanks to performance point. At the performance point, the stresses and deformations of the structural elements are compared with the limit values and this comparison gives valuable results about durability of the structure against the seismic actions. The seismic performance of the structure is assessed according to these compression results and necessary strengthening methods are applied to structure if retrofitting is needed.

In this project, performance point of the masonry bridge was obtained the procedure which is defined in DLH 2008, Appendix C. According to code, the nonlinear spectral displacement is a function of linear spectral displacement which can be defined as follows.

$$S_{\mathrm{di1}} = S_{\mathrm{de1}}.C_{\mathrm{R1}} \tag{5.17}$$

where;

S_{di1}: nonlinear spectral displacement for the first fundamental mode

C_{R1}: spectral displacement ratio for the first mode

In order to calculate spectral displacement ratio for the first mode, C_{R1}, following procedure which is defined in DLH 2008 was used.

Case 1.

If $T_1^{(1)} > T_{\mathrm{S}}$ or $(\omega_1^{(1)})^2 < \omega_s^2$;

$$C_{\mathrm{R1}} = 1.0$$

which means

$$S_{\mathrm{di1}} = S_{\mathrm{de1}}$$

In case of periods greater than corner period T_{S}, the capacity curve will be represented by the line with a slope corresponding to $(\omega_1^{(1)})^2$ of the first mode.

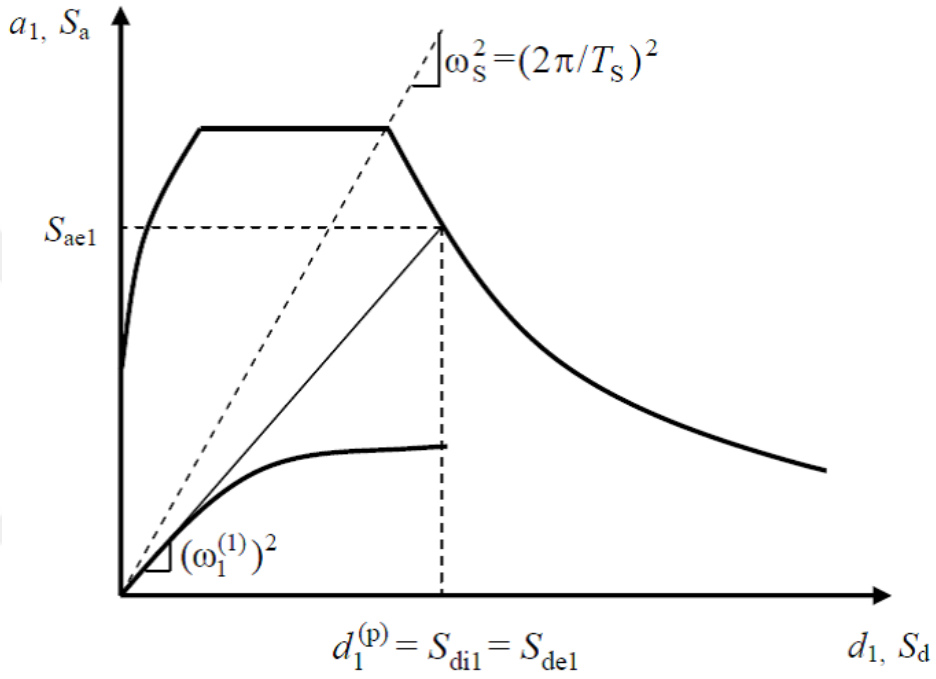

Figure 5.17. Capacity curve and design spectrum for Case 1

Case 2.

If $T_1^{(1)} < T_{\mathrm{S}}$ or $(\omega_1^{(1)})^2 > \omega_s^2$;

$$C_{\mathrm{R1}} = \frac{1 + (R_{\mathrm{y1}} - 1)\, T_{\mathrm{S}} / T_1^{(1)}}{R_{\mathrm{y1}}} \tag{5.18}$$

$$R_{\mathrm{y1}} = \frac{S_{\mathrm{ae1}}}{a_{\mathrm{y1}}} \tag{5.19}$$

where;

R_{y1}: strength reduction factor for the first mode

a_{y1}: equivalent yield acceleration for the first mode

For periods less than corner period, the value of the coefficient C_{R1} is used as defined above.

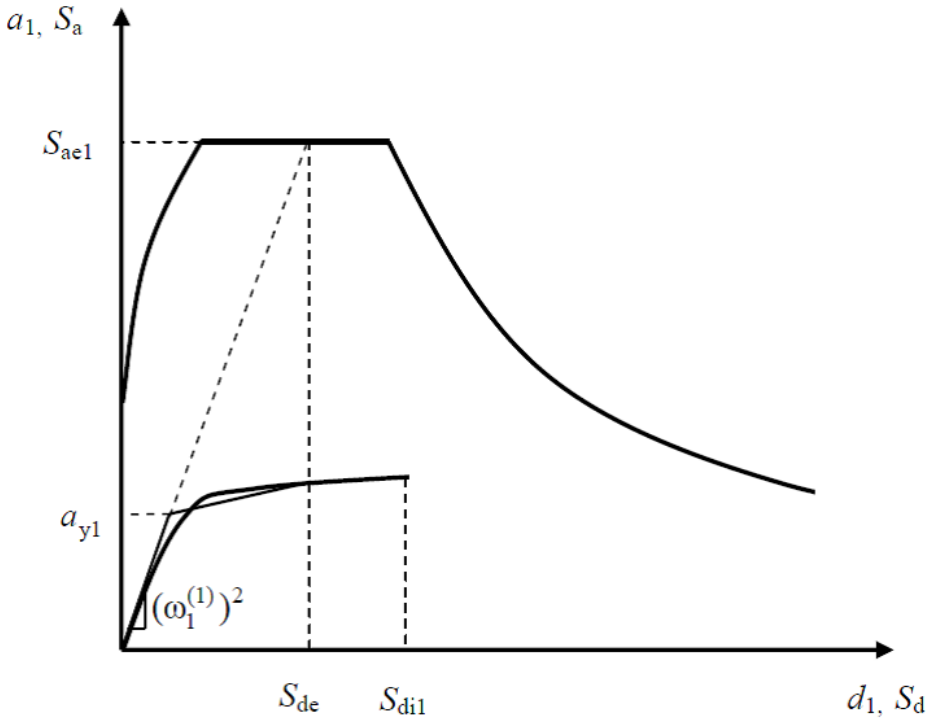

Figure 5.18. Capacity curve and design spectrum for Case 2

In equations which are described in Case 1. and Case 2.; $T_1^{(1)}$is natural vibration period for the first fundamental mode, T_S is corner period at which spectrum changes from being independent of period to being inversely proportional to period and ω_S is natural angular frequency for the first mode.

The relationship between modal capacity curve and demand curve was represented in Figure 5.19. According to this figure, spectral displacement ratio for the first mode, C_{R1}, was calculated by using Case 2.

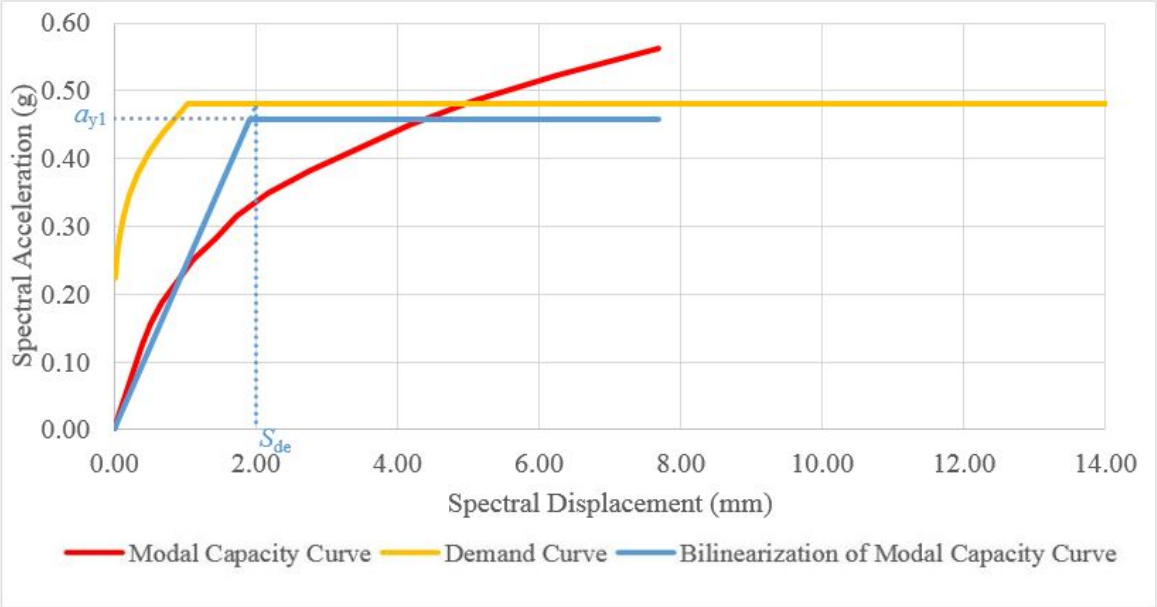

Figure 5.19. Relationship between modal capacity curve and demand curve

Table 5.7 represents the performance points parameters obtained from defined calculations.

Table 5.7. Performance point parameters

a_y(g)	S_{ae1}(g)	S_{de1}(mm)	R_{y1}	C_{R1}	S_{di1}(mm)
0.46	0.48	2.01	1.05	1.10	2.20

The pushover analysis results show that the inelastic spectral displacement of the masonry bridge is 2.20 mm. which represents the performance point of the structure.

5.2.4. Results

Figure 5.20 and Figure 5.21 represent the stress distributions in X direction and in Z directions at the performance point.

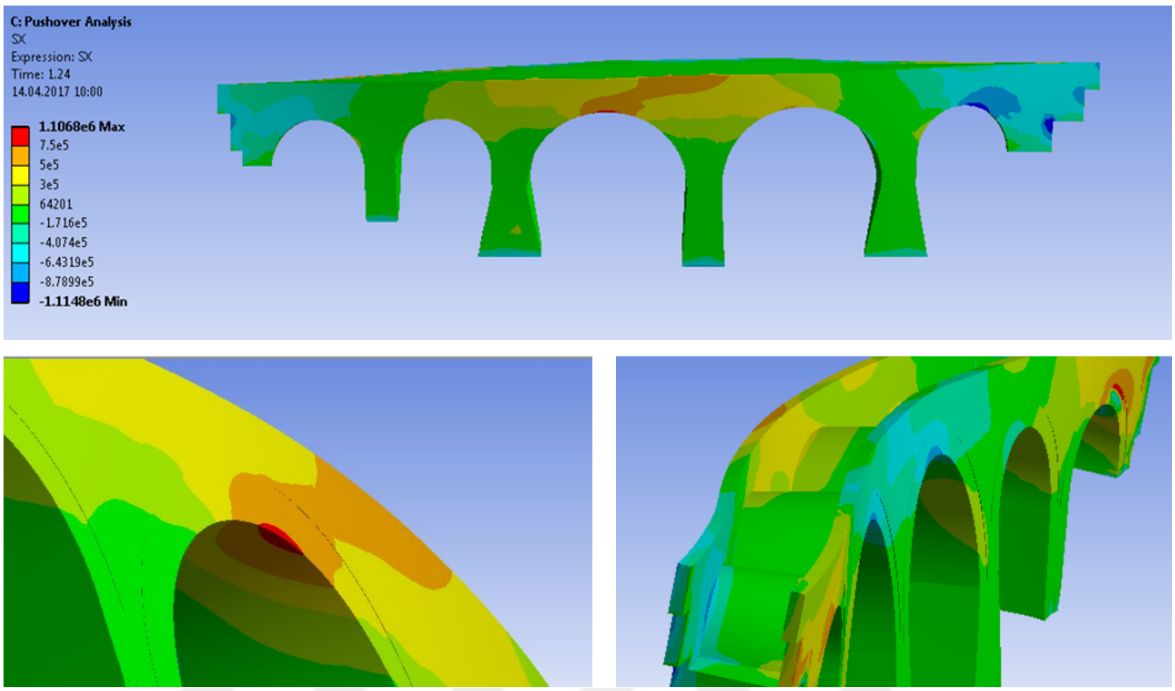

Figure 5.20. Stress distribution in X direction at the performance point

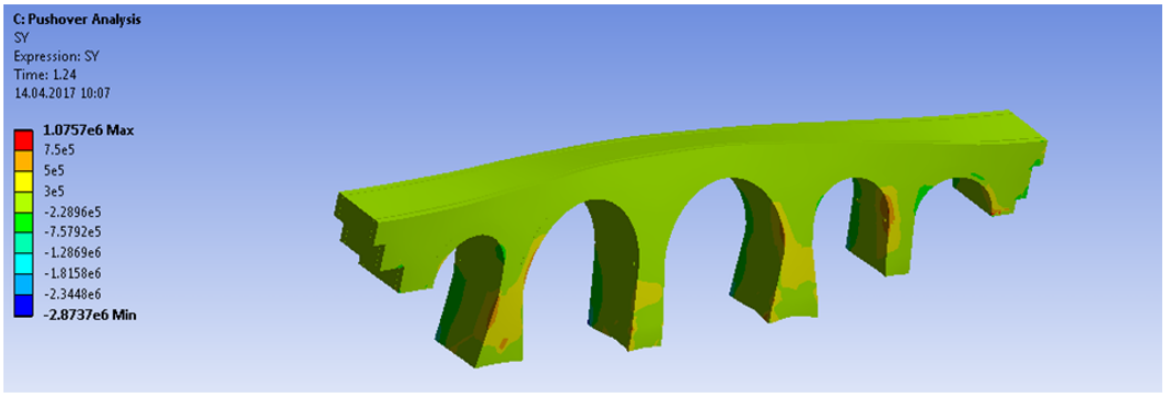

Figure 5.21. Stress distribution in Z direction at the performance point

Based on stresses obtained from pushover analysis, stress distribution in the spandrel wall extends along the arch span and creates some cracks along the keystone of the middle arch barrel, however tensile stresses did not penetrate into inner surface of middle arch barrel and it is not expected to result with a partial failure from the bridge as shown in Figure 5.20. Also, the spandrel wall was exposed to large amount of tensile stresses, but these tensile stresses do not exceed the capacity of masonry. Moreover, tensile stresses along the end of the edge arch barrels in Z direction was in limit value of strength. On the other hand, pushover analysis results show that compression stresses of the structural elements were in limit value of strength and there is no damage due to compression.

5.3. Nonlinear Time History Analysis (NLTHA)

NLTHA is common and effective way to characterize the dynamic inelastic response of the structures. When compared with pushover analysis, NLTHA produces inelastic deformations of structural elements with low uncertainty. In NLTHA, the dynamic inelastic response of structure is highly depended the characteristic behavior of ground motion, so increasing number of ground motion analysis increases the reliability of results. That is, NLTHA analysis is inevitable method in order to obtain close to the truth behavior of structure under seismic loading.

5.3.1. Ground Motion Record Selection

In this study, ground motion records were selected from *Peer Strong Motion Database NGA-West 2 Ground Motion Selection Tool* and *Strong Ground Motion Database of Turkey* to perform nonlinear time history analyses. For this purpose, 11 earthquake records were used to simulate seismic load on the masonry bridge. Selected ground motions were scaled according to procedure defined in DLH 2008. This methodology was described in following expression;

(i) First of all, the response spectrums of transverse and longitudinal components of earthquake records were combined by Square Roots of the Sum of the Squares

(SRSS) method.

(ii) After that, combined response spectra of the selected ground motions were scaled in a way that, geometric mean of response spectrums of earthquake records is coherent with 1.3 times design spectrum which was obtained for pushover analysis according to DLH 2008 based on earthquake level which was selected D2, location of the masonry bridge and soil investigation report.

(iii) In a fact that, the geometric mean of response spectra of selected earthquakes was controlled in order to provide that it should not below 1.3 times design spectrum between $0.2T_1$ and $1.5T_1$, where T_1 is the fundamental period of the masonry bridge.

(iv) In addition, DLH 2008 suggests that the time between the first and last points of earthquake record exceeding +/- 0.05g should not be less than 15 seconds and five times the fundamental period of structure. Therefore, time history of selected ground motions were controlled in order to implement this rule.

The information of selected earthquakes were given in Table 5.8. Also, the coherence between the SRSS of scaled response spectra of selected ground motion and target spectrum was indicated in Figure 5.22.

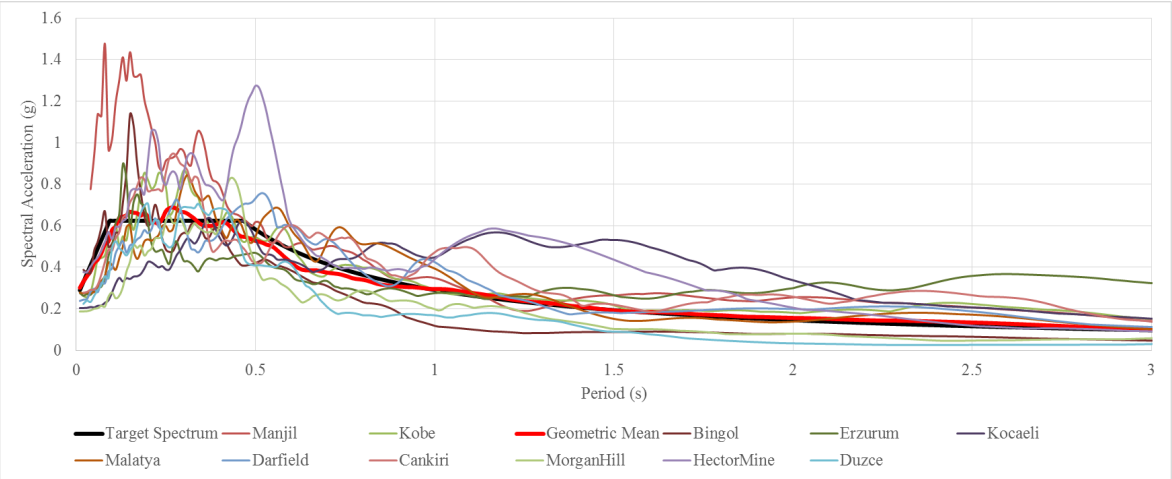

Figure 5.22. Response spectra of selected ground motions, their mean and the target spectrum

Table 5.8. Properties of the selected ground motions

No	Name	Station	Year	Distance (km)	Magnitude	Scale Factor
1	Manjil	Abbar	1990	12.55	7.37	0.54
2	Kobe	Sakai	1995	28.08	6.39	1.28
3	Bingol	Bingol Environment and Urbanization Directorate	2003	2.23	6.60	0.44
4	Erzurum	Erzurum Horosan Meteorology Directorate	1983	22.60	6.60	1.12
5	Kocaeli	Kutahya	1999	145.06	7.51	1.33
6	Malatya	Adiyaman Golbasi State Hospital	1986	23.93	6.00	1.94
7	Darfield	Christchurch Cashmere High School	2010	17.64	7.00	0.70
8	Cankiri	Cankiri Cerkes Meteorology Directorate	2000	8.19	6.39	3.03
9	Morgan Hill	San Justo Dam	1984	31.88	6.19	1.75
10	Hector Mine	Hector	1999	10.35	7.13	0.86
11	Duzce	Irigm 487	1999	2.65	7.14	0.53

NLTH analysis in ANSYS software uses direct integration method for calculations, so the damping matrix is required. The mass and stiffness matrices are needed in order to define damping matrix of the structure. Rayleigh Damping which is most well-known method is used to create the mass and stiffness matrices. Equation 5.19 shows that linear combination of the initial mass and stiffness matrices establish the damping matrix of the structure. According to *Dynamic of Structures, Chapter 3 (Chopra, 1995)*, mass and stiffness matrices are created by using below equations.

$$\mathrm{C} = \alpha.\mathrm{M} + \beta.\mathrm{K} \tag{5.20}$$

In this equation, C represents damping matrix, M is the mass matrix and K shows the stiffness matrix. The coefficients, α and β, are obtained by using following equations.

$$\alpha = \xi.\frac{2.\omega_\mathrm{i}.\omega_\mathrm{j}}{\omega_\mathrm{i} + \omega_\mathrm{j}} \tag{5.21}$$

$$\beta = \xi.\frac{2}{\omega_\mathrm{i} + \omega_\mathrm{j}} \tag{5.22}$$

In above equations, ω_i and ω_j are the natural frequencies of the ith and j^{th} modes and ξ is damping ratio. In this study, α and β were calculated 0.864 and 1.950e-4, respectively.

5.3.2. Results

After NLTH analysis, stresses of structural elements were controlled in X and Z direction for each earthquake. Moreover, maximum displacement of control node which was also selected for pushover analysis was controlled for every ground motions. Stress results were showed in below figures for each earthquake.

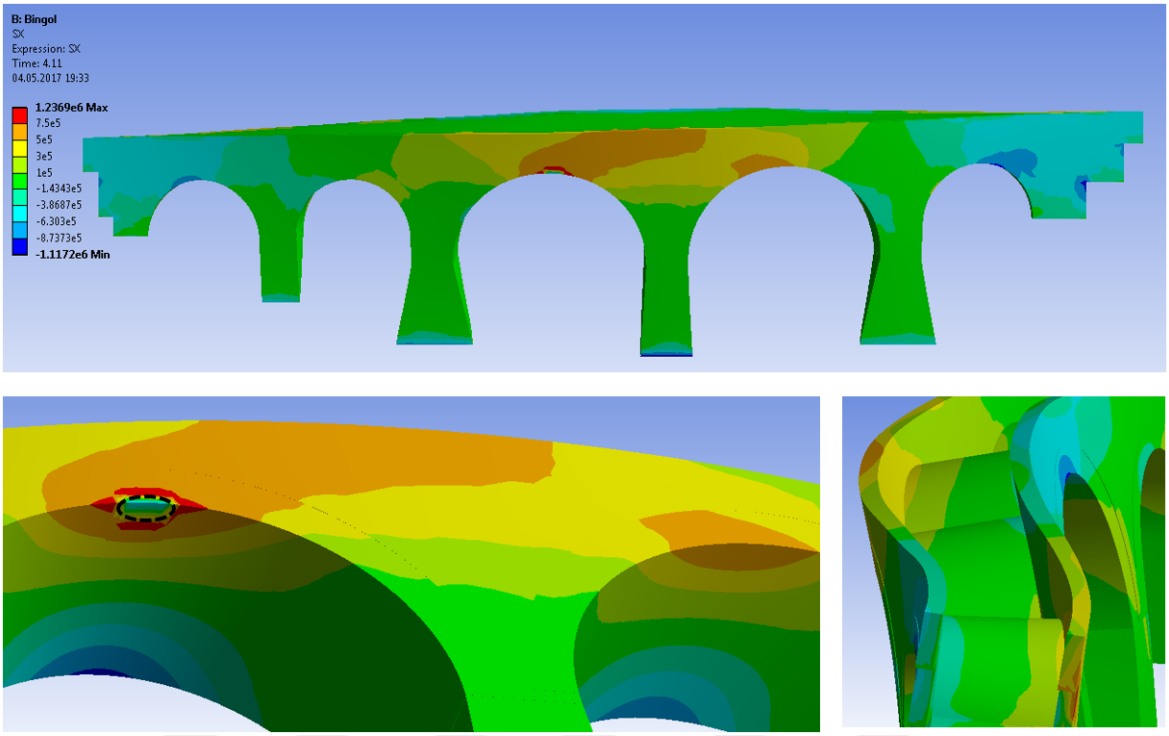

Figure 5.23. Stress distribution for Bingol in X direction

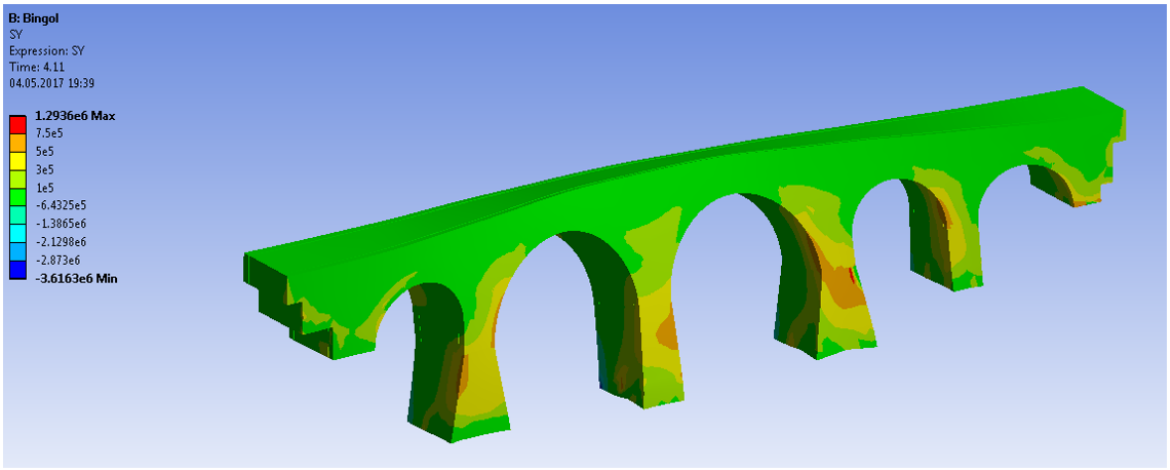

Figure 5.24. Stress distribution for Bingol in Z direction

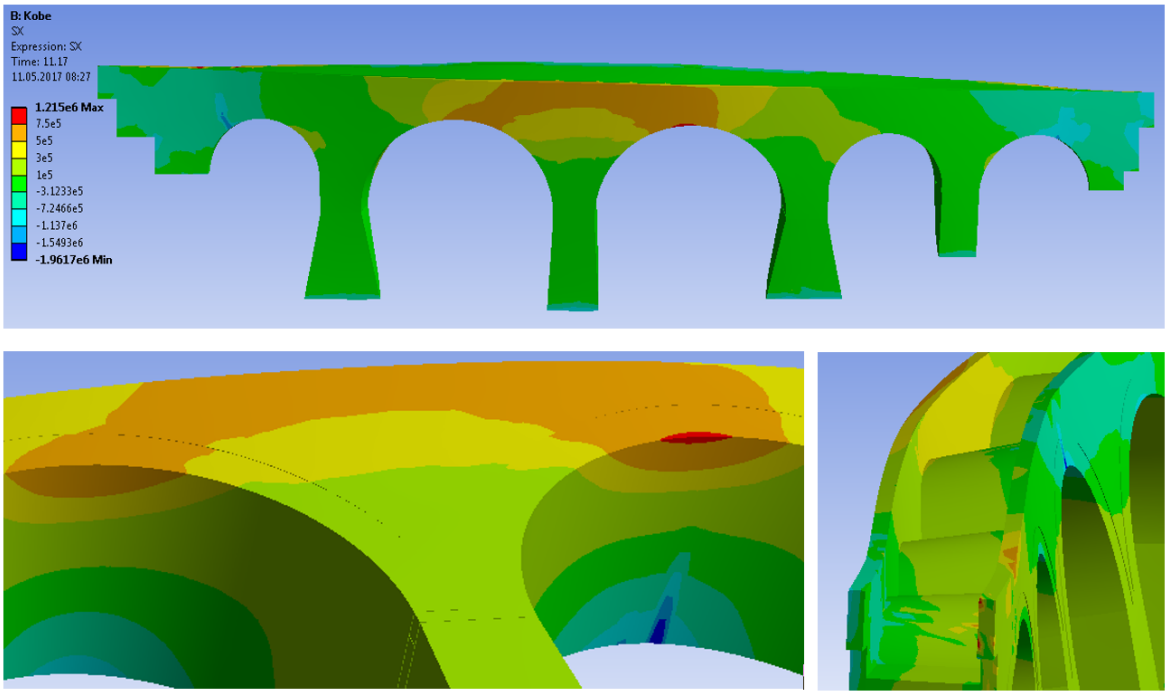

Figure 5.25. Stress distribution for Kobe in X direction

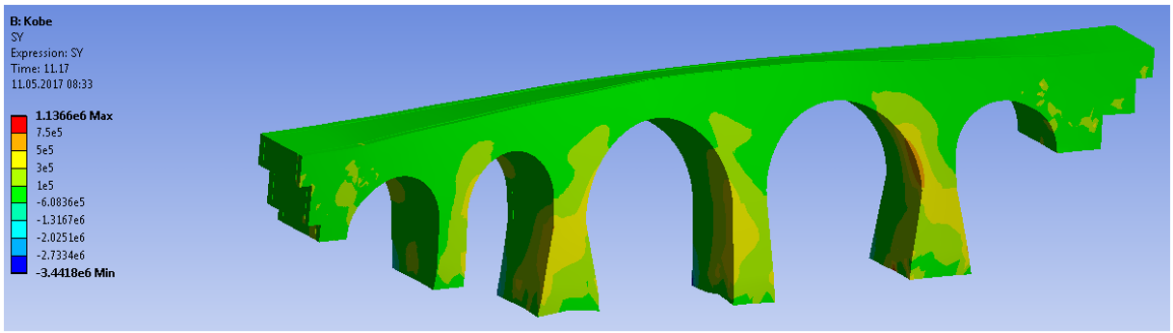

Figure 5.26. Stress distribution for Kobe in Z direction

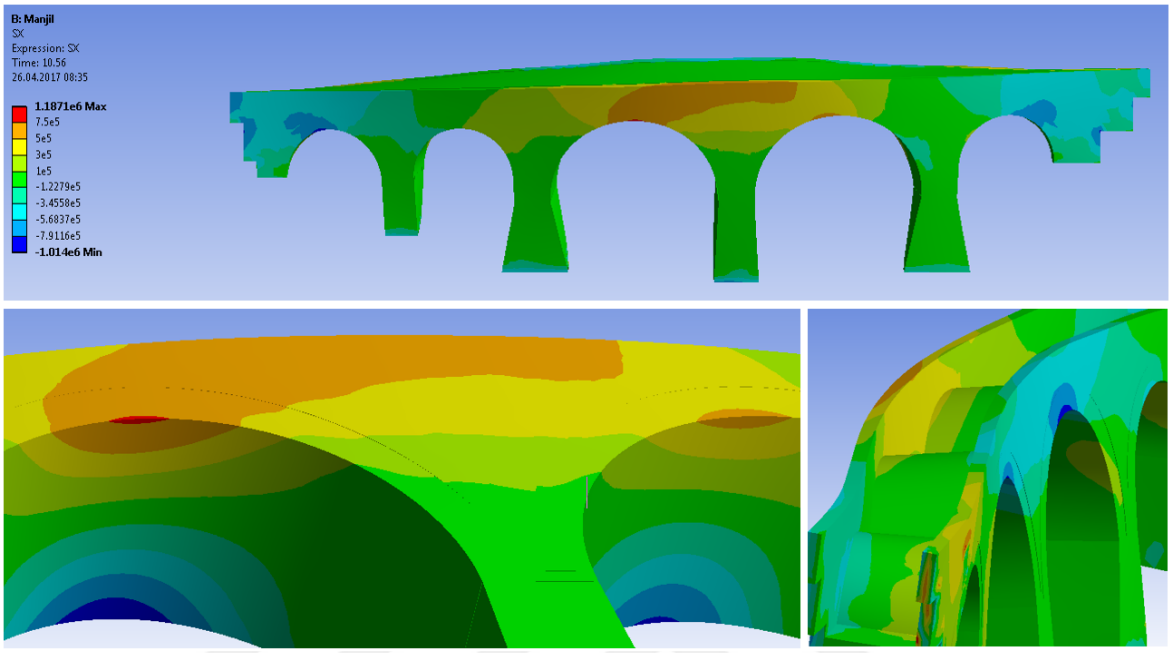

Figure 5.27. Stress distribution for Manjil in X direction

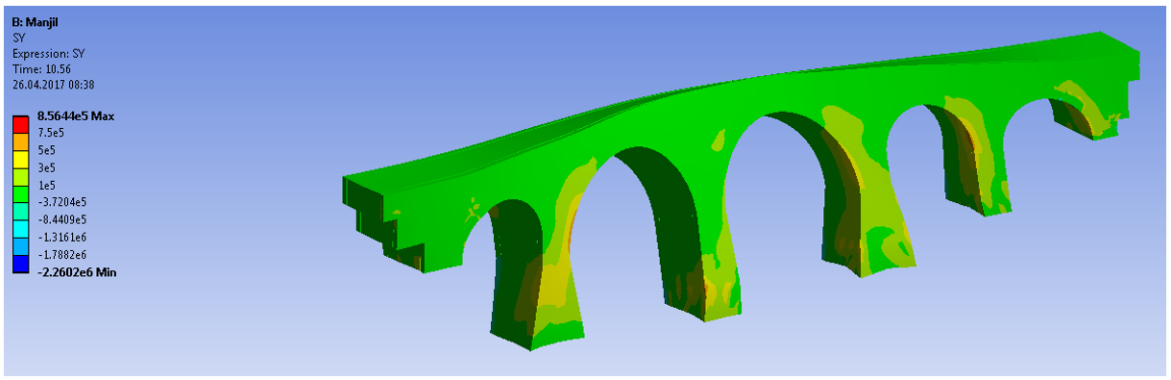

Figure 5.28. Stress distribution for Manjil in Z direction

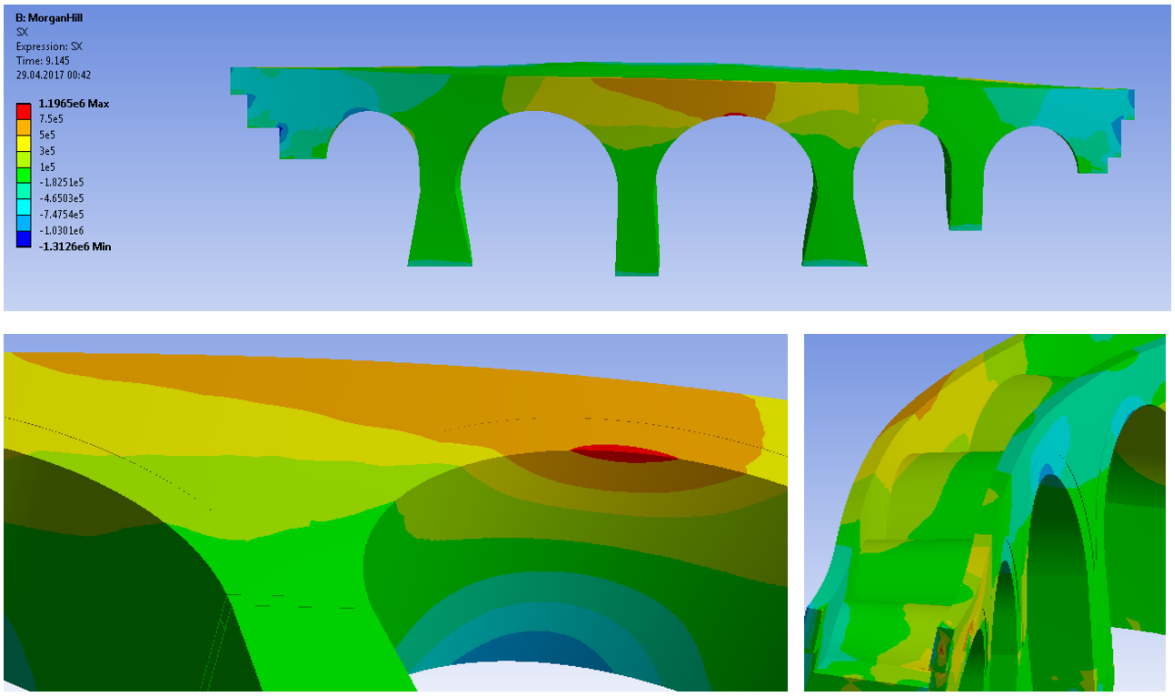

Figure 5.29. Stress distribution for Morgan Hill in X direction

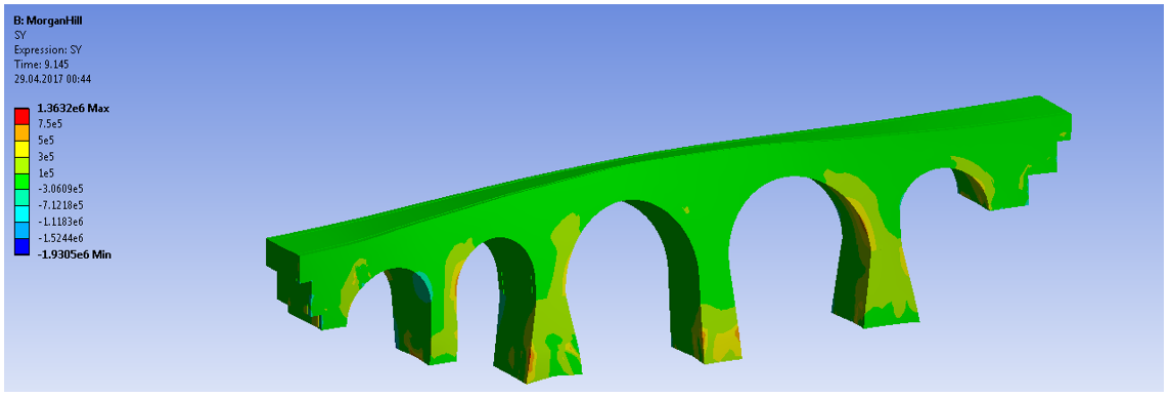

Figure 5.30. Stress distribution for Morgan Hill in Z direction

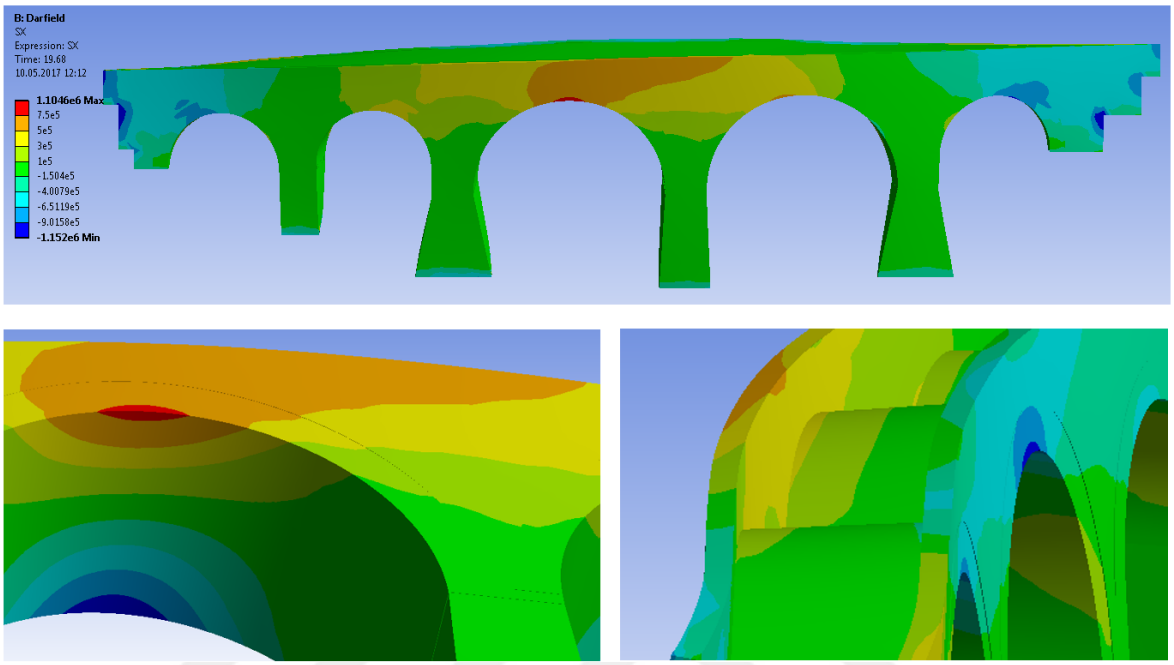

Figure 5.31. Stress distribution for Darfield in X direction

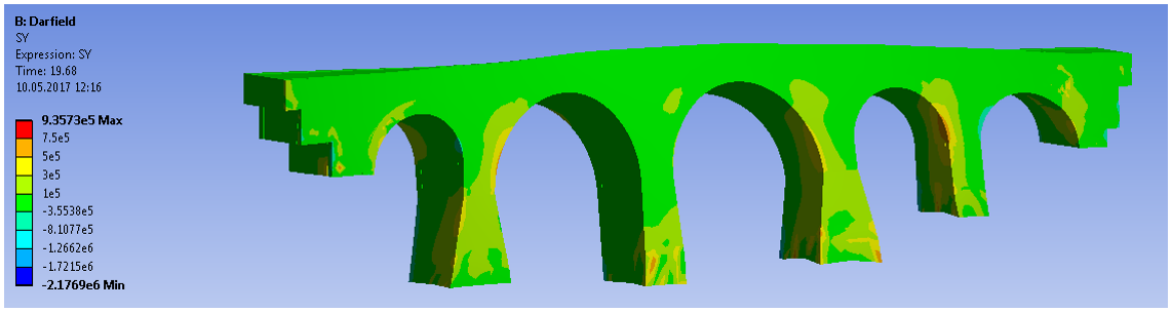

Figure 5.32. Stress distribution for Darfield in Z direction

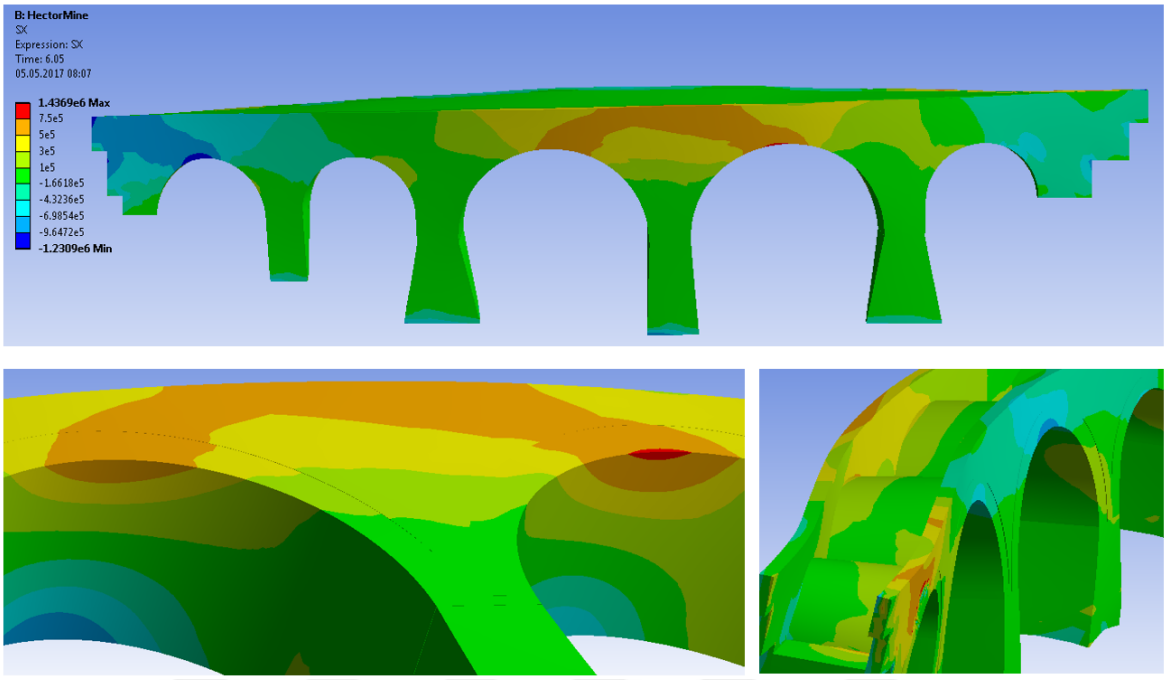

Figure 5.33. Stress distribution for Hector Mine in X direction

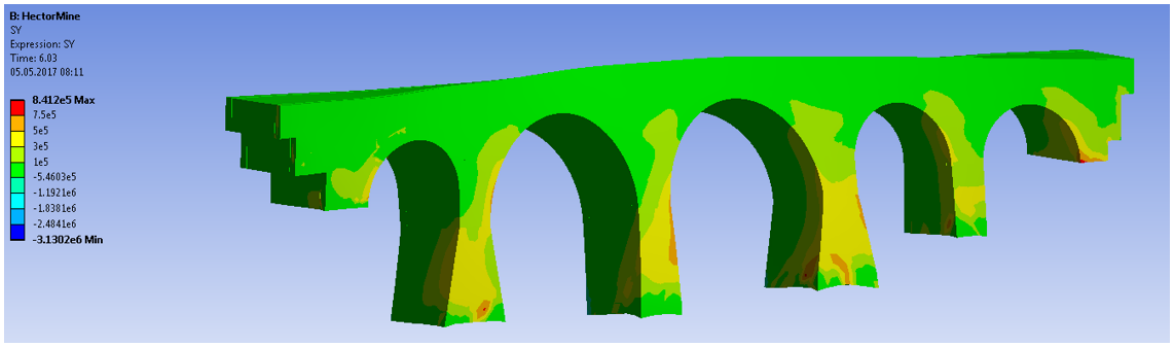

Figure 5.34. Stress distribution for Hector Mine in Z direction

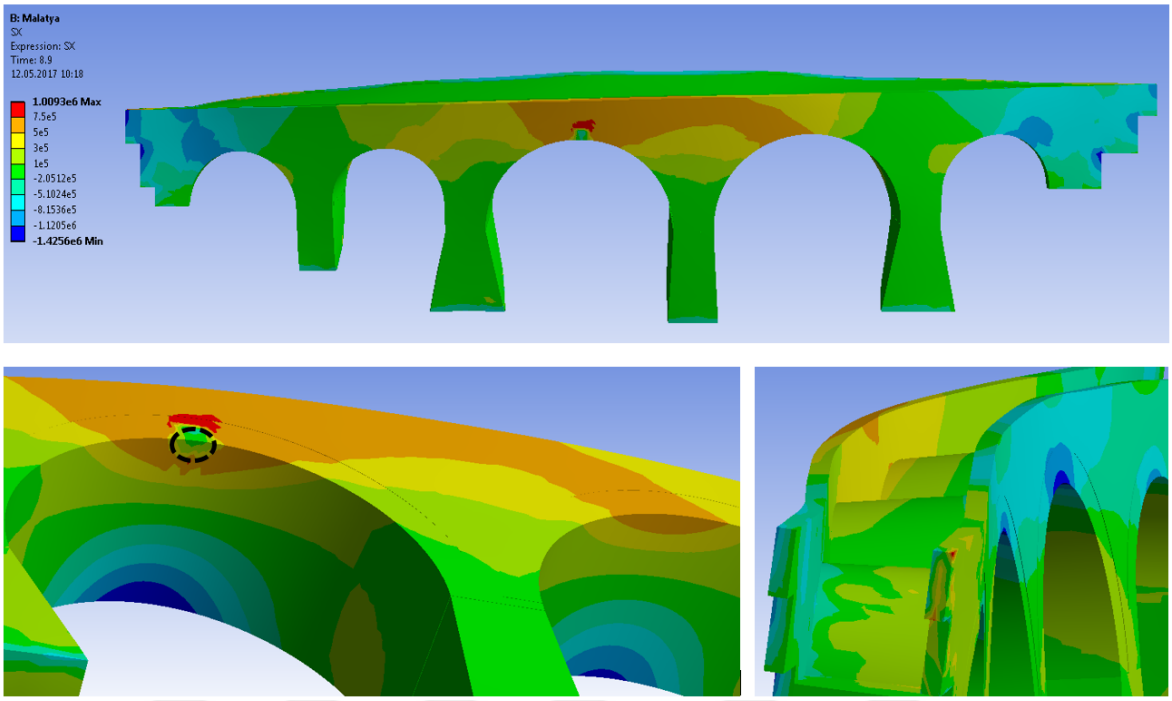

Figure 5.35. Stress distribution for Malatya in X direction

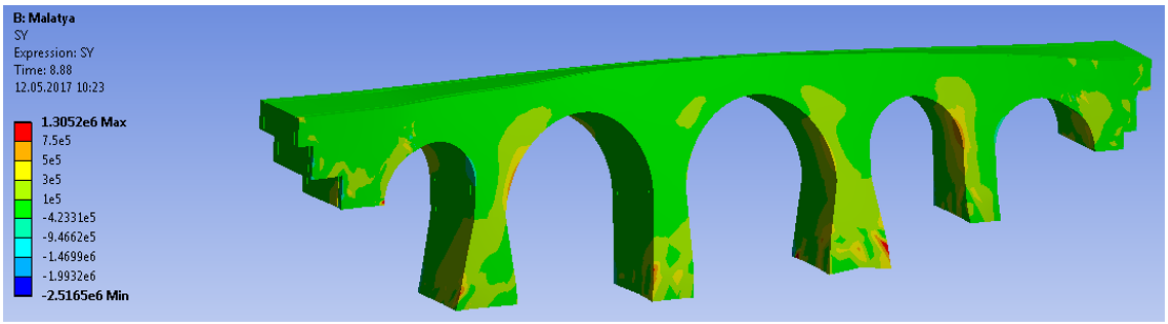

Figure 5.36. Stress distribution for Malatya in Z direction

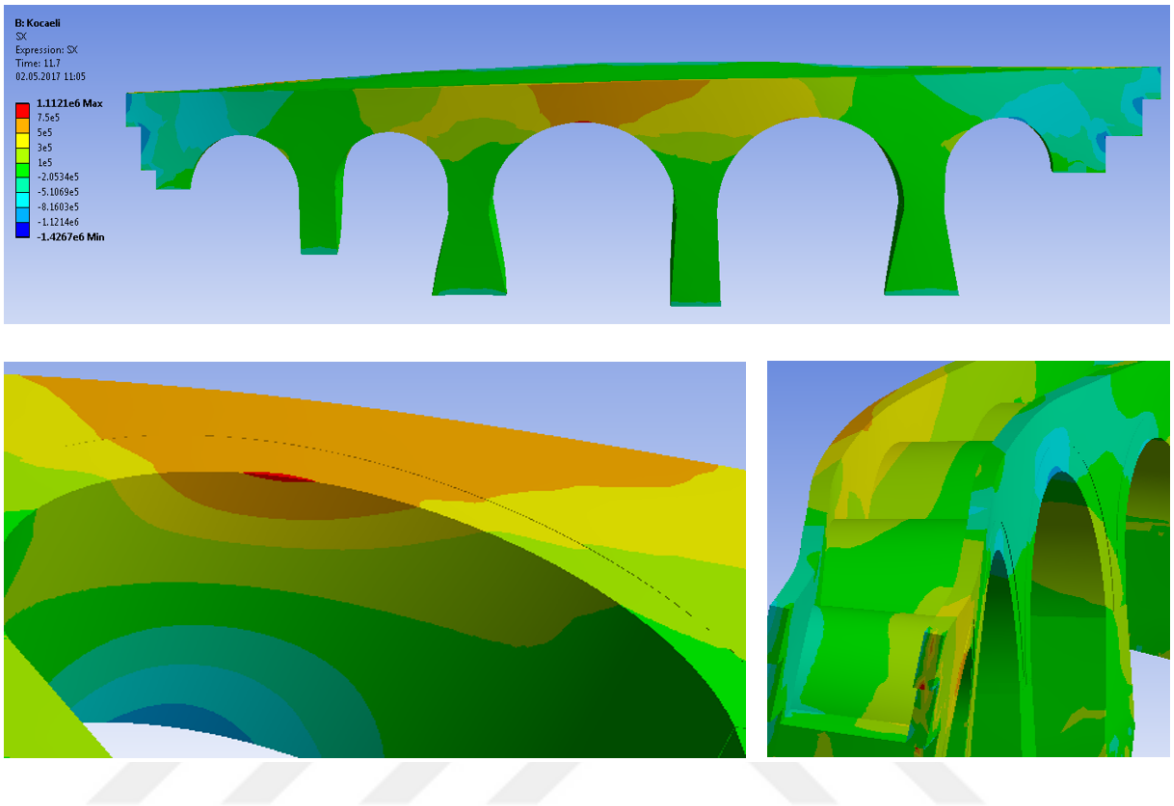

Figure 5.37. Stress distribution for Kocaeli in X direction

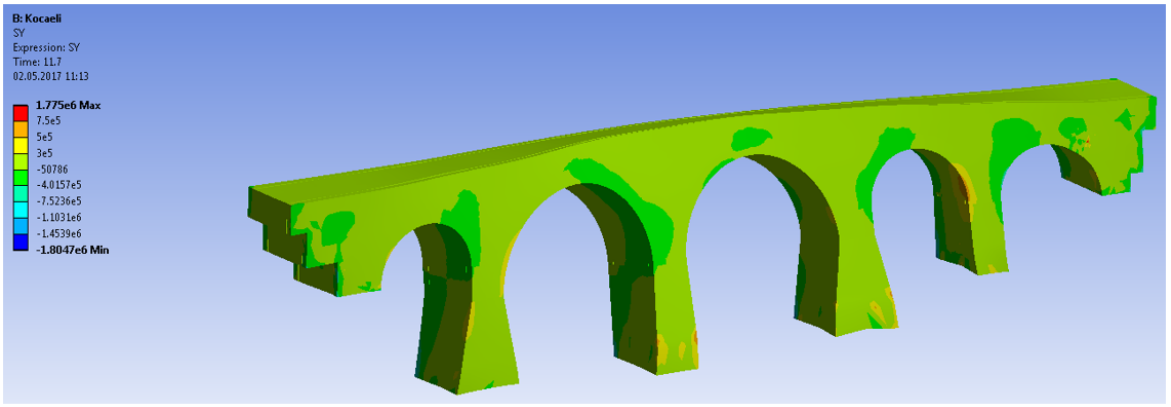

Figure 5.38. Stress distribution for Kocaeli in Z direction

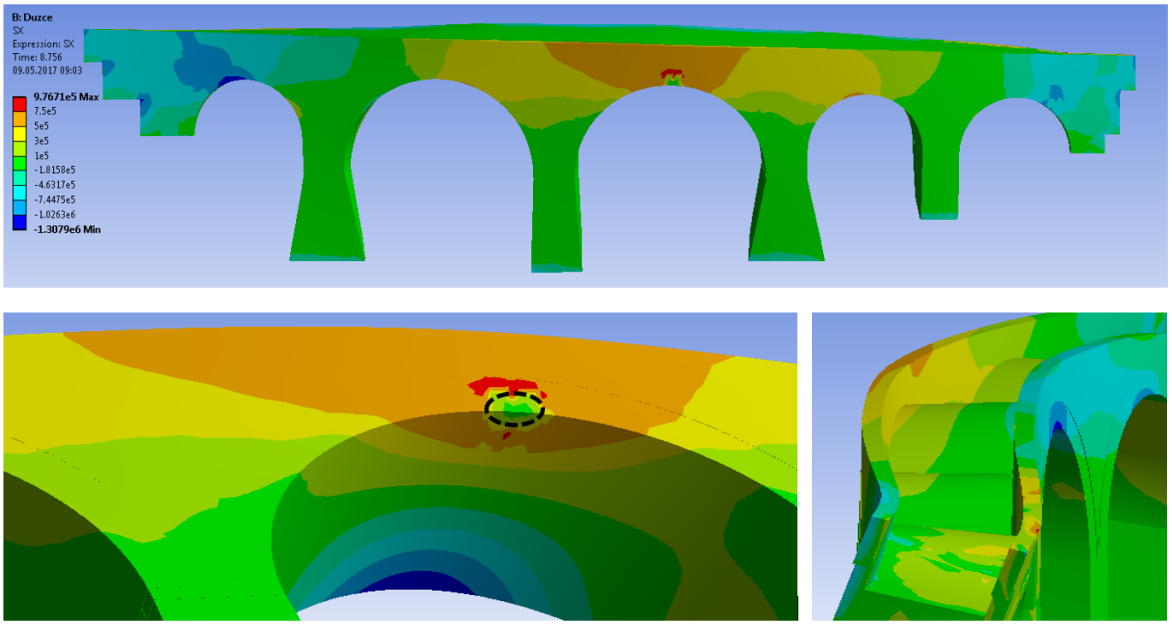

Figure 5.39. Stress distribution for Duzce in X direction

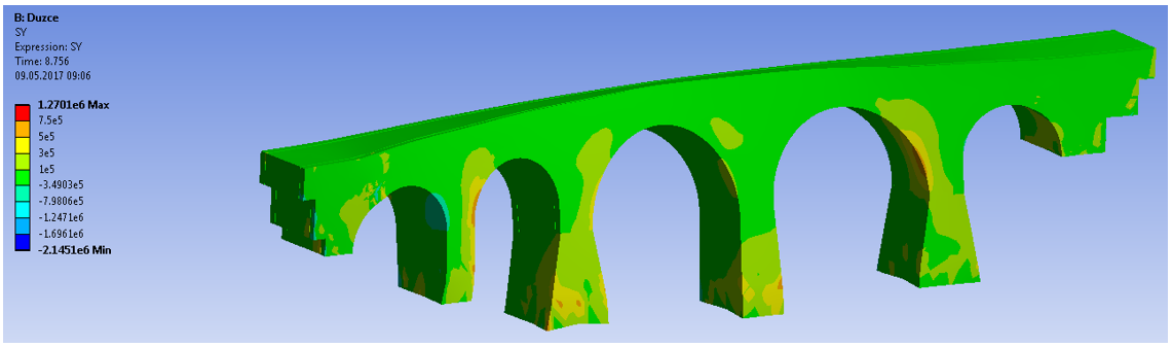

Figure 5.40. Stress distribution for Duzce in Z direction

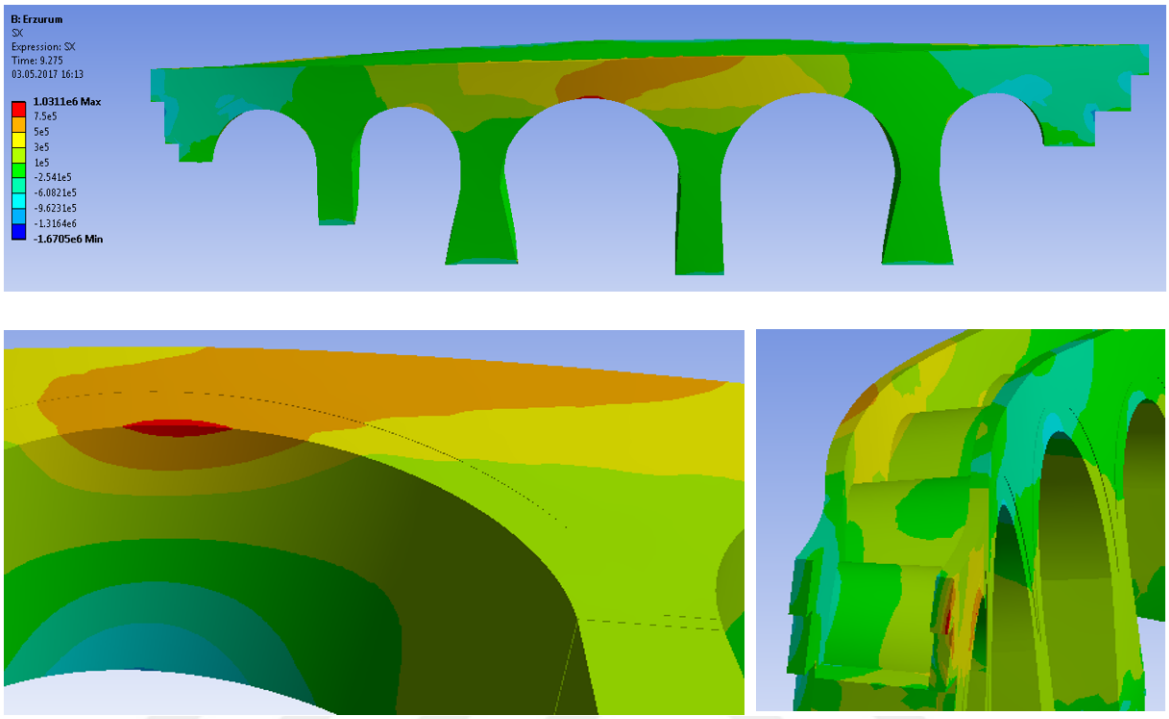

Figure 5.41. Stress distribution for Erzurum in X direction

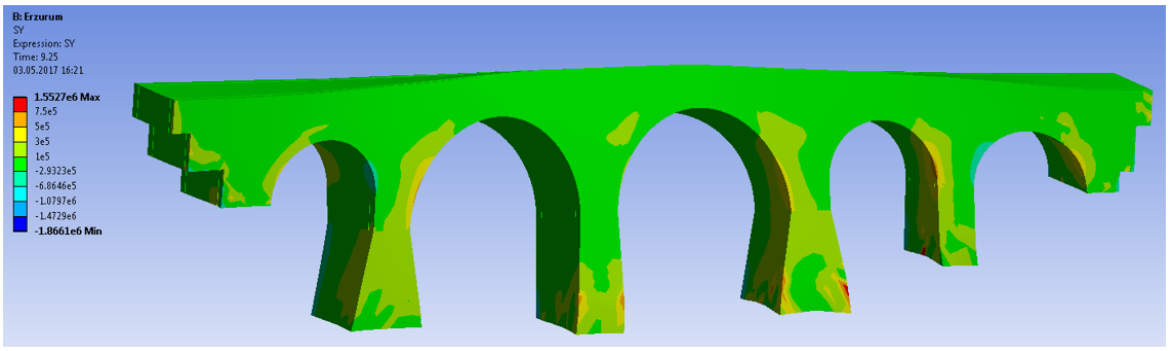

Figure 5.42. Stress distribution for Erzurum in Z direction

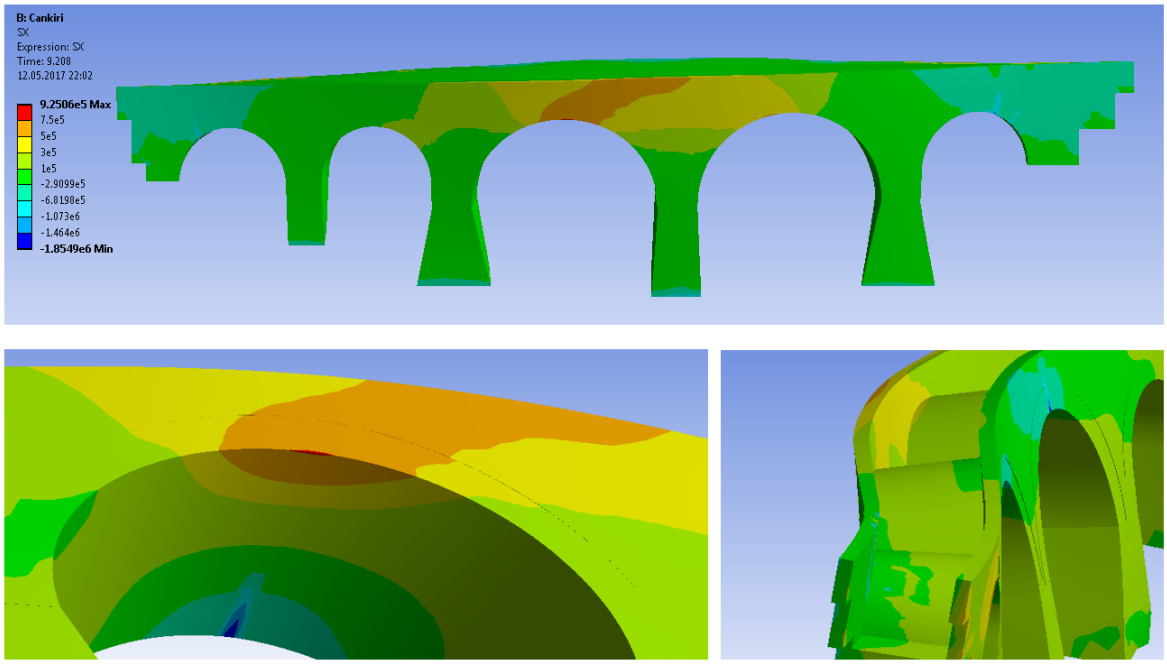

Figure 5.43. Stress distribution for Cankiri in X direction

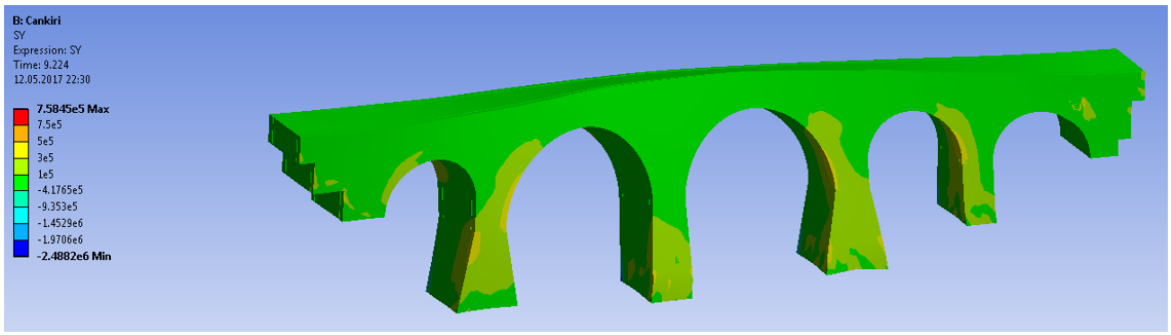

Figure 5.44. Stress distribution for Cankiri in Z direction

Table 5.9 presents the maximum displacement of control node for each ground motion and their arithmetic mean and geometric mean results.

Table 5.9. Displacement results of control node for NLTHA

Earthquake	**Maximum Displacement (mm)**
Bingol	3.56
Kobe	4.49
Manjil	4.40
Morgan Hill	4.02
Darfield	4.46
Hector Mine	3.76
Malatya	5.35
Kocaeli	3.91
Duzce	4.66
Erzurum	5.08
Cankiri	3.35
Geometric Mean	**4.24**
Geometric Mean-Spectral Displacement	**3.21**

Based on stresses obtained from NLTHA, stress distribution in the spandrel wall extends along the arch span and creates some cracks along the keystone of the middle arch barrel, which were represented with black dashed line on above figures, however tensile stresses did not penetrate into inner surface of middle arch barrel and it is not expected to result with a partial failure from the bridge. Also, the spandrel wall was exposed to large amount of tensile stresses, but these tensile stresses do not exceed the capacity of masonry. Actually, as in pushover analysis, crack (or crush) in NLTHA represents that a section of structural component reaches its tensile (or compressive) strength. After that point, this section could not carry any extra load, and stress of this section drops to zero for successive loading. Collapse of structure is observed

at the failure point if width of the area reaching the capacity increases during time history analysis. It is fact that, tensile stress distribution is beginning from arch barrel and continuing along the spandrel wall but the amount of tensile stresses for each earthquake are different. For instance, cracks penetrate to wide range on the arch barrel for Malatya earthquake, but same conclusion cannot be obtained for Cankiri and Kocaeli earthquakes. Also, high tensile stresses were created along the end of the edge arch barrels in Z direction but these tensile stresses were in limit value of strength for each earthquake. On the other hand, NLTHA results show that compression stresses of the structural elements were in limit value of strength and there is no damage due to compression. Besides, maximum displacements of control node show variability. It is related to amount of crack penetration along the structural elements of the bridge. If the amount of the crack along the arch barrel and spandrel wall is high, the total stiffness of the structure decreases and the maximum displacement of control node increases. Displacement of control node is maximum for Malatya earthquake. The geometric mean of spectral displacement of control node was obtained 3.21 mm.

5.4. Comparison of NLSA and NLTHA

Pushover analysis is recommended in many seismic codes, so it is very common analysis method for performance based design and performance assessment. Pushover analysis is more suitable method and gives more reliable results for short and regular bridges because the higher mode effects are limited for these types of structures. On the other hand, NLTHA is common and effective way to characterize the dynamic inelastic response of the structures. When compared with pushover analysis, NLTHA produces inelastic deformations of structural elements with low uncertainty. In NLTHA, the dynamic inelastic response of structure is highly depended the characteristic behavior of ground motion, so increasing number of ground motion analysis increases the reliability of results. That is, NLTHA analysis is inevitable method in order to obtain close to the truth behavior of structure under seismic loading.

According to nonlinear analysis results, stress distributions of structural elements in X direction and in Z direction are similar for NLSA and NLTHA. For both type of

analyses, middle arch barrel and spandrel wall above this arch barrel were exposed to high tensile stresses such that tensile stresses penetrated from outer surface of middle arch barrel and continue along spandrel wall. However, these tensile stresses did not penetrate into inner surface of middle arch barrel. Also, it created some cracks along the keystone of the middle arch barrel. However, this cracks does not establish partial failure on the masonry bridge. Although, spandrel walls were exposed to high tensile stresses due to seismic action, these tensile stresses do not exceed the capacity of masonry. Also, high tensile stresses in Z direction can be seen along the end of edge arch barrels, but these tensile stresses do not exceed the strength capacity of masonry. On the other hand, the compressive stresses were within the limits for both type of analyses.

On the other hand, displacement of control node is around 3.21 mm and 2.20 mm for NLTHA and NLSA respectively. The results show that displacement of control node for NLTHA exceeds that of NLSA. One of the reason of that may be that geometric mean of response spectra of selected ground motion stays above of target spectrum around the fundamental period of the structure.

6. CONCLUSION

6.1. Summary and Results

In this study, summary of a comprehensive project on seismic performance assessment of historical stone arch bridges on Samsun – Sivas railway line was presented. Stone arch bridges have significant structural uncertainties as other historical structures. It was seen that modal values based on material properties obtained from literature or material testing may give significantly different values than the actual ones. Therefore, dynamic identification and FEM updating of these bridges were carried out to obtain more representative FEM and carry out more reliable seismic assessment.

Modal parameters of the masonry bridge were identified from vibration measurements under ambient condition, hammer impact loading and train passing by using Enhanced Frequency Domain Decomposition algorithm. FEM of the masonry bridge was updated based on identified modal parameters. For FEM updating, a Matlab code, which automatically creates FEM's by changing the values of the chosen structural parameters within pre-determined limits, was utilized.

After obtaining updated FEM, seismic performance assessment of the bridges was carried out by pushover analysis and nonlinear dynamic analysis. For nonlinear analyses, FEM of the masonry bridge was established in ANSYS software. In order to reflect properly the material non-linearity for FEM in ANSYS, smeared crack model was used. This solid element model has an ability to capture cracking in tension and crushing in compression of structural components.

Demand curve was created according to DLH 2008 by considering earthquake level which was selected D2, coordinates of bridge and soil investigation report in order to obtain performance point of the masonry bridge after pushover analysis. 11 earthquake records were used to perform nonlinear time history analyses. In order to properly simulate seismic load on the masonry bridge, the horizontal components

of the selected earthquake motions were combined by Square Roots of the Sum of the Squares (SRSS) method and combined response spectra of the selected ground motions were scaled in a way that, geometric mean of response spectra of earthquake records is coherent with 1.3 times design spectrum which was obtained for pushover analysis according to DLH 2008 based on earthquake level which was selected D2, location of the masonry bridge and soil investigation report.

NLSA and NLTHA results show that there was no global structural deficiency i.e.no significant strength overcome on piers and arches of all bridges on the line. However, it can be seen from nonlinear analyses results that stress distribution in the spandrel wall extends along the arch span and creates some cracks along the keystone of the middle arch barrel which is not expected to result with a partial failure from the bridge. Also, the spandrel wall and end of the edge arch barrels were exposed to large amount of tensile stresses, but these tensile stresses do not exceed the capacity of masonry. Moreover, the displacement of control node at performance point of NLSA is similar to the geometric mean of displacement of control node at NLTHA. On the other hand, structural deficiencies were observed on spandrel walls for bridges with wider arches and higher seismic demand.

The outcomes of the study indicate that determination of modal frequencies, mode shapes and damping ratios by using identification techniques is very crucial in order to identify the current behavior of the masonry bridges. The use of unrealistic modal values may lead to unsafe or conservative assessments. Also, FEM updating based on identified modal results is very essential step to create accurate FEM's for seismic assessment of masonry bridges because updating results show that Young's modulus of masonry and soil are very far from literature values. More proper stress distributions and deformations were obtained on the structural components thanks to updated material values. It must be certainly stated that dynamic tests of a large number of historical arch bridges, which were built in similar years and on a railway route, uniquely contributed to the understanding the dynamic behaviors of such bridges. Moreover, updating of FEM's by considering identified dynamic behaviors of the bridges and generation of code based spectrum for a representative group of

bridges located on a railway route played an essential role in enhancing the seismic performance evaluation of the railway bridges. Therefore, system identification and FEM updating studies are strongly recommended to verify the result of nonlinear simulations of masonry bridges in order to improve the current seismic design practice. Also, the results of nonlinear analyses were obtained similarly for two analysis types. However, NLTHA creates inelastic deformations of structural elements with low uncertainty and produces more reliable results when compared with pushover analysis. Therefore, NLTHA is recommended for seismic assessment of these types of structures.

6.2. Future Works

In the project, nonlinear analyses represented that 12 out of 41 bridges were in need of strengthening on their spandrel walls if they have wider arches and higher seismic demand and this paper presents one of these 12 bridges. This study can be improved with the following future works.

- Other identification methods such as Stochastic Subspace Identification (SSI) and Autoregressive Moving Average (ARMA) can be very useful to discuss the effects of identification methods.
- The laboratory tests will be very useful in order to represent properly relationship between mortar and stone as well as the relationship between fill and masonry structure.
- The effects of strengthening methods to stress distribution of structural components and crack penetrations will be investigated in order to decide the most effective strengthening methodology.
- Showing the difference between the nonlinear analyses results of updated and non-updated FEM may be more representative and memorable in probabilistic view.
- To establish micro model with considering stone and mortar separately will be very useful to discuss the differences of nonlinear results for macro model and micro model.

REFERENCES

1. Structural Components of Masonry Bridges, 2003, http://www.pinterest.com, accessed at July 2017.

2. Ponte Vecchio Bridge, Inside Inferno in Florence, 2009, http://www.insideinferno.com, accessed at May 2017.

3. Pont du Gar Bridge, Yann De Fareins, 2007, http://www.pontdugard.fr/en, accessed at May 2017.

4. Puente Trajan Bridge, 2008,http://www.flickriver.com, accessed at May 2017.

5. Examples of Bridge from Romans in Turkey, Ersin Demirel, 2005, http://www.atlasdergisi.com, accessed at May 2017.

6. Railway Line Map of Turkey, Turkish State Railways, 2009, http://www.tcdd.gov.tr, accessed at May 2017.

7. Aoki T., Sabia D., Rivella D., and Komiyama T, "Structural Characterization of a Stone Arch Bridge by Experimental Tests and Numerical Model Updating", *International Journal of Architectural Heritage*, 1, 227-250, 2007.

8. Altunisik A.C., Bayraktar A., Sevim B., and Birinci F., "Vibration-based Operational Modal Analysis of the Mikron Historic Arch Bridge After Restoration", *Civil Engineering and Environmental Systems*, 28, 247-259, 2011.

9. Banerji P., Chikermane S., "Condition Assessment of a Heritage Arch Bridge Using a Novel Model Updation Technique", *Journal of Civil Structural Health Monitoring*, 2, 1-16, 2012.

10. Costa C., Arêde A., Costa A., Caetano E., Cunha, A., and Magalhães F., "Updating Numerical Models of Masonry Arch Bridges by Operational Modal Analysis", *International Journal of Architectural Heritage*, 9, 760-774, 2015.

11. Fanning P.J., and Boothby T.E., "Three Dimensional Modelling and Full-scale Testing of Stone Arch Bridges", *Computers and Structures*, 79, 2645-2662, 2001.

12. Orban Z., and Guterman M., "Assessment of Masonry Arch Railway Using Non-destructive In-situ Testing Methods", *Engineering Structures*, 31, 2287-2298, 2009.

13. Domede N., Sellier A., and Stablon T., "Structural Analysis of Multi-span Railway Masonry Bridge Combining In-situ Observations, Laboratory Tests and Damage Modelling", *Engineering Structures*, 56, 837-849, 2013.

14. Pelà L., Aprile A., and Benedett A., "Seismic Assessment of Masonry Arch Bridges", *Engineering Structures*, 31, 1777-1788, 2009.

15. Pelà L., Aprile A., and Benedett A., "Comparison of Seismic Assessment Procedures for Masonry Arch Bridges", *Engineering Structures*, 38, 381-394, 2013.

16. Zampieri P., Zanini M.A., and Modena C., "Simplified Seismic Assessment of Multi-span Masonry Arch Bridges", *Bulletin of Earthquake Engineering*, 13, 2629-2646, 2015.

17. Tecchio G., da Porto F., Zampieri P., Modena C., and Bettio C., "Static and Seismic Retrofit of Masonry Arch Bridges: Case studies", *Bridge Maintenance, Safety, Management, Resilience and Sustainability*, 33, 1094-1098, 2012.

18. Behnamfar F., and Afshari M., "Collapse analysis and strengthening of stone arch bridges against earthquake", *International Journal of Architectural Heritage*, 7, 1-25, 2013.

19. LDH125 Locomotive, 2011, http://www.le-rail.ch, accessed at May 2016.

20. Brincker R., Zhang L., and Andersen P., "Modal Identification of Output – only Systems Using Frequency Domain Decomposition", *Smart Materials and Structures*, 10, 441-445, 2001.

21. North Anatolian Fault, General Directorate of Mineral Research and Exploration, 2010, http://www.mta.gov.tr/v3.0/, accessed at May 2017.

22. Barraza J. A. C.,*Numerical Model for Nonlinear Analysis of Masonry Walls*, Ph.D. Thesis, Rheinisch-Westfälischen Technischen Hochschule Aachen University, 2012.

23. AFAD, Strong Ground Motion Database of Turkey, Boğaziçi University, Kandilli Observatory and Earthquake Research Institute, http://kyhdata.deprem.gov.tr/2K/kyhdata-v4.php

24. Peer Strong Ground Motion Database, 2005, "The Pacific Earthquake Engineering Research", Center and the Unisversity of California.

25. DLH, 2008, "Technical Earthquake Regulation Concerning Construction of Coastal and Port Structures, Railroads, Airports by the Ministry of Transport, Maritime and Communication", Ankara.

26. Chopra A., *Dynamics Of Structures,Theory and Applications to Earthquake Engineering (2nd Edition b.)*, New Jersey Prentice-Hall, 2001.

27. The mathworks INC, MATLAB User's Guide, 2015.